UNIVERSITÀ DEGLI STUDI DI VERONA

DIPARTIMENTO DI MEDICINA

SCUOLA DI DOTTORATO IN SCIENZE DELLA VITA E DELLA SALUTE

DOTTORATO DI RICERCA IN PROTEOMICA CLINICA

XXIV° CICLO / ANNO 2009

TITOLO DELLA TESI DI DOTTORATO:

INTEGRATED ANALYSIS OF NOVEL SIGNAL TRANSDUCTION PATHWAYS IN RED CELLS FROM PATIENTS WITH NEUROACANTHOCYTOSIS

S.S.D. MED 09

Coordinatore: Prof. Oliviero Olivieri

Firma _____

Tutor: Prof.ssa Lucia De Franceschi

Firma _____

Dottorando: Dott. Carlo Tomelleri

Firma _____

INDEX

ABSTRACT

Neuroacanthocytosis (NA) is a group of rare genetic disorders that share similar neurological clinical manifestations and the presence of thorny red cells in the peripheral circulation, the acanthocytes. The two core NA diseases are Chorea-Acanthocytosis (ChAc) and McLeod Syndrome (MLS). Since acanthocytes are an hallmark of NA, studying the mechanisms underlying the generation of acanthocytes might shed light on the pathogenesis of NA syndromes. Here, we present a set of studies on the signaling mechanisms and structural changes in red cells from ChAc and MLS patients.

In the first study, we evaluated tyrosine phosphorylation of red cells from ChAc patients by proteomics analysis. Increased Tyr-phosphorylation state of several membrane proteins including band 3, β-spectrin and adducin was found in ChAc RBCs. In particular, band 3 was highly phosphorylated on the Tyr-904 residue, a functional target of Lyn, but not on Tyr-8, a functional target of Syk. In ChAc RBCs band 3 Tyr-phosphorylation by Lyn was independent of the canonical Syk mediated pathway. The ChAc-associated alterations in RBC membrane-protein organization appear to be the result of increased Tyr-phosphorylation leading to altered linkage of band 3 to the junctional complexes involved in anchoring the membrane to the cytoskeleton. We propose this altered association between cytoskeleton and membrane proteins as a novel mechanism in the generation of acanthocytes in ChAc.

In the second study, we combined phosphoproteomics datasets on ChAc and MLS with network topology analysis to predict signaling sub-networks involved in acanthocyte generation. We identified all the interactomic shortest paths linking the two proteins mutated in NA syndromes, respectively chorein and XK, to the differentially phosphorylated proteins in our proteomics data. Then, we refined the analysis considering only restricted clusters of highly interacting signaling proteins which can be involved in acanthocyte formation in both diseases. We identified a cluster of 14 kinases that might be related to red cell shape alterations and deserve further investigation.

As preliminary study in the context of an international collaboration we analyzed red cells from Neurodegeneration with Brain Iron Accumulation (NBIA) patients and their first degree relatives. Our aim was to assess the presence of acanthocytes in these subjects and to study their structural characteristics.

In the last study, we validated a new co-polymer based on acrylamide and polyvinyl alcohol bearing olefinic moieties in proteomic analysis of red cells. This new hydrogel is easy to handle and its macroporosity makes it suitable for the separation of high molecular weight proteins such as chorein.

RIASSUNTO

Il termine neuroacantocitosi (NA) raggruppa diverse malattie genetiche rare che condividono manifestazioni neurologiche simili e la presenza di globuli rossi stellati nella circolazione periferica, gli acantociti. Le due principali malattie classificate come NA sono Corea acantocitosi (ChAc) e sindrome di McLeod (MLS).

Poiché la presenza di acantociti è una caratteristica comune di questi disordini, lo studio dei meccanismi alla base della loro formazione può aiutare a comprendere la patogenesi delle NA. In questa tesi viene presentata una serie di studi sui meccanismi di signaling e sulle modificazioni strutturali di globuli rossi di pazienti di ChAc e MLS.

Nel primo studio abbiamo analizzato con tecniche di proteomica la fosforilazione in tirosina di globuli rossi di pazienti affetti da ChAc .

Nei globuli rossi di questi pazienti abbiamo riscontrato un aumento della fosforilazione in tirosina su diverse proteine di membrana e legate alla membrana tra cui banda 3, β-spectrina e adducina. In particolare, la fosforilazione sul residuo Tyr-904 della banda 3, target della chinasi Lyn, era molto elevata, mentre sul residuo Tyr-8 della stessa proteina, target della chinasi Syk, non abbiamo riscontrato un aumento della fosforilazione. Nei pazienti di ChAc, la fosforilazione della banda 3 da parte di Lyn è indipendente dal meccanismo canonico di fosforilazione sequenziale mediato da Syk.

Le alterazioni dell'organizzazione delle proteine di membrana correlate con ChAc sembrano quindi essere il risultato di un aumento della fosforilazione in tirosina che porta a cambiamenti nel legame della banda 3 con i ponti multiproteici tra la membrana e il citoscheletro. Proponiamo quindi quest'alterazione nell'associazione tra membrana e citoscheletro mediata da fosforilazione in tirosina come un nuovo meccanismo che porta alla formazione di acantociti in ChAc.

Nel secondo studio abbiamo combinato i nostri set di dati fosfo-proteomici su eritrociti di pazienti di ChAc e MLS con l'analisi topologica di network proteici per predirre quali sub-network della trasduzione del segnale possano essere coinvolti nella formazione degli acantociti.

Abbiamo identificato tutte le interazioni che legano le due proteine mutate nelle due patologie in esame (rispettivamente coreina e XK) con le proteine differenzialmente fosforilate dei nostri dati sperimentali. Quindi, abbiamo analizzato nello specifico solo cluster di proteine coinvolte nella trasduzione del segnale che interagiscono molto strettamente tra loro e che possono essere coinvolte nella formazione di acantociti in entrambe le patologie. Abbiamo identificato un cluster di 14 chinasi che possono essere coinvolte in tale processo e meritano ulteriori approfondimenti.

Come studio preliminare nel contesto di una collaborazione internazionale abbiamo analizzato globuli rossi da pazienti affetti da Neurodegenerazione con Accumulo di Ferro nel Cervello (NBIA) e di loro parenti di primo grado. Il nostro scopo era quello di determinare se fossero presenti acantociti nei pazienti e nei soggetti correlati ma privi di sintomi clinici e di studiare le caratteristi che strutturali dei loro eritrociti.

Nell'ultimo studio abbiamo validato con l'applicazione a tecniche di analisi proteomica un nuovo copolimero basato su acrilamide e polivinil alcool modificato con gruppi olefinici. Questo nuovo idrogel è semplice da maneggiare anche a basse concentrazioni e la sua macroporosità lo rende particolarmente adatto alla separazione di proteine ad alto peso molecolare quale la coreina.

INTRODUCTION

Red blood cell shape and membrane organization

Red blood cell main function of exchanging carbon dioxide with oxygen and bringing it throughout the human body via blood vessels claims for a very efficient structure of this peculiar cell. The discoidal shape of the erythrocyte maximizes the surface to volume ratio to increase the oxygen rate exchange [1]. Red cell plasma membrane plasticity and its viscoelastic properties make it possible for these cells to pass through the microcapillaries in peripheral circulation, turning back to the discoidal shape right after deformation, several times per minute during their whole lifespan (120 days ca).

The maintenance of an optimal red cell surface to volume ratio and membrane stability in response to either mechanical or osmotic stress is assured by the functional cross-talk between the lipid bilayer, the integral membrane proteins and the peripheral proteins. In this system are involved (i) integral membrane proteins such as band 3 that spanning through the membrane, support the lipid bilayer and participate to the membrane anchoring to the cytoskeletal network; (ii) the ion transport systems: exchangers and channels involved in red cell volume regulation and (iii) the peripheral proteins as α- and β-spectrin.

Two major multiprotein complexes bridge the red cell membrane, via band 3 dimers or tetramers, with the cytoskeleton network: the 4.1 or junctional complex and the ankyrin complex [2]. The deformability of red cells during their life-span in the peripheral circulation is related to the maintenance of the asymmetric membrane lipid bilayer, an optimal lipid-protein cross-talk and the rearrangement of the cytoskeleton.

The main component of red cell cytoskeleton are spectrins. Spectrins are high molecular weight proteins (250kDa ca), that form heterodimers which connect to each other by head-to-head interaction to generate linear tetramers. Such tetramers are organized in hexagons by tail interaction with short actin filaments, resulting in a highly elastic bidimensional lettice [3].

Band 3 has multiple functions in red cells such as bicarbonate/chloride exchange, docking site for glycolytic enzymes such as aldolase or GAPDH, thereby regulating ATP production, and docking of antioxidant/chaperone proteins such as Prx-2 [4].

Most studies on red cell membrane organization and function have been carried out on hereditary red cell membrane disorders involving protein(s) from the multiprotein bridges or from the cytoskeleton [5][6]. Progresses in the knowledge of red cell membrane-cytoskeleton dynamic interactions have been also made after the development of mouse models lacking specific proteins of red cell membrane [7].

Recent studies have suggested that changes in membrane protein phosphorylation state plays an important role in the modulation of red cell membrane protein-protein functional

cross-talk and in the stability of multi-protein structures affecting red cell membrane mechanical properties and, in some cases, red cell morphology [8, 9]

Changes in the phosphorylation state of either tyrosine (Tyr) or serine/threonine (Ser/Thr) residues on band 4.1 [10-12], ankyrin [13], band 3 [8] and spectrins [14], have been reported to affect protein structure or protein stability, which in turn modifies protein-protein interaction in the complex and dynamic organization of red cell membrane-cytoskeleton network.

Abnormal Tyr-phosphorylation profiles of red cell membrane proteins have been observed in inherited red cell disorders such as sickle cell disease [15], spherocytosis, stomatocytosis or G6PD deficiency [16] as well as in malaria infected red cells [17], suggesting a key role of phosphorylation events in red cell homeostasis.

Among red cell membrane proteins, band 3 is the most studied since it is the most abundant integral membrane protein and is characterized by several phosphorylable sites.

Tyr-phosphorylation state of band 3, much more than its Ser/Thr phosphorylation state, seems to affect red cell morphology since higher levels of band 3 Tyr-phosphorylation correlate with the appearance of crenated cells [18]. The process of Tyr-phosphorylation of band 3 is tightly regulated, is elicited by volume decrease and Ca2+ loading, and involves two Tyr-kinases: Syk and the Src family kinase Lyn, which are balanced by phosphatases PTP1B and SHPTP-2 action through a still partially known mechanism [19, 20].

Namely, activated Syk phosphorylates band 3 at the N-terminus (residues 8 and 21) generating an SH-2 domain docking site for Lyn that subsequently phosphorylates band 3 between the cytoplasmic and membrane domain (residue 359) and at the C-terminus (residue 904). Native dephosphorylated status is then restored by phosphatases recruited to the membrane [21]. In red cells from healthy subjects Tyr-phosphorylation of band 3 increases with red cell aging, possibly due to lack of phosphatase activity or to oxidative damage related to cell senescence [20].

Neuroacanthocytosis syndromes

Neuroacanthocytosis (NA) denotes a group of rare genetic diseases that share similar neurological symptoms (including choreic movements, dyskinesia, dystonia, dysphagia, dysarthria, areflexia, seizures and cognitive impairment) due to basal ganglia degeneration and presence, in variable percentage, of spiculated erythrocytes in the peripheral circulation, known as acanthocytes [22, 23].

The two main diseases classified as NA are Chorea-Acanthocytosis (ChAc) and McLeod Syndrome (MLS). In the past few years other diseases have been added to the NA syndromes group [24]: (a) Huntington Disease Like 2 (HDL-2) caused by the expansion of a trinucleotide in the *jph3* gene, coding for Junctophilin 3 and (b) abetalipoproteinemia (ABL), characterized by the absence of plasma betalipoproteins, due to mutations in the MTP

gene coding for microsomal triglyceride transfer protein. Finally, another hereditary neurodegenerative disease characterized by the presence of acanthocytes in peripheral blood and basal ganglia degeneration, is Pantothenate Kinase Associated Neurodegeneration (PKAN), that is caused by mutations in the *pank2* gene coding for Pantothenate Kinase 2. Recently PKAN has been classified among the Neurodegeneration with Brain Iron Accumulation (NBIA) syndromes due to the characteristic accumulation of iron in the globus pallidus [25].

ChAc is a typically autosomal recessive disease caused by mutations on the *VPS13A* gene coding for chorein [26], a high molecular weight protein which possible function has been extrapolated by similarities with other organisms: the yeast Vps13p and the *Dictyostelium discoideum* TipC proteins [27]. In yeast, the Vps13p protein is involved in protein trafficking of various transmembrane proteins in particular in the recruitment of three membrane proteins to the trans-Golgi network (TGN): Kex2p, a Golgi-endoprotease, Ste13p, a dipeptidyl aminopeptidase and Vps10p, a cargo-sorting receptor, which delivers the cargo enzymes to the prevacuolar compartment (PCV) that is similar to human late endosome [28-31]. In ChAc patients several mutations including frameshifts, nonsense, splice-site, missense mutations and deletion of whole exons, resulting in low or absent synthesis of chorein or normal expression of a functionally defective protein have been reported [32-34]. Chorein has been shown to be expressed in mature red cells and to be partially or completely absent in red cells from patients with ChAc. Chorein detection by a polyclonal antibody has been proposed as fast molecular diagnosis of chorea acanthocytosis [35] together with the genetic analysis of the *VPS13A* locus.

The neurological clinical presentation of ChAc is in young adult but may also occur at younger ages, increased serum creatine kinase may precede the neurological symptoms, and sometimes is associated with hepatosplenomegaly and, more rarely, with cardiac myopathies [36-39]

MLS is a recessive, X-linked disease due to mutations in the *xk* gene coding for XK protein, a membrane protein predicted to have 10 transmembrane domains and the structural characteristics of a membrane transport of still unknown role [40]. The XK protein is covalently linked to Kell glycoprotein by a single disulphide bond forming a membrane protein complex part of the junctional complex anchoring the membrane to the cytoskeleton [41-43]. Analysis of the expression of Kell and XK on the membrane is used for diagnosis, while the molecular genetic testing of the *xk* locus is available only on a research basis. The absence of the red cell XK protein and the reduction of Kell antigens are associated with the presence of acanthocytes and compensated hemolytic anemia. Clinical features of MLS include late onset (between the fourth and sixth decade of life), myopathy and cardiomyopathy [44].

Acanthocytes in Neuroacanthocytosis

Although the molecular defects underlying NA have been described and partially characterized, to date, the mechanism of generation of acanthocytes and the way they are related to neurodegenerative clinical manifestations remains still unclear.

A study based on electron microscopy showed that both for MLS and ChAc acanthocytes the distribution of cytoskeletal structures is irregular as compared to normal red cells and is characterized by condensation of filamentous structures around the base of protrusions and only small amounts of spectrin based structures in inward bent areas [45].

Since in NA no abnormalities in the abundance of membrane or membrane associated proteins have been reported, it is likely that the processes leading to acanthocyte formation are connected to alteration of red cell membrane protein structure and/or function, possibly involving the stability of multiprotein complexes bridging the membrane to the cytoskeleton network.

In one case of ChAc increased membrane serine-threonine phosphorylation levels mainly of band 3 and spectrin, increased levels of band 3 tyrosine phosphorylation and increased casein-kinase membrane activity have been described [46].

The observation of an increased amount of Nε (γ-glutamyl)-lysine isopeptide cross-links, a product of tissue transglutaminase, in red cells from some patients, is also suggesting the presence of a perturbation of the anchoring bridges [47]. Transglutaminase 2 catalyzes the organization of a protein multicomplex cross-linked by the Nε (γ-glutamyl) lysine isopeptide. The main protein involved is band 3 through its Gln-30 residue, together with bridging proteins as ankyrin and band 4.1 and with cytoskeleton proteins such as spectrins [48, 49].

The how and why of the combination of neuronal degeneration in the basal ganglia with the formation of acanthocytes in patients with various neuroacanthocytosis syndromes is still far from being fully understood. Further studies need to be carried out to understand the events involved in the pathogenesis of NA syndromes. In view of the specific and characteristic association of acanthocytosis with neurodegeneration, red cells, constitute an interesting research target.

References

1. Chakraborty, S., V. Balakotaiah, and A. Bidani, *Diffusing capacity reexamined: relative roles of diffusion and chemical reaction in red cell uptake of O2, CO, CO2, and NO.* J Appl Physiol, 2004. **97**(6): p. 2284-302.
2. Anong, W.A., et al., *Adducin forms a bridge between the erythrocyte membrane and its cytoskeleton and regulates membrane cohesion.* Blood, 2009. **114**(9): p. 1904-12.
3. Liu, S.C., et al., *Alteration of the erythrocyte membrane skeletal ultrastructure in hereditary spherocytosis, hereditary elliptocytosis, and pyropoikilocytosis.* Blood, 1990. **76**(1): p. 198-205.
4. Walsh, S.B. and G.W. Stewart, *Anion exchanger 1: Protean function and associations.* Int J Biochem Cell Biol. **42**(12): p. 1919-22.
5. Iolascon, A., S. Perrotta, and G.W. Stewart, *Red blood cell membrane defects.* Rev Clin Exp Hematol, 2003. **7**(1): p. 22-56.
6. Delaunay, J., *The molecular basis of hereditary red cell membrane disorders.* Blood Rev, 2007. **21**(1): p. 1-20.
7. van den Akker, E., et al., *Band 3 multiprotein complexes in the red cell membrane; of mice and men.* Blood Cells Mol Dis. **45**(1): p. 1-8.
8. Ferru, E., et al., *Regulation of membrane-cytoskeletal interactions by tyrosine phosphorylation of erythrocyte band 3.* Blood. **117**(22): p. 5998-6006.
9. Pantaleo, A., et al., *Current knowledge about the functional roles of phosphorylative changes of membrane proteins in normal and diseased red cells.* J Proteomics. **73**(3): p. 445-55.
10. Gauthier, E., et al., *Phosphorylation-dependent perturbations of the 4.1R-associated multiprotein complex of the erythrocyte membrane.* Biochemistry. **50**(21): p. 4561-7.
11. Manno, S., Y. Takakuwa, and N. Mohandas, *Modulation of erythrocyte membrane mechanical function by protein 4.1 phosphorylation.* J Biol Chem, 2005. **280**(9): p. 7581-7.
12. Betz, T., et al., *ATP-dependent mechanics of red blood cells.* Proc Natl Acad Sci U S A, 2009. **106**(36): p. 15320-5.
13. Cianci, C.D., M. Giorgi, and J.S. Morrow, *Phosphorylation of ankyrin down-regulates its cooperative interaction with spectrin and protein 3.* J Cell Biochem, 1988. **37**(3): p. 301-15.
14. Tang, H.Y. and D.W. Speicher, *In vivo phosphorylation of human erythrocyte spectrin occurs in a sequential manner.* Biochemistry, 2004. **43**(14): p. 4251-62.
15. George, A., et al., *Altered phosphorylation of cytoskeleton proteins in sickle red blood cells: the role of protein kinase C, Rac GTPases, and reactive oxygen species.* Blood Cells Mol Dis. **45**(1): p. 41-5.
16. Pantaleo, A., et al., *Irreversible AE1 tyrosine phosphorylation leads to membrane vesiculation in G6PD deficient red cells.* PLoS One. **6**(1): p. e15847.
17. Pantaleo, A., et al., *Analysis of changes in tyrosine and serine phosphorylation of red cell membrane proteins induced by P. falciparum growth.* Proteomics. **10**(19): p. 3469-79.
18. Bordin, L., et al., *Functional link between phosphorylation state of membrane proteins and morphological changes of human erythrocytes.* Biochem Biophys Res Commun, 1995. **213**(1): p. 249-57.
19. Bordin, L., et al., *Band 3 is an anchor protein and a target for SHP-2 tyrosine phosphatase in human erythrocytes.* Blood, 2002. **100**(1): p. 276-82.
20. Ciana, A., G. Minetti, and C. Balduini, *Phosphotyrosine phosphatases acting on band 3 in human erythrocytes of different age: PTP1B processing during cell ageing.* Bioelectrochemistry, 2004. **62**(2): p. 169-73.
21. Brunati, A.M., et al., *Sequential phosphorylation of protein band 3 by Syk and Lyn tyrosine kinases in intact human erythrocytes: identification of primary and secondary phosphorylation sites.* Blood, 2000. **96**(4): p. 1550-7.
22. Walker, R.H., H.H. Jung, and A. Danek, *Neuroacanthocytosis.* Handb Clin Neurol. **100**: p. 141-51.
23. Walker, R.H., et al., *Neurologic phenotypes associated with acanthocytosis.* Neurology, 2007. **68**(2): p. 92-8.

24. Walker, R.H., et al., *Developments in neuroacanthocytosis: expanding the spectrum of choreatic syndromes.* Mov Disord, 2006. **21**(11): p. 1794-805.
25. Gregory, A., B.J. Polster, and S.J. Hayflick, *Clinical and genetic delineation of neurodegeneration with brain iron accumulation.* J Med Genet, 2009. **46**(2): p. 73-80.
26. Velayos-Baeza A, L., C., Dobson-Stone, C., Monaco, A.P. , *The function of chorein*, in *Neuro-acanthocytosis syndromes II*, S. Walker RH, S., Danek, A., Editor. 2008, Springer-Verlag: Berlin Heildelberg. p. 87-105.
27. Stege, J.T., M.T. Laub, and W.F. Loomis, *tip genes act in parallel pathways of early Dictyostelium development.* Dev Genet, 1999. **25**(1): p. 64-77.
28. Abazeed, M.E., J.M. Blanchette, and R.S. Fuller, *Cell-free transport from the trans-golgi network to late endosome requires factors involved in formation and consumption of clathrin-coated vesicles.* J Biol Chem, 2005. **280**(6): p. 4442-50.
29. Abazeed, M.E. and R.S. Fuller, *Yeast Golgi-localized, gamma-Ear-containing, ADP-ribosylation factor-binding proteins are but adaptor protein-1 is not required for cell-free transport of membrane proteins from the trans-Golgi network to the prevacuolar compartment.* Mol Biol Cell, 2008. **19**(11): p. 4826-36.
30. Foote, C. and S.F. Nothwehr, *The clathrin adaptor complex 1 directly binds to a sorting signal in Ste13p to reduce the rate of its trafficking to the late endosome of yeast.* J Cell Biol, 2006. **173**(4): p. 615-26.
31. Brickner, J.H. and R.S. Fuller, *SOI1 encodes a novel, conserved protein that promotes TGN-endosomal cycling of Kex2p and other membrane proteins by modulating the function of two TGN localization signals.* J Cell Biol, 1997. **139**(1): p. 23-36.
32. Dobson-Stone, C., et al., *Mutational spectrum of the CHAC gene in patients with chorea-acanthocytosis.* Eur J Hum Genet, 2002. **10**(11): p. 773-81.
33. Rampoldi, L., et al., *A conserved sorting-associated protein is mutant in chorea-acanthocytosis.* Nat Genet, 2001. **28**(2): p. 119-20.
34. Velayos-Baeza, A., et al., *Analysis of the human VPS13 gene family.* Genomics, 2004. **84**(3): p. 536-49.
35. Dobson-Stone, C., et al., *Chorein detection for the diagnosis of chorea-acanthocytosis.* Ann Neurol, 2004. **56**(2): p. 299-302.
36. Kageyama, Y., et al., *A new phenotype of chorea-acanthocytosis with dilated cardiomyopathy and myopathy.* Mov Disord, 2007. **22**(11): p. 1669-70.
37. Lossos, A., et al., *Early clinical heterogeneity in choreoacanthocytosis.* Arch Neurol, 2005. **62**(4): p. 611-4.
38. Danek, A., et al., *Neuroacanthocytosis: new developments in a neglected group of dementing disorders.* J Neurol Sci, 2005. **229-230**: p. 171-86.
39. Rampoldi, L., A. Danek, and A.P. Monaco, *Clinical features and molecular bases of neuroacanthocytosis.* J Mol Med (Berl), 2002. **80**(8): p. 475-91.
40. Ho, M., et al., *Isolation of the gene for McLeod syndrome that encodes a novel membrane transport protein.* Cell, 1994. **77**(6): p. 869-80.
41. Arnaud, L., et al., *Identification and characterization of a novel XK splice site mutation in a patient with McLeod syndrome.* Transfusion, 2009. **49**(3): p. 479-84.
42. Calenda, G., et al., *Identification of two new members, XPLAC and XTES, of the XK family.* Gene, 2006. **370**: p. 6-16.
43. Singleton, B.K., et al., *McLeod syndrome resulting from a novel XK mutation.* Br J Haematol, 2003. **122**(4): p. 682-5.
44. Danek, A., et al., *McLeod neuroacanthocytosis: genotype and phenotype.* Ann Neurol, 2001. **50**(6): p. 755-64.
45. Terada, N., et al., *Ultrastructural changes of erythrocyte membrane skeletons in chorea-acanthocytosis and McLeod syndrome revealed by the quick-freezing and deep-etching method.* Acta Haematol, 1999. **101**(1): p. 25-31.
46. Olivieri, O., et al., *Increased membrane protein phosphorylation and anion transport activity in chorea-acanthocytosis.* Haematologica, 1997. **82**(6): p. 648-53.
47. Melone, M.A., et al., *Abnormal accumulation of tTGase products in muscle and erythrocytes of chorea-acanthocytosis patients.* J Neuropathol Exp Neurol, 2002. **61**(10): p. 841-8.

48. Lorand, L. and R.M. Graham, *Transglutaminases: crosslinking enzymes with pleiotropic functions.* Nat Rev Mol Cell Biol, 2003. **4**(2): p. 140-56.
49. Murthy, S.N., et al., *Residue Gln-30 of human erythrocyte anion transporter is a prime site for reaction with intrinsic transglutaminase.* J Biol Chem, 1994. **269**(36): p. 22907-11.
50. Matte, A., et al., *Peroxiredoxin-2 expression is increased in beta-thalassemic mouse red cells but is displaced from the membrane as a marker of oxidative stress.* Free Radic Biol Med. **49**(3): p. 457-66.

blood

2011 118: 5652-5663
Prepublished online September 27, 2011;
doi:10.1182/blood-2011-05-355339

Erythrocyte membrane changes of chorea-acanthocytosis are the result of altered Lyn kinase activity

Lucia De Franceschi, Carlo Tomelleri, Alessandro Matte, Anna Maria Brunati, Petra H. Bovee-Geurts, Mariarita Bertoldi, Edwin Lasonder, Elena Tibaldi, Adrian Danek, Ruth H. Walker, Hans H. Jung, Benedikt Bader, Angela Siciliano, Emanuela Ferru, Narla Mohandas and Giel J. C. G. M. Bosman

Blood (print ISSN 0006-4971, online ISSN 1528-0020), is published weekly by the American Society of Hematology, 2021 L St, NW, Suite 900, Washington DC 20036.

Erythrocyte membrane changes of chorea-acanthocytosis are the result of altered Lyn kinase activity

Lucia De Franceschi,[1] *Carlo Tomelleri,[1] *Alessandro Matte,[1] Anna Maria Brunati,[2] Petra H. Bovee-Geurts,[3] Mariarita Bertoldi,[4] Edwin Lasonder,[5] Elena Tibaldi,[2] Adrian Danek,[6] Ruth H. Walker,[7,8] Hans H. Jung,[9] Benedikt Bader,[6] Angela Siciliano,[1] Emanuela Ferru,[1,10] Narla Mohandas,[11] and Giel J. C. G. M. Bosman[3]

[1]Department of Medicine, University of Verona, Verona; Italy; [2]Department of Biochemistry, University of Padova, Padova, Italy; [3]Department of Biochemistry and Nijmegen Centre for Molecular Life Sciences, Radboud University Nijmegen Medical Centre, Nijmegen, The Netherlands; [4]Department of Life and Reproduction Sciences, Section of Biochemistry, University of Verona, Verona, Italy; [5]Centre for Molecular and Biomolecular Informatics, Nijmegen Centre for Molecular Life Sciences, Radboud University Nijmegen Medical Centre, Nijmegen, The Netherlands; [6]Department of Neurology, Ludwig Maximilians Universität, Munich, Germany; [7]Department of Neurology, James J. Peters Veterans Administration Medical Center, Bronx, NY and [8]Mount Sinai School of Medicine, New York, NY; [9]University Hospital of Zurich, Zurich, Switzerland; [10]Department of Genetic, Biology and Biochemistry, University of Torino, Torino, Italy; and [11]New York Blood Center, New York, NY

Acanthocytic RBCs are a peculiar diagnostic feature of chorea-acanthocytosis (ChAc), a rare autosomal recessive neurodegenerative disorder. Although recent years have witnessed some progress in the molecular characterization of ChAc, the mechanism(s) responsible for generation of acanthocytes in ChAc is largely unknown. As the membrane protein composition of ChAc RBCs is similar to that of normal RBCs, we evaluated the tyrosine (Tyr)–phosphorylation profile of RBCs using comparative proteomics. Increased Tyr phosphorylation state of several membrane proteins, including band 3, β-spectrin, and adducin, was noted in ChAc RBCs. In particular, band 3 was highly phosphorylated on the Tyr-904 residue, a functional target of Lyn, but not on Tyr-8, a functional target of Syk. In ChAc RBCs, band 3 Tyr phosphorylation by Lyn was independent of the canonical Syk-mediated pathway. The ChAc-associated alterations in RBC membrane protein organization appear to be the result of increased Tyr phosphorylation leading to altered linkage of band 3 to the junctional complexes involved in anchoring the membrane to the cytoskeleton as supported by coimmunoprecipitation of β-adducin with band 3 only in ChAc RBC-membrane treated with the Lyn-inhibitor PP2. We propose this altered association between membrane skeleton and membrane proteins as novel mechanism in the generation of acanthocytes in ChAc. (*Blood*. 2011;118(20):5652-5663)

Introduction

Chorea-acanthocytosis (ChAc) is a rare autosomal recessive neurodegenerative disorder of the neuroacanthocytosis group.[1-3] ChAc is characterized by a neurodegeneration of the basal ganglia, which is associated with the presence of acanthocytes, abnormal erythrocytes with thorn-like protrusions, in the peripheral circulation.[1-3] Molecular studies have identified mutation(s) of the *VPS13A* gene (chromosome 9), encoding a 360-kDa protein chorein of unknown function that is ubiquitously expressed in the brain.[2,4-6] To date, 92 mutations on the *VPS13A* gene have been reported, resulting in low or absent synthesis of chorein or in expression of a functionally defective protein at normal levels.[2,4-6] Chorein has been detected in mature RBCs but it is partially or completely absent in RBCs from patients with ChAc.[6] Because of the lack of knowledge on the structure of chorein and on its interaction with other proteins, we can only speculate on the role of chorein in RBC homeostasis.

In the RBC membrane, 2 major multiprotein complexes bridge the lipid bilayer with the integral membrane proteins to the spectrin-actin cytoskeleton: the ankyrin complex and the junctional or 4.1R complex.[7] Electron microscopy of ChAc RBCs reveals ultrastructural abnormalities in the membrane skeleton as indicated by a heterogeneous distribution of the cytoskeleton. Condensed skeletal structures around protrusions and a less filamentous structure in some large membrane patches indicate a perturbation of membrane cytoskeleton network associated with the membrane protrusions that characterize acanthocytes.[8] These structural data were also supported by the observation that ChAc patients have a fraction of dense RBCs containing acanthocytes with a reduced cell K^+ content compared with normal controls.[9] RBCs from ChAc patients did not show overall abnormalities in RBC membrane protein composition and content, although there is accumulating evidence for neuroacanthocytosis-specific abnormalities in band 3 structure and function.[10] Increased membrane serine-threonine phosphorylation levels, mainly of band 3 and spectrin, increased levels of band 3 tyrosine (Tyr) phosphorylation, and increased activity of membrane-associated casein-kinase has also been described in ChAc RBCs.[11] Increased amounts of N^{ε} (γ-glutamyl) lysine isopeptides associated with the RBC membrane have also been reported in a few ChAc patients, indicating a possible perturbation of the anchoring bridges between the membrane and the cytoskeleton.[12,13] There are no consistent data indicating a

Submitted May 17, 2011; accepted September 7, 2011. Prepublished online as *Blood* First Edition paper, September 27, 2011; DOI 10.1182/blood-2011-05-355339.

*C.T. and A.M. contributed equally to this study.

The online version of this article contains a data supplement.

The publication costs of this article were defrayed in part by page charge payment. Therefore, and solely to indicate this fact, this article is hereby marked "advertisement" in accordance with 18 USC section 1734.

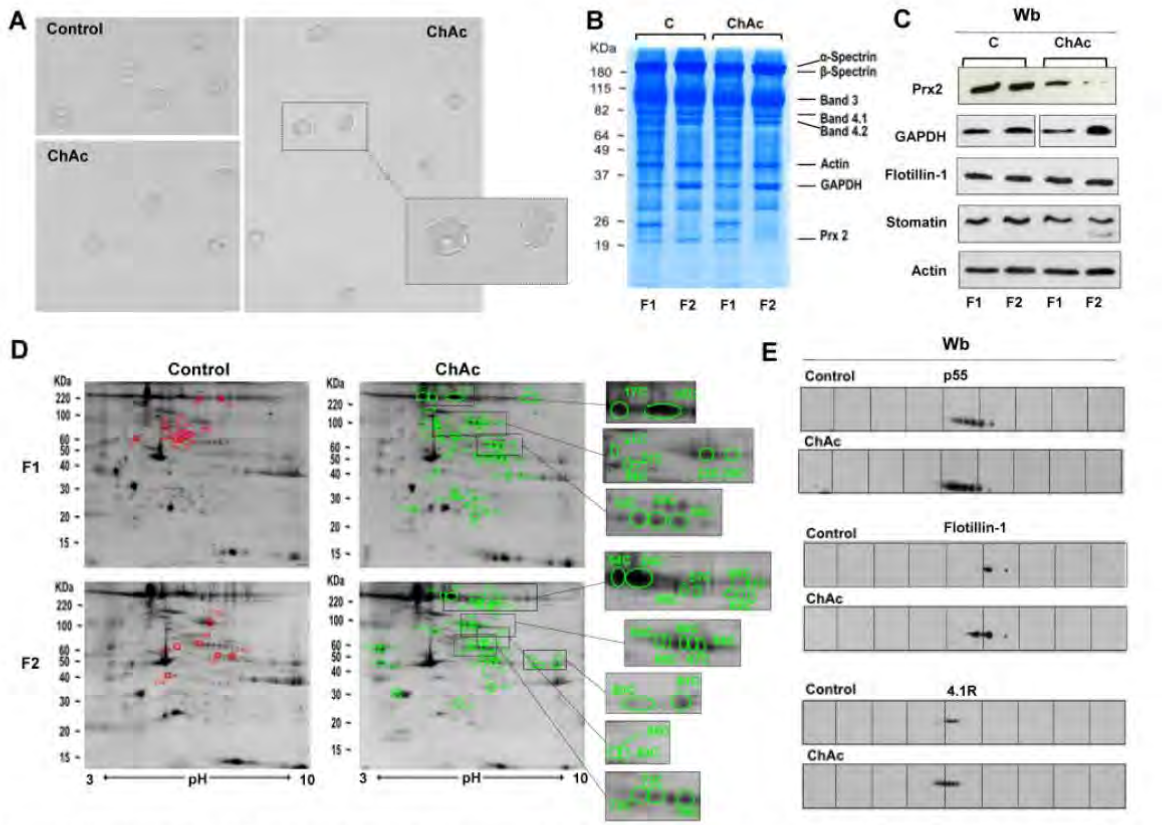

Figure 1. Proteomic analysis of RBC membrane fractions shows differences in ChAc compared with healthy controls. (A) Morphology of RBCs from control and ChAc subjects. (B-E) RBCs from control (C) and ChAc were fractionated in fraction 1 (F1) corresponding to a density < 1.074, containing reticulocytes, and fraction 2 (F2) corresponding to a density > 1.092, containing acanthocytes. (B) The fractionated RBC membrane proteins were separated by 1DE and stained with colloidal Coomassie blue. The bands that were identified by mass spectrometry are indicated: β-spectrin (accession no. P11277), 48% coverage; β-spectrin (accession no. P02549), 52% coverage; band 3 (accession no. P027330), 25% coverage; band 4.1R (accession no. P11171), 22% coverage; band 4.2 (accession no. P16452), 18% coverage; β-actin (accession no. P60709), 26% coverage; GAPDH (accession no. P04406), 18% coverage; and Prx-2 (accession no. P32119), 32% coverage. The figure shows a representative of 9 experiments performed with similar results. (C) Western blot (Wb) analysis of RBC membranes separated by 1DE with specific antibodies against Prx-2, GAPDH, flotillin-1, and stomatin proteins of fractionated RBCs from controls (C) and ChAc subjects. Actin was used as loading control. The data are representative for 8 experiments. (D-E) The membrane proteins of fractionated RBCs (see "Study design") were separated by 2DE. Twin 2DE gels were run: one stained with colloidal Coomassie and the other transferred to membrane for Western blot analysis. (D) The colloidal Coomassie blue–stained gels underwent image analysis, and differently expressed proteins were identified by mass spectrometry (see "Comparative proteomic analysis"; supplemental Methods). Red and green spots indicated the differently expressed proteins based on image analysis. The identified proteins are reported in supplemental Table 2. The figures show 1 representative experiment from a total 8 experiments performed. (E) Western blot (Wb) analysis of the 2DE maps with specific anti–protein p55 antibody on F1 RBCs from control and ChAc subjects (validating the differently expressed spots 32C, 33C, and 34C in panel 1D and supplemental Table 2), anti–flotillin-1 antibody on F1 RBCs from control and ChAc subjects (validating the differently expressed spots 40C in panel D and supplemental Table 2), and anti–protein 4.1R antibody on F2 RBCs from control and ChAc subjects (validating the differently expressed spots 64C-68C in panel D and supplemental Table 2). The figures show one representative experiment of 3 experiments performed with similar results.

relation between lipid content and/or composition and acanthocytosis in ChAc patients.

The recent development of proteomic techniques has yielded a description of RBC membrane proteome, mainly in normal RBCs.[14-18] We used comparative proteomics to study membrane proteome of RBCs from patients with ChAc in relation to normal controls. Differences between normal and ChAc RBCs included changes in Tyr phosphorylation state of band 3, β-spectrin, and other members of the anchoring complexes in ChAc RBCs. We also found abnormal activation of Lyn, a Tyr-kinase of the Src family, independent from its canonical signaling pathway involving primary phosphorylation of Syk. These finding suggest that altered phosphorylation of band 3 and membrane skeletal proteins may play a role in the development of acanthocyte morphology in ChAc.

Methods

Study design

We studied 9 patients with ChAc based on clinical neurologic manifestations, presence of acanthocytes (Figure 1A), and confirmation by either immunoblot analysis for chorein and/or molecular analysis for *VPS13A* mutations as previously described.[6] The demographic and molecular data of patients are reported in Table 1. Blood was obtained by venipuncture using EDTA as an anticoagulant, according to the guidelines approved by the local Ethics Committees for human subject studies of all participating institutions involved. Blood samples (ChAc patients and healthy control donors) were shipped to Verona and Nijmegen at 4°C and processed immediately after arrival. Erythrocytes were isolated from whole blood after removal of white blood cells and platelets as previously described.[19] Because ChAc patients have a dense fraction of RBCs

Table 1. Demographic and molecular data of control and ChAc subjects

	Sex	Age, y	Molecular defect/WB analysis for chorein
Controls (n = 12)	9 females/3 males	35.6 ± 2.3	
ChAc 1	Female	35	Intron 3: c.188–5T > G (splice site); mutation on other allele unknown/ND
ChAc 2	Female	34	ND/chorein absent
ChAc 3	Female	30	Exon 37: c.4286G > C;p.A1428P; intron 55: c.7806G > A;p.P2602P (splice site)/chorein absent
ChAc 4	Female	40	Exon 34: c.3889C > T; p.R1297X; exon 36: c.4216del; p.V1406CfsX20/ND
ChAc 5	Male	47	Intron 22: c.2288 + 2T > C; (splice site mutation); intron 61: c.8472–1G > C; (splice site mutation)/ND
ChAc 6	Female	56	(homozygous) Exon 13: c.1115del; p.K372SfsX2/ND
ChAc 7	Male	32	ND/chorein absent
ChAc 8	Female	38	Intron 6: c.495 + 5G > A (splice site mutation); exon 40: c.4903_4906del; p.K1635VfsX6/ND
ChAc 9	Female	40	ND/chorein absent

WB indicates Western blot; and ND, not determined.

enriched in acanthocytes,[9] we analyzed RBCs separately according to RBC density.

For semiquantitative proteome analyses, we separated the RBCs in 1 of 2 ways. Cells were separated into 5 fractions (I-V) based on volume and density using counter flow centrifugation followed by Percoll gradient centrifugation, with fraction I containing the youngest and fraction V the oldest erythrocytes and acanthocytes. The membrane proteomes of these fractions were analyzed as described previously.[15]

Alternatively, RBCs were separated into 2 fractions: fraction 1 (F1) corresponding to a density < 1.074, containing reticulocytes, and fraction 2 (F2) corresponding to a density > 1.092, containing acanthocytes, for proteomic analysis by 2-dimensional electrophoresis matrix-assisted laser desorption/ionization time-of-flight mass spectrometry, which requires a relatively large amount of proteins for the analysis.[19,20] Where indicated, control RBCs were incubated in the presence of sodium orthovanadate as previously described by Bordin et al.[21]

RBC morphology, membrane preparation, and membrane cytoskeleton extraction

To study cell morphology, RBCs were fixed as previously described by Matte et al[22] and imaged using a Leica TCS SP5 II microscope equipped with an objective HCX PL APO λ blue 63.0×, NA 1.40 oil.

RBC membrane fractions were obtained by lysing 1 volume of packed cells in 10 volumes of ice-cold phosphate lysis buffer (5mM Na_2HPO_4, pH 8.0, in the presence of protease inhibitors, cocktail tablet, Roche Diagnostics; 3mM benzamidine, 1mM Na_3VO_4). Samples were incubated for 10 minutes on ice and centrifuged for 10 minutes at 12 000*g* at 4°C. Membranes were then washed 4 times by centrifugation at 12 000*g* at 4°C with phosphate lysis buffer until they appeared almost white.[15]

To assess the strength of the interaction between cytoskeleton and the lipid bilayer, cytoskeletal proteins were extracted by resuspending membranes (100 μg of total protein) in 1 mL of 100mM Na_2CO_3, pH 11. The suspension was passed 5 times through a 25-gauge needle, mixed and incubated for 30 minutes at 4°C. Soluble proteins were removed by centrifugation for 30 minutes at 200 000*g*. This procedure was repeated twice. Proteins from pelleted membranes were extracted by either detergent or NaCl. Briefly, packed erythrocyte membranes were incubated for 1 hour at 4°C with 50mM Tris-HCl, pH 7.5, 10% glycerol, 1mM sodium orthovanadate, and protease inhibitor cocktail in the absence or the presence of either 1% Triton X-100[22] or 0.6M NaCl. After ultracentrifugation, the supernatants and precipitates were analyzed by 1-dimensional electrophoresis (1DE) and either stained with colloidal Coomassie or transferred to membranes for immunoblot analysis with the appropriate antibody.[22]

Comparative proteomic analysis

Semiquantitative proteomic analysis. All the analyses were performed essentially as previously described.[15] Details are reported in supplemental Methods (available on the *Blood* Web site; see the Supplemental Materials link at the top of the online article). Samples of various origins were quantified by the label-free peptide counting method emPAI, which calculates protein abundance, as has been applied for a quantitative analysis of RBC membranes during storage.[15] Data were normalized using the median emPAI value per sample. This protocol has been shown to result in a reliable identification of all erythrocyte membrane proteins and to enable semiquantification of the major protein species.[15] To be able to apply this method to multiple samples in an efficient and cost-effective manner, we reduced the running time of the SDS-PAGE step and extended the running time of the HPLC gradient from 1.5 to 4 hours. This "one-slice" method yielded 300 to 400 reliably identified proteins, comparable with those found earlier by us and others using one-dimensional as well as 2-dimensional electrophoresis.[15,23,24]

Gel electrophoresis of RBC membrane. For 1DE, RBC membranes were solubilized in sample buffer (50mM Tris, pH 6.8, 100mM β-mercaptoethanol, 2% volume/volume SDS, 10% volume/volume glycerol, a few grains of bromophenol blue), and loaded on to either 8% or 10% polyacrylamide gels. Whenever peroxiredoxin-2 (Prx-2) was evaluated, RBCs were lysed in the presence of NEM (100mM) in the phosphate lysis buffer and solubilized in sample buffer with NEM (100mM).[19,20,22] For 2-dimensional electrophoresis (2DE), RBC membranes were delipidated and separated by 2DE as previously described.[19,20,22] Details are presented in supplemental Methods. After electrophoresis, the gels were stained with colloidal Coomassie followed by image analysis using "Progenesis SameSpots" software (Non Linear Dynamics).[20] Details of image analysis are reported in supplemental Methods. The selected bands or spots were identified by 2DE matrix-assisted laser desorption/ionization time-of-flight mass spectrometry/mass spectrometry analysis (see supplemental Methods for more details).

Immunoblot analysis and dephosphorylation of blotted proteins

Proteins were transferred from 1D or 2D gels to membranes for immunoblot analysis and probed with specific antibodies as previously described[19,20] (see also supplemental Methods for details). Dephosphorylation of blotted proteins was carried out as described in supplemental Methods.

Peptides and recombinant proteins

The phosphopeptide of band 3 (amino acids 1-26) and its unphosphorylated analog were synthesized as described previously.[25] The recombinant GST-Lyn/SH3 domain was expressed and purified according to the protocol described by Trentin et al.[26] The GST-Lyn/SH2 domain was expressed and purified as previously reported.[27]

Phosphorylation of erythrocyte membranes

Erythrocyte membranes (3 μg protein) were phosphorylated for 10 minutes at 30°C in 30 μL of an incubation mixture containing 50mM Tris-HCl, pH

7.5, 10mM $MnCl_2$, 30μM ATP, 200μM sodium orthovanadate, and 15nM of exogenous Lyn Tyr kinase, purified from rat spleen.[27] When required, the phosphorylation assays were carried out in the absence or presence of the GST-Lyn/SH2 domain or the GST-Lyn/SH3 domain, respectively. The solubilized membranes were analyzed by immunoblot with the anti–p-Tyr antibody. The membranes were reprobed with anti–β-actin antibody as a loading control. When indicated, washed RBCs from control and ChAc subjects were incubated with and without the Src family kinase inhibitors PP1 (10μM) and PP2 (10μM) as previously reported.[19,27]

Preparation of Syk-phosphorylated membranes of erythrocytes

Membranes were phosphorylated by 15nM $p36^{Syk}$ for 10 minutes in 50mM Tris-HCl, 10mM $MnCl_2$, 30μM ATP, and 200μM sodium orthovanadate. Syk-phosphorylated membranes were separated from $p36^{Syk}$, ATP, and other reagents by centrifugation and washed twice as previously reported.[27]

Identification of putative phosphorylation targets of Lyn by sequence and structure analyses

The sequences of the different Tyr-phosphorylated proteins were obtained from the NCBI reference sequence database using their accession numbers. They were analyzed by means of the GPS Version 2.0 software to identify putative Lyn target sites.[28] Details are reported in supplemental Methods.

Results

Proteomic analysis of ChAc RBC membranes shows differences compared with membranes from healthy controls

Analysis of ChAc RBC membrane proteins by 1DE followed by protein staining showed that the membrane protein composition of ChAc RBCs was very similar to that of RBCs from healthy controls, except for a band at approximately 20 kDa, which was markedly reduced in the high-density (F2) fraction of RBCs of ChAc patients (Figure 1B). This band was excised from the gel and identified by mass spectrometry as Prx-2. Analysis of the RBC membrane protein composition by comparative semiquantitative proteomic approach showed an enrichment in ChAc RBC membranes for spectrin, ankyrin, and protein 4.2 major component of the ankyrin complex (supplemental Table 1). The concentrations of the raft-associated flotillins did not differ between control and ChAc samples. However, stomatin, another raft-associated protein, was conspicuously enriched in the ChAc samples (supplemental Table 1). The membrane association of GAPDH was variable with an increase in 2 of 3 ChAc patients and a decrease in one ChAc patient (supplemental Table 1). In addition, proteins of the small G protein family were hardly detectable in the control samples but were abundant in the patients' membrane fractions. All membrane samples contained similar amounts of heat shock proteins (data not shown). Immunoblot analysis with specific antibodies confirmed: (1) a reduction of membrane-associated Prx-2 in both low- and high-density fractions of ChAc RBCs compared with controls; (2) an increased membrane association of GAPDH in the high-density fraction of ChAc RBCs that were enriched in acanthocytes compared with normal controls; and (3) a similar membrane content of flotillin 1 in ChAc and control RBCs (Figure 1C).

For a more detailed analysis, we performed 2DE followed by identification of the differently expressed proteins by mass spectrometry. Using a 2-fold abundance as the selection criterion (see "Comparative proteomic analysis"), we detected 50 spots that were differently expressed in high-density fraction (F2) of ChAc RBCs and 41 spots differently expressed in low-density fraction (F1) of ChAc RBCs (Figure 1D; supplemental Table 2). It is to be noted that our protein identifications are in strong accordance with previously published 2DE maps of RBC membrane.[14,20] The identified proteins were divided into 8 functional clusters: I, proteins of the anchoring complexes; II, cytoskeleton proteins; III, raft-related proteins; IV, membrane channels and transporters; V, intracellular signaling proteins; VI, metabolic enzymes; VII, proteins of the ubiquitin-proteasome system; and VIII, stress response proteins and chaperones.[20] We validated the 2DE data by immunoblot analysis of some of the identified proteins: protein p55 in F1 fractionated RBCs, flotillin-1 in F1 fractionated RBCs, and protein 4.1 in F2 fractionated RBCs (Figure 1E). The differences in membrane and cytoskeleton proteins in ChAc RBC observed in 2DE maps were mainly related to protein 2DE mobility shift, possibly reflecting protein post-translational modifications, such as phosphorylation (Figure 1D-E; supplemental Table 2). This is also supported by the similar abundance of membrane and cytoskeleton proteins in 1DE analysis of ChAc and control RBC membranes (Figure 1B).

Differential extraction of membrane proteins reveals differences in membrane organization in ChAc RBCs

To explore putative ChAc-associated changes in membrane organization, we assessed the strength of binding of the major erythrocyte membrane and cytoskeletal proteins to the lipid bilayer by analyzing the proteome after incubation of the membrane fractions with 100mM Na_2CO_3, pH 11 (see "RBC morphology, membrane preparation, and membrane cytoskeleton extraction"). In controls, this alkaline treatment led to the virtual disappearance of most cytoskeletal and membrane-associated proteins, such as spectrin, ankyrin, and GAPDH. This was accompanied by enrichment of most integral membrane proteins, including band 3 and Glut1, and by a large increase in the concentration of stomatin (supplemental Table 3). The loss of GPC, but not GPA, suggests that a considerable fraction of the GPC molecules is extracted together with the cytoskeleton. As in control samples, extraction of ChAc membranes resulted in the depletion of the same proteins as seen in normal membranes and also in enrichment for most integral membrane proteins with band 3 as a notable exception (supplemental Table 3).

Because recent studies have suggested that changes in membrane protein phosphorylation state play an important role in the modulation of RBC membrane protein-protein functional cross-talk and stability of multiprotein structures,[29,30] we studied the Tyr phosphorylation profile of RBC membrane from control and ChAc subjects.

The Tyr-phosphorylation state of ChAc RBC membrane proteins is increased compared with normal controls

Evaluation of the Tyr phosphorylation pattern of RBC membranes from normal and ChAc density-separated RBCs by immunoblot analysis showed a higher Tyr phosphorylation state of various membrane proteins in ChAc RBCs (Figure 2).

The 2DE Tyr-phospho maps confirmed the presence of trains of Tyr-phosphorylated proteins in the gel area corresponding to the differently expressed spots noted in 2DE maps: ankyrin (17-18C in F1 and 54C-57C and 60C-62C in F2 from ChAc RBCs), protein 4.1R (21C, 23C, 25 C in F1 and 64C-68C in F2 from ChAc RBCs), protein p55 (32C-34C in F1 from ChC RBCs) and dematin (88C-89C in F2 from ChAc RBCs; Figure 1D; supplemental Table 2). These data are also supported by the absence of reactivity when

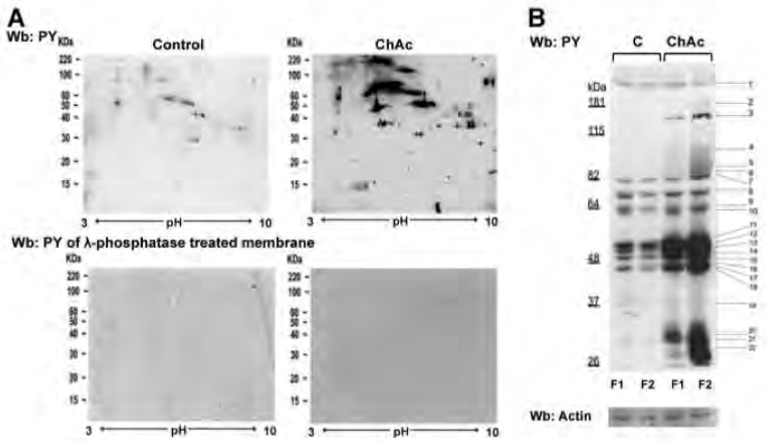

Figure 2. Tyr phosphorylation of RBC membrane protein is increased in ChAc compared with normal controls. RBCs from control (C) and ChAc subjects were fractionated as described in "Study design" and in the legend of Figure 1B-E. Western blot (Wb) analysis with specific anti–phosphotyrosine (PY) antibodies of RBC membrane proteins separated by either bidimensional electrophoresis (2DE) or monodimensional electrophoresis (1DE). (A) Twin 2DE gels were run: one used for colloidal Coomassie-stained gels (Figure 1D) and the other for the Western blot analysis with specific anti–phosphotyrosine (PY) antibodies. Top panel: Membranes of high-density RBC fraction (F2) from control (C) and ChAc subjects. Similar results were also obtained in low-density RBC fraction (F1) from control and ChAc (data not shown). Bottom panel: Dephosphorylation of blotted proteins by recombinant λ protein phosphatase (400 U/mL). The blotted membranes were incubated in TBS containing 1% BSA, 0.1% Triton X-100, 2mM $MnCl_2$ (overnight at 4°C), and then probed with anti–phosphotyrosine antibodies. The data are representative for 3 experiments with similar results. (B) 1DE gels (13 cm) were blotted for Western blot (Wb) analysis with specific anti–phosphotyrosine (PY) antibodies. The bands with different staining intensities were identified by mass spectrometry (Table 2; "Comparative proteomic analysis"; supplemental Methods). Actin was used as a loading control. The data are representative of 8 experiments. See also supplemental Figure 1B for densitometric analysis of the Tyr phosphorylation profile of the RBC membrane proteins.

the membranes were treated with λ-phosphatase, which was used to remove phosphate groups from blotted proteins (Figure 2A bottom panel). The differently Tyr-phosphorylated proteins were excised from the 1D-stained gels and identified by mass spectrometry (Figure 2B). According to their functions, the identified proteins were divided into 8 functional clusters: I, membrane protein, band 3; II, cytoskeleton network proteins β-spectrin and β-actin; III, ankyrin complex proteins, ankyrin, band 4.2; IV, membrane junctional complex proteins, band 4.1, p55, β-adducin; V, intracellular signaling protein; VI, metabolic enzymes, such as GAPDH; VII, stress response proteins, such as catalase; and VIII cell trafficking protein, such as Ras-related proteins (Table 2). Of note, we found a Tyr-phosphorylated β-spectrin fragment in both F1 and F2 fractions from ChAc patients, and we identified a phosphopeptide of β-adducin (R.MLDNLGYR.T) in the dense RBC fraction from ChAc subjects (Table 2). These results

Table 2. Proteins with different degrees of Tyr phosphorylation in RBC membranes from control and ChAc subjects

Band no.	AC	Protein	Theoretical protein MW, kDa	Matching peptide	Coverage, %
1	P11277	β-spectrin (SPTB1)	246.468	146	50
2	P16157	Ankyrin (ANK1)	206.265	20	22
3	Q8WX82	β-I Spectrin form β I α 3 (fragment; Q8WX82)	117.549	14	20
4	P02730	Band 3 anion transport protein (B3AT)	101.792	16	18
5	P02730	Band 3 anion transport protein (B3AT)	101.792	23	24
6	Q9H4B4	Serine threonine protein kinase PLK3 (PLK3)	71.629	6	8
7	P35612	β-adducin (ADDB)	80.854	9	11
8	P11171	Band 4.1 (EPB41)	97.017	10	24
9	P16452	Band 4.2 (EPB42)	77.009	9	12
10	Q9H4B4	Serine threonine protein kinase PLK3 (PLK3)	71.629	6	11
11	Q00013	55-kDa erythrocyte membrane protein (EM55)	52.296	19	34
12	Q00013	55-kDa erythrocyte membrane protein (EM55)	52.296	6	18
13	P47895	Aldehyde dehydrogenase family 1 member A3 (AL1A3)	56.108	3	6
14	P04040	Catalase (CATA)	59.756	4	9
15	O94921	Serine threonine protein kinase PFTAIRE-1 (CDK14)	53.057	5	10
16	Q14012	Calcium calmodulin-dependent protein kinase type 1 (KCC1A)	41.337	4	10
17	P60709	β-actin (ACTB)	41.737	10	34
18	Q96GD4	Serine threonine protein kinase 12 (AURKB)	39.311	4	15
19	P04406	Glyceraldehyde-3-P-dehydrogenase (G3P)	36.053	9	36
20	P27105	Stomatin (STOM)	31.731	10	40
21	P00918	Carbonic anhydrase 2 (CAH2)	29.246	3	11
22	Q96E17	Ras-related protein Rab-3C (RAB3C)	25.952	3	17

The corresponding bands are indicated in Figure 2B. The success rate of protein identification by matrix-assisted laser desorption/ionization time-of-flight mass spectrometry/mass spectrometry was 82% ± 6.7% (n = 9).

AC indicates accession number; and MW, molecular weight.

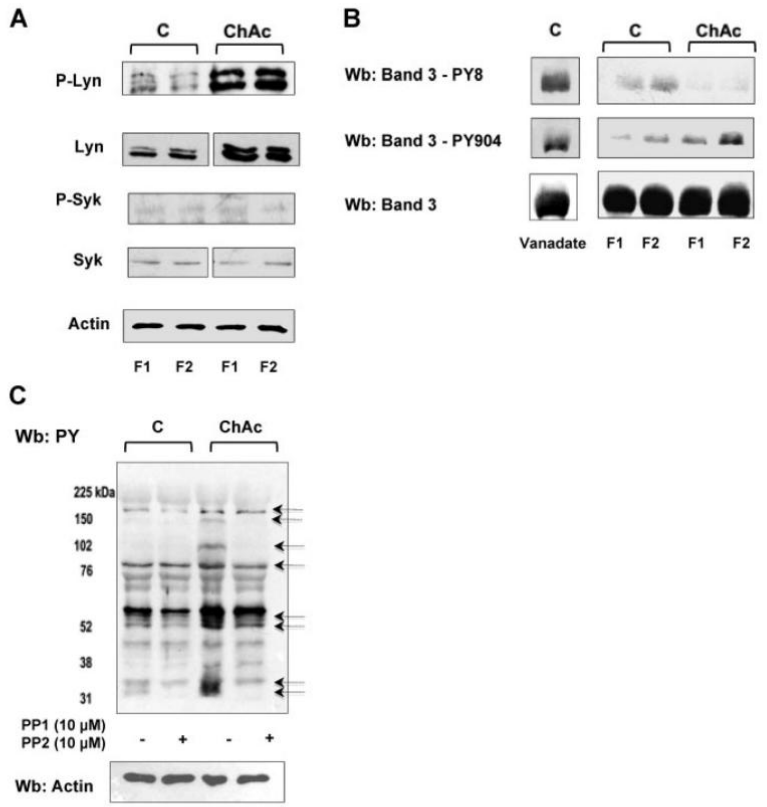

Figure 3. ChAc RBCs show increased Lyn Tyr kinase associated with the membrane. RBCs from control (C) and ChAc were fractionated as described in "Study design" and in the legend of Figure 1B-E. (A) Western blot analysis with specific antibodies of membrane-associated Tyr kinase Lyn and phospho-Lyn (p-Lyn), Syk, and phospho-Syk (p-Syk). Actin was used as a loading control. Shown is a representative of 6 experiments. Vertical line(s) have been inserted to indicate a repositioned gel lane. (B) Western blot (Wb) analysis with specific antibodies against Tyr-8 on the N-terminal of band 3, as a Syk target, and Tyr-904 on the transmembrane domain of band 3 (as a Lyn target). We used normal RBCs treated with Na-vanadate (see "Study design") as positive controls. Total band 3 was used as loading control. (C) Western blot (Wb) analysis with specific anti–phosphotyrosine (PY) antibodies of high-density fraction (F2) of RBCs from control (C) and ChAc subjects are shown. The F2 RBCs were incubated with or without the Src family kinase inhibitors PP1 (10μM) and PP2 (10μM) as previously reported.[19] The arrows indicated the bands affected by PP1-PP2 treatment in ChAc RBCs compared with untreated ChAc RBCs. The data are representative of 3 experiments (on 6-cm gels). Actin was used as a loading control. The data are representative of 3 experiments. Similar results were also obtained with cells from low density fraction (F1) control and ChAc RBCs (data not shown).

suggest that altered phosphorylation may contribute to acanthocytosis in ChAc.

Lyn is abnormally activated in ChAc RBCs and is independent from Syk sequential phosphorylation

Because Tyr-kinase Syk and the Src family kinase Lyn have been described as being involved in modulating band 3 function in healthy RBCs,[27] we studied membrane association of Syk and Lyn in control and ChAc erythrocytes.

In both F1 and F2 RBCs from ChAc patients, we observed an increased membrane association of active Lyn (phospho-Lyn, Figure 3A). In contrast, the amount of membrane-bound total and active Syk (phospho-Syk) was almost undetectable in ChAc and barely detectable in control RBCs (Figure 3A). We previously reported a sequential phosphorylation of band 3 catalyzed by the concerted action of Syk and Lyn, with Tyr-8 and Tyr-21 being first targeted by Syk and thereby serving as docking sites for the Src homology domain 2 (SH2) of Lyn. Lyn, once recruited, phosphorylates Tyr-359 and Tyr-904 of band 3[27] as well as other proteins, such as spectrins and adducin (unpublished data).

We used specific antibodies against Tyr-8 on the N-terminal of band 3, as a Syk target, and Tyr-904 on the transmembrane domain of band 3, as a Lyn target. We found increased Tyr phosphorylation at Tyr-904 compared with normal RBCs (Figure 3B). Phosphorylation of residue Tyr-8 was almost absent in both fractions from ChAc RBCs and only slightly detectable in normal RBCs. Since we have previously reported that activated Syk might be present in the cytoplasm in a truncated form,[21] we evaluated Syk activity in the cytoplasm. Syk activity was similar in the cytoplasm of normal and ChAc RBCs (data not shown), suggesting a peculiar membrane recruitment of Lyn to ChAc membranes that occurs independent of preceding phosphorylation of band 3 by Syk.

To evaluate whether the Tyr-phospho profile of ChAc RBC membrane might be affected by in vitro Lyn inhibition, we incubated control and ChAc RBCs with both PP1 and PP2, Src family kinase inhibitors, to obtain a more stable inhibition of kinase activity. As shown in Figure 3C, in ChAc RBCs the PP1/PP2 treatment markedly reduced Tyr-phosphorylation state of several bands, including band 3, thus supporting the role of Src kinase as determinant of the peculiar ChAc RBC membrane Tyr-phosphorylation profile.

Because the amount of Lyn was markedly higher in ChAc erythrocytes than in control RBCs, we characterized Lyn RBC membrane association. Lyn was almost entirely solubilized by the treatment with Triton-X 100 in both control and ChAc RBCs (Figure 4A lanes 2 and 3 and lanes 7 and 8). However, treatment with high ionic strength medium (0.6M NaCl, see "Study design") resulted in remarkably increased extraction of Lyn from ChAc RBC membranes compared with that from membranes of control cells, accounting for the increased Lyn concentration (Figure 4A lanes 4 and 5 vs lanes 9 and 10). These data suggest there are several pools of Lyn in ChAc RBCs, which associate with the membrane by multiple modes. This is corroborated by the observation that a fraction of Lyn was released from ChAc RBC membranes by agents capable of disrupting the SH2 domain/phospho-Tyr interaction, such as GST-Lyn/SH2 and the phosphorylated NH2 terminus of band 3 (Figure 4B).

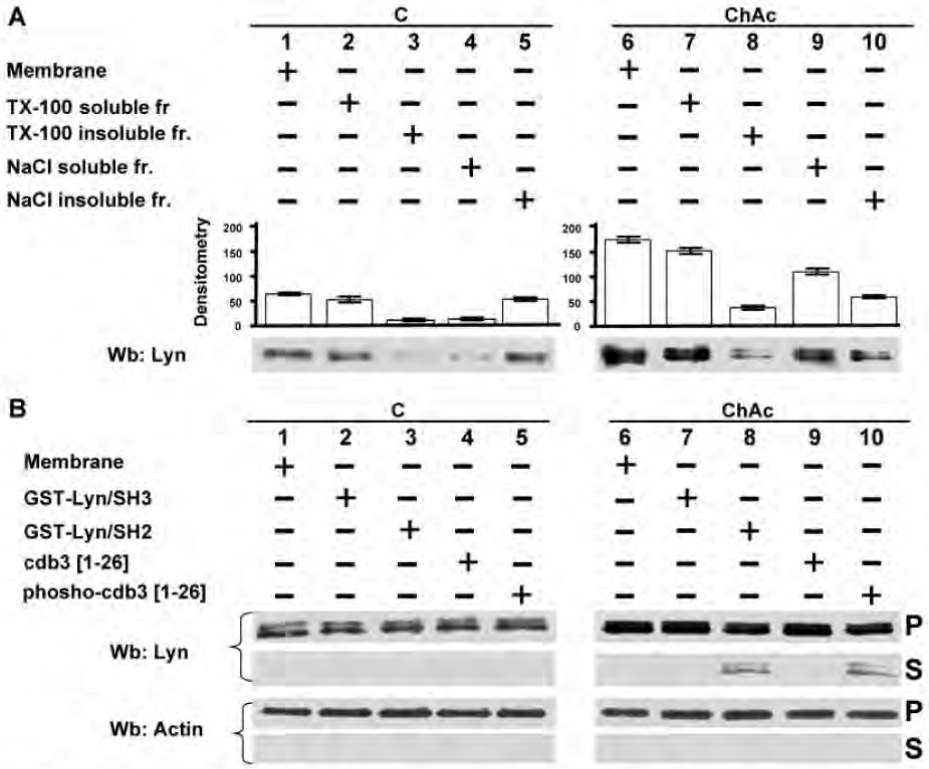

Figure 4. Modes of interaction of Lyn with membranes from ChAc RBCs. (A) Membranes of F2 RBCs from control (C) and ChAc subjects were extracted with Triton X-100 or NaCl (see "RBC morphology, membrane preparation, and membrane cytoskeleton extraction") and assayed after ultracentrifugation for the presence of Lyn by Western blot (Wb) analysis. The data shown here are obtained with F2 ChAc RBCs. Similar data were obtained with F1 control and ChAc RBCs (data not shown). (B) Membranes of F2 RBCs from control (C) and ChAc subjects were incubated in the presence or absence of GST-Lyn/SH3, GST-Lyn/SH2, cdb3, or phospho (p)–cdb3 and assayed after ultracentrifugation for Lyn in the resulting soluble (S) and pellet (P) fractions for the presence of Lyn by Western blot (Wb) analysis. Similar data were obtained from F1 control and ChAc RBCs (data not shown). The membranes were reprobed with anti–actin antibody as loading control.

Exogenous Lyn phosphorylates several targets in ChAC RBC membrane independent of Syk

We then evaluated whether in ChAc RBCs the ability of Lyn to phosphorylate RBC membrane proteins in vitro was still dependent on a Syk-related mechanism. Preparations from control and ChAc RBC membranes were washed free of the phosphatase inhibitor vanadate and resealed with exogenous Lyn in the presence and absence of GST-Lyn/SH2 and GST-Lyn/SH3 domains. Exogenous Lyn was shown to phosphorylate ChAc membrane proteins much more efficiently than control fractions (Figure 5). In addition, the Tyr phosphorylation profile remained unaltered in the presence of the GST-Lyn/SH3 domain, with only a slight decrease when the GST-Lyn/SH2 domain was added (Figure 5). These data indicate that the ability of Lyn to Tyr-phosphorylate ChAc membrane proteins is not dependent on a preceding membrane binding and activity of Syk as previously reported for control RBCs.[27] Thus, ChAc-associated alterations in the membrane protein organization may allow Lyn to target its substrates independently from Syk. Interestingly, exogenous Lyn promotes Tyr phosphorylation of membrane proteins other than band 3, similarly to that observed in the naturally occurring Tyr phosphorylation profile of ChAc RBC membranes (Figures 3A and 5). It is of note that in vitro phosphorylation of ChAc RBC membrane by exogenous Lyn involved a smaller number of proteins (bands) at molecular weights lower than 48 kDa compared with intact ChAc RBCs. Otherwise, these proteins showed reduced Tyr phosphorylation in PP1/PP2-treated ChAc RBCs, suggesting that Lyn might be also part of other signaling pathways involving other kinases or play a role as downstream regulator of phosphatase(s) similarly to what we previously described in other RBC models.[31,32]

Bioinformatic analysis of the differentially Tyr-phosphorylated proteins reveals Lyn targets in ChAc RBCs

To evaluate the presence of possible Lyn targets on ChAc RBC membrane proteins differentially Tyr-phosphorylated, we carried out an extensive bioinformatic analysis of putative Lyn target sites in the Tyr-phosphorylated proteins identified. This analysis reveals that approximately 75% of the proteins have at least one highly Lyn-selective site (Table 3). Only 3 of them (aldehyde dehydrogenase, carbonic anhydrase, and glyceraldehyde dehydrogenase) show low specificity and 2 (stomatin and rab) an even lower specificity for Lyn, with increased specificity for other Src kinase members (data not shown). Because we found a highly phosphorylated β-spectrin peptide in the proteomic analysis and also identified a β-adducin phosphopeptide, we carried out a sequence structure analysis of β-spectrin or β-adducin to further characterize the Lyn targets in these 2 proteins. The analysis of the sequence of β-spectrin for Lyn-directed peptides with a high threshold score more than 2.4 identified 5 peptides (Table 3). An intercrossed search to identify whether these peptides could also serve as substrates for Src Tyr kinases restricted the Lyn-specific target

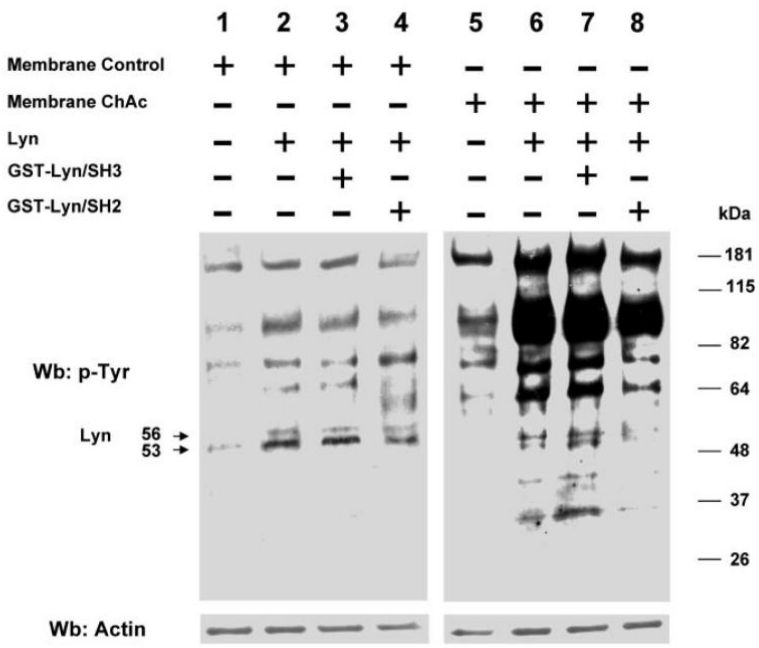

Figure 5. Phosphorylation patterns of normal and ChAc RBC membranes by exogenous Lyn. Membranes of high-density fraction (F2) of RBCs from control (C) and ChAc subjects were incubated without (lanes 1 and 5) or with exogenous Lyn (lanes 2-4 and 6-8) and with GST-Lyn/SH3 (lanes 3 and 7) or GST-Lyn/SH2 (lanes 4 and 8), respectively. Samples were then analyzed by Western blot (Wb) analysis with anti–phosphotyrosine antibodies. Similar data were obtained with F1 control and ChAc RBCs (data not shown). The membranes were reprobed with anti–actin antibody as loading control.

sequences to 2 Tyr residues Tyr-307 and Tyr-1590. Inspection of the 3D structure indicated that the Tyr-307 is located inside the triple-helical bundle, whereas Tyr-1590 is in the linker region preceding repeat 14, at the interface of the ankyrin binding domain (repeats 14 and 15)[33-35] (Table 3). The phosphopeptide of β-adducin (Tyr-377) is a specific target of Lyn with little specificity for Src (Table 3) and is located in a highly conserved sequence of the neck domain of the protein.[36]

Lyn-mediated phosphorylation of ChAc membranes alters the interaction of band 3 with β-adducin

We then evaluated the role of Lyn-dependent phosphorylation of band 3 in the interaction with β-adducin in ChAc RBCs compared with normal erythrocytes. We first phosphorylated band 3 by exogenous Syk with or without exogenous Lyn using normal RBC membranes and then extracted by Triton-X (Figure 6A). The immunoprecipitated band 3 from the resulting extract was further subjected to immunoblot analysis with anti–adducin antibody. As shown in Figure 6B, in control erythrocytes the presence of β-adducin in the band 3 immunoprecipitate was dramatically decreased only if the membranes were sequentially phosphorylated by Syk and Lyn. Because in ChAc RBCs we have shown band 3 Tyr-phosphorylated by Lyn independently from Syk phosphorylation, we immunoprecipitated band 3 from ChAc extracts, and we observed a small amount of β-adducin coimmunoprecipitated. This increased further when membranes were incubated in the presence of the Src kinase inhibitor PP2, suggesting that the altered Lyn activity was implicated in the mechanism of association between band 3 and β-adducin in ChAc RBCs.

Discussion

An integrated proteomic approach enabled us to analyze the perturbation of membrane protein organization in ChAc RBCs at the molecular level. Our analysis indicated that this membrane perturbation mainly affects the multiprotein complexes that anchor the cytoskeleton to the membrane through band 3. The ChAc-related alterations in the membrane association of GAPDH and hemoglobin also suggest a perturbation of their binding sites on band 3. These observations are in agreement with the reduction in association of Prx-2 with the membrane, which may be the result of unavailability of the Prx-2 docking site on band 3, as has also been reported in β-thalassemic RBCs.[22] These data confirm and extend previous observations of neuroacanthocytosis-associated alterations on band 3[10] and extend these to ChAc-specific alterations in band 3 function.

Previous studies have shown that the Tyr phosphorylation state of RBC membrane proteins is involved in regulation of membrane cohesion and mechanical stability.[29] Accordingly, we found that several membrane proteins are highly Tyr-phosphorylated in ChAc RBCs compared with controls. These proteins are band 3 and other components of the 2 anchoring complexes. Because band 3 is part of both complexes, these findings suggest that phosphorylation-induced perturbation of protein-protein interactions may be centered on band 3. Changes in the protein phosphorylation state can modify protein-protein interactions and thereby multiprotein complex formation and/or functions.[37,38]

Previous studies documented that the Syk-Lyn signaling pathway working in concert can modify band 3 function in healthy RBCs.[27] It is noteworthy that we found increased association of active Lyn with the ChAc membranes in the absence of Syk. This is surprising because Syk is responsible for the primary Tyr phosphorylation of band 3 that precedes membrane recruitment of Lyn in normal RBCs.[27] In ChAc membranes, the membrane-associated form of Lyn was normally solubilized by detergent but differentially partitioned by ionic strength extraction. These data point toward a contribution of electrostatic interactions in Lyn binding and suggest the existence of different pools of Lyn associated with the membrane. A small amount of Lyn was displaced from the

Table 3. Bioinformatic analysis of the differently Tyr-phosphorylated proteins identified in ChAc RBCs

Band no.	AC	Protein	Lyn-target	Score
1	P11277	β-spectrin (SPTB1)	Y-307*	2.447
			Y-474	3.596
			Y-493	3.383
			Y-660	4.128
			Y-1590*	3
2	P16157	Ankyrin (ANK1)	Y-884	3.83
			Y-1468	2.362
			Y-1750	2.447
3	Q8WX82	β-I spectrin form β I σ 3 (fragment) (Q8WX82)	Y-307*	2.447
			Y-474	3.596
			Y-493	3.383
			Y-660	4.128
			Y-1590*	3
4	P027330	Band 3 anion transport protein (B3AT)	Y-8	8.809
			Y-21	6.553
			Y-46	4.149
			Y-359	4.702
			Y-904	5.915
5	P027330	Band 3 anion transport protein (B3AT)	Y-8	8.809
			Y-21	6.553
			Y-46	4.149
			Y-359	4.702
			Y-904	5.915
6	Q9H4B4	Serine threonine protein kinase PLK3 (PLK3)	Y-136	2.383
7	P35612	β-adducin (ADDB)	Y-377*	0.66
8	P11171	Band 4.1 (EPB41)	Y-374	2.489
9	P16452	Band 4.2 (EPB42)	Y-435	2.085
10	Q9H4B4	Serine threonine protein kinase PLK3 (PLK3)	Y-136	2.383
11	Q00013	55-kDa erythrocyte membrane protein (EM55)	Y-331	2.468
			Y-429	2.83
12	Q00013	55-kDa erythrocyte membrane protein (EM55)	Y-331	2.468
			Y-429	2.83
13	P47895	Aldehyde dehydrogenase family 1 member A3 (AL1A3)	Y-497	1.683†
14	P04040	Catalase (CATA)	Y-260	1.809
15	O94921	Serine threonine protein kinase PFTAIRE-1 (CDK14	Y-135	4.17
16	Q14012	Calcium calmodulin-dependent protein kinase type 1 (KCC1A)	Y-20	2.872
			Y-235	2.723
17	P60709	β-actin (ACTB)	Y-240	2.702
18	Q96GD4	Serine threonine protein kinase 12 (AURKB)	Y-8	2.319
19	P04406	Glyceraldehyde-3-P-dehydrogenase (G3P)	Y-255	1.66†
20	P27105	Stomatin (STOM)	Y-60	0.213‡
			Y-123	0.404‡
			Y-124	0.234‡
			Y-252	0.426‡
21	P00918	Carbonic anhydrase 2 (CAH2)	Y-40	1.511†
			Y-51	1.745†
			Y-114	1.681†
22	Q96E17	Ras related protein Rab-3C (RAB3C)	Y-17	0.809‡
			Y-29	0.383‡
			Y-50	0.298‡
			Y-92	0.638‡
			Y-99	0.596‡
			Y-100	0.638‡
			Y-110	0.191‡
			Y-131	0.234‡

*Identified phosphopeptides of β-spectrin and β-adducin.
†Low threshold analysis.
‡Very low threshold analysis.

ChAc membrane by the addition of GST-Lyn/SH2 or the phosphorylated cytoplasmic domain of band 3. This suggests the unmasking of the Lyn domain on band 3, which allows Lyn to bind independently from the action of Syk. The conspicuous increase in Tyr phosphorylation state of ChAc RBC membrane proteins by exogenous Lyn supports this hypothesis.

Bioinformatic analyses show that in large part the differentially Tyr-phosphorylated proteins identified in ChAc indeed contain

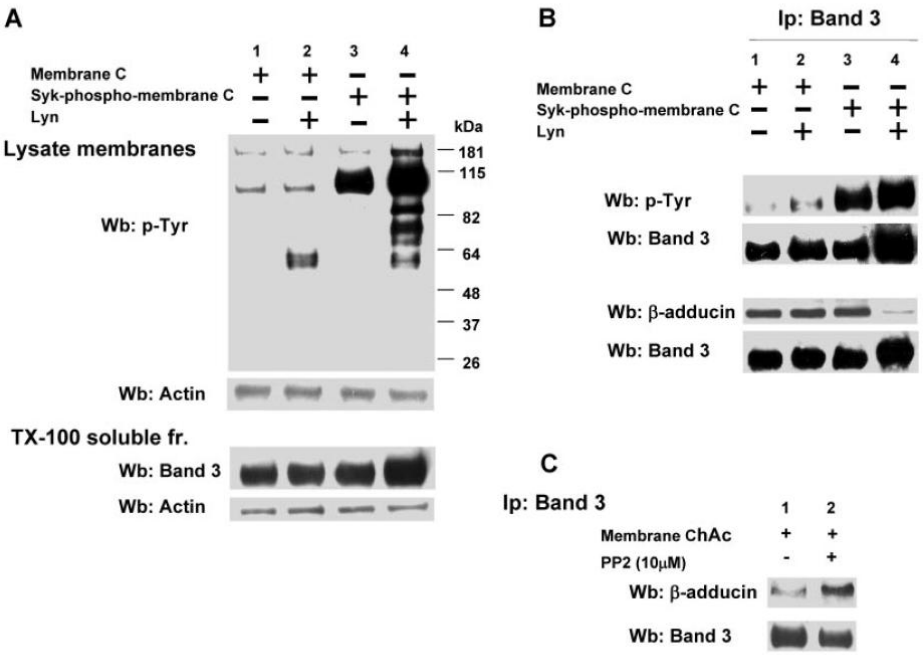

Figure 6. Effect of phosphorylation of RBC membranes by Syk and/or Lyn on band 3 binding to β-adducin in normal and ChAc RBC membranes. (A) Membranes (lanes 1 and 2) or Syk-phospho-membranes (lanes 3 and 4) of F2 RBCs from control (C) were incubated without (lanes 1 and 3) or with exogenous Lyn (lanes 2 and 4) and subjected to Western blot analysis with anti–phospho-Tyr (anti–pTyr) antibody (top panel) or were extracted with Triton X-100 and assayed after ultracentrifugation for the presence of band 3 by Western blot analysis (bottom panel). The membranes were reprobed with anti–actin antibody as loading control. (B) Band 3 was immunoprecipitated from membranes (lanes 1 and 2) and Syk-phospho-membranes (lanes 3 and 4) of F2 RBCs from C after incubation without (lanes 1 and 3) or with exogenous Lyn (lanes 2 and 4). The immunoprecipitates were subjected to Western blot analysis with anti–pTyr (top panel), anti–β-adducin antibody. The blots were also probed with anti–band 3 antibody. (C) Band 3 was immunoprecipitated from membranes of F2 ChAc RBCs previously incubated without or with the inhibitor PP2 (10μM). The immunoprecipitates were subjected to Western blot analysis with anti–β-adducin antibody. The blots were also probed with anti–band 3 antibody. The figure is representative of 3 independent experiments.

Lyn-specific targets or putative Src kinase family substrates. In addition, the sequence-structure study allowed us to propose specific Lyn phosphorylation sites on β-adducin and β-spectrin, supporting the multitarget action of abnormally activated Lyn in ChAc RBCs. Notably, Tyr-377 of β-adducin, which is phosphorylated in ChAc RBCs, is highly conserved.[36] This residue is located in the neck region that is involved in association of adducin monomers to heterodimers, thereby constituting the functionally active form of the protein. This conserved sequence in the neck region of adducin is also involved in the organization of an amphiphilic structure, which is important in mediating protein-protein interactions.[39] In ChAc RBCs, β-adducin was coimmunoprecipitated with band 3 only in the presence of the Src kinase inhibitor PP2, whereas in control erythrocytes there was a requirement for sequential Syk-Lyn band 3 phosphorylation. Thus, changes in the Tyr phosphorylation state of β-adducin in this region probably affect its interactions with the other proteins of the junctional complexes and thereby the stability of the RBC membrane protein bridges.

Our data suggest a novel mechanism in generation of acanthocytes in ChAc in addition to those reported in McLeod syndrome, a neuroacanthocytosis-related disorder, and in abetalipoproteinemia. In these diseases, acanthocytes formation has been related to either the absence of the XK membrane protein convalently linked to the Kell glycoprotein and part of the multiprotein 4.1 juctional complex as in McLeod syndrome or to the abnormal membrane lipid composition (increased sphingomielin/lecithin ratio) with abnormalities of lipid-lipid interaction within membrane as in abetaliproteinemia.[40,41] In ChAc RBCs, there is no indication of abnormalities in either membrane lipid composition or membrane and cytoskeletal protein content. We did, however, find alterations in Tyr-phosphorylation state of membrane proteins and in the signal transduction pathway. Thus, we propose that in ChAc RBCs the "Lyn storm" might affect the organization of the complexes bridging the membrane to the cytoskeleton, most likely by inducing abnormal protein interactions through the opening of SH2 binding sites in a Syk-independent manner. This might result in the heterogeneous distribution of the cytoskeleton as observed in electron microscopy studies,[8] and may be similar to the concentration of Lyn in plasma membrane patches of activated platelets, adjacent to granules.[42,43] In addition, abnormal Lyn phosphorylation might also contribute to altered vesiculation of ChAc RBCs. Lyn has been found in association with the exosomes that are excreted by reticulocytes, containing lipid raft domains, and in vesicles from mature RBCs.[44-46] Together with the indication for a stomatin-specific, raft-based process in vesicle formation in vitro,[47] this supports the hypothesis that vesicle formation is an important, active process in the formation of acanthocytes. This is in agreement with increased concentrations in ChAc RBC membranes of various small G-proteins involved in vesicle formation and transport.[10]

In conclusion, our data link, for the first time, the presence of abnormal RBCs in patients with ChAC with evidence for an independent and strong Lyn activation. The ChAc-associated alterations in RBC membrane-protein organization appear to be the result of increased Tyr phosphorylation leading to altered linkage

of band 3 to the junctional complexes involved in anchoring the membrane to the cytoskeleton. The latter may promote an increased degree of freedom of the junctional complexes bridging the membrane to the cytoskeleton and affect the association of the cytoskeleton with the plasma membrane. The present data open new ways to explore the pathobiology of acanthocytes and pathophysiologic mechanisms of neurodegeneration in patients with neuroacanthocytosis.

Acknowledgments

This work was supported by the Advocacy for Neuroacanthocytosis Patients (B.B., P.H.B.-G., E.L., G.J.C.G.M.B., and L.D.F.), Carl H. and Elizabeth S. Pforzheimer III, New York (B.B., P.H.B.-G., E.L., G.J.C.G.M.B., and R.H.W.), Ginger and Glenn Irvine, London (P.B., E.L., and G.J.C.G.M.B.) and Telethon (grant GPP07007, L.D.F.). Preliminary data were generated by Dr Christan Pozzobon.

Authorship

Contribution: L.D.F. and G.J.C.G.M.B. designed the experiments and analyzed the data; N.M. designed the study and wrote the manuscript; C.T., L.D.F., G.J.C.G.M.B., P.H.B.-G., A.S., and A.M. performed the experiments; M.B. performed the protein structure analysis and wrote the manuscript; A.M.B. and E.T. performed part of the Lyn analysis, analyzed the data, and wrote the manuscript; A.D., R.H.W., H.H.J., and B.B. performed neurologic diagnosis; A.D., B.B., R.H.W., and H.H.J. provided blood samples and confirmed diagnosis; E.F. performed part of the analysis by mass spectrometry; E.L. and C.T. performed bioinformatic analysis of the proteomic data; and all authors reviewed the manuscript.

Conflict-of-interest disclosure: The authors declare no competing financial interests.

Correspondence: Lucia De Franceschi, Department of Medicine, University of Verona, P.le L Scuro, 10, 37134 Verona, Italy; e-mail: lucia.defranceschi@univr.it.

References

1. Danek A, Jung HH, Melone MA, Rampoldi L, Broccoli V, Walker RH. Neuroacanthocytosis: new developments in a neglected group of dementing disorders. *J Neurol Sci.* 2005;229–230: 171-186.
2. Danek A, Walker RH. Neuroacanthocytosis. *Curr Opin Neurol.* 2005;18(4):386-392.
3. Jung HH, Danek A, Frey BM. McLeod syndrome: a neurohaematological disorder. *Vox Sang.* 2007; 93(2):112-121.
4. Rampoldi L, Danek A, Monaco AP. Clinical features and molecular bases of neuroacanthocytosis. *J Mol Med.* 2002;80(8):475-491.
5. Velayos-Baeza A, Levecque C, Dobson-Stone C, Monaco AP. The function of chorein. In: Walker RH, Saiki S, Danek A, eds. *Neuro-acanthocytosis Syndromes II.* Berlin, Germany: Springer-Verlag; 2008:87-105.
6. Dobson-Stone C, Velayos-Baeza A, Filippone LA, et al. Chorein detection for the diagnosis of chorea-acanthocytosis. *Ann Neurol.* 2004;56(2):299-302.
7. Mohandas N, Gallagher PG. Red cell membrane: past, present, and future. *Blood.* 2008;112(10): 3939-3948.
8. Terada N, Fujii Y, Ueda H, et al. Ultrastructural changes of erythrocyte membrane skeletons in chorea-acanthocytosis and McLeod syndrome revealed by the quick-freezing and deep-etching method. *Acta Haematol.* 1999;101(1):25-31.
9. Clark MR, Aminoff MJ, Chiu DT, Kuypers FA, Friend DS. Red cell deformability and lipid composition in two forms of acanthocytosis: enrichment of acanthocytic populations by density gradient centrifugation. *J Lab Clin Med.* 1989;113(4): 469-481.
10. Bosman GJCGM, de Franceschi L. Neuroacanthocytosis-related changes in erythrocyte membrane organization and function. In: Walker RH, Saiki S, Danek A, eds. *Neuroacanthocytosis syndromes II.* Berlin, Germany: Springer; 2008.
11. Olivieri O, De Franceschi L, Bordin L, et al. Increased membrane protein phosphorylation and anion transport activity in chorea-acanthocytosis. *Haematologica.* 1997;82(6):648-653.
12. Murthy SN, Wilson J, Zhang Y, Lorand L. Residue Gln-30 of human erythrocyte anion transporter is a prime site for reaction with intrinsic transglutaminase. *J Biol Chem.* 1994;269(36):22907-22911.
13. Melone MA, Di Fede G, Peluso G, et al. Abnormal accumulation of tTGase products in muscle and erythrocytes of chorea-acanthocytosis patients. *J Neuropathol Exp Neurol.* 2002;61(10):841-848.
14. Pasini EM, Kirkegaard M, Mortensen P, Lutz HU, Thomas AW, Mann M. In-depth analysis of the membrane and cytosolic proteome of red blood cells. *Blood.* 2006;108(3):791-801.
15. Bosman GJ, Lasonder E, Luten M, et al. The proteome of red cell membranes and vesicles during storage in blood bank conditions. *Transfusion.* 2008;48(5):827-835.
16. Bosman GJ, Willekens FL, Werre JM. Erythrocyte aging: a more than superficial resemblance to apoptosis? *Cell Physiol Biochem.* 2005;16(1):1-8.
17. Pasini EM, Lutz HU, Mann M, Thomas AW. Red blood cell (RBC) membrane proteomics: II. Comparative proteomics and RBC patho-physiology. *J Proteomics.* 2010;73(3):421-435.
18. Pasini EM, Lutz HU, Mann M, Thomas AW. Red blood cell (RBC) membrane proteomics: I. Proteomics and RBC physiology. *J Proteomics.* 2010;73(3):403-420.
19. De Franceschi L, Biondani A, Carta F, et al. PT-Pepsilon has a critical role in signaling transduction pathways and phosphoprotein network topology in red cells. *Proteomics.* 2008;8(22):4695-4708.
20. Siciliano A, Turrini F, Bertoldi M, et al. Deoxygenation affects tyrosine phosphoproteome of red cell membrane from patients with sickle cell disease. *Blood Cells Mol Dis.* 2010;44(4):233-242.
21. Bordin L, Ion-Popa F, Brunati AM, Clari G, Low PS. Effector-induced Syk-mediated phosphorylation in human erythrocytes. *Biochim Biophys Acta.* 2005;1745(1):20-28.
22. Matte A, Low PS, Turrini F, et al. Peroxiredoxin-2 expression is increased in beta-thalassemic mouse red cells but is displaced from the membrane as a marker of oxidative stress. *Free Radic Biol Med.* 2010;49(3):457-466.
23. Bosman GJ, Lasonder E, Groenen-Dopp YA, Willekens FL, Werre JM, Novotny VM. Comparative proteomics of erythrocyte aging in vivo and in vitro. *J Proteomics.* 2010;73(3):396-402.
24. van Gestel RA, van Solinge WW, van der Toorn HW, et al. Quantitative erythrocyte membrane proteome analysis with Blue-native/SDS PAGE. *J Proteomics.* 2010;73(3):456-465.
25. Donella-Deana A, James P, Staudenmann W, et al. Isolation from spleen of a 57-kDa protein substrate of the tyrosine kinase Lyn: identification as a protein related to protein disulfide-isomerase and localisation of the phosphorylation sites. *Eur J Biochem.* 1996;235(1):18-25.
26. Trentin L, Frasson M, Donella-Deana A, et al. Geldanamycin-induced Lyn dissociation from aberrant Hsp90-stabilized cytosolic complex is an early event in apoptotic mechanisms in B-chronic lymphocytic leukemia. *Blood.* 2008;112(12):4665-4674.
27. Brunati AM, Bordin L, Clari G, et al. Sequential phosphorylation of protein band 3 by Syk and Lyn tyrosine kinases in intact human erythrocytes: identification of primary and secondary phosphorylation sites. *Blood.* 2000;96(4):1550-1557.
28. Xue Y, Ren J, Gao X, Jin C, Wen L, Yao X. GPS 2.0, a tool to predict kinase-specific phosphorylation sites in hierarchy. *Mol Cell Proteomics.* 2008; 7(9):1598-1608.
29. Pantaleo A, De Franceschi L, Ferru E, Vono R, Turrini F. Current knowledge about the functional roles of phosphorylative changes of membrane proteins in normal and diseased red cells. *J Proteomics.* 2010;73(3):445-455.
30. Ferru E, Giger K, Pantaleo A, et al. Regulation of membrane-cytoskeletal interactions by tyrosine phosphorylation of erythrocyte band 3. *Blood.* 2011;117(22):5998-6006.
31. De Franceschi L, Villa-Moruzzi E, Biondani A, et al. Regulation of K-Cl cotransport by protein phosphatase 1alpha in mouse erythrocytes. *Pflugers Arch.* 2006;451(6):760-768.
32. Mallozzi C, De Franceschi L, Brugnara C, Di Stasi AM. Protein phosphatase 1alpha is tyrosine-phosphorylated and inactivated by peroxynitrite in erythrocytes through the src family kinase fgr. *Free Radic Biol Med.* 2005;38(12): 1625-1636.
33. Ipsaro JJ, Huang L, Gutierrez L, MacDonald RI. Molecular epitopes of the ankyrin-spectrin interaction. *Biochemistry.* 2008;47(28):7452-7464.
34. Ipsaro JJ, Harper SL, Messick TE, Marmorstein R, Mondragon A, Speicher DW. Crystal structure and functional interpretation of the erythrocyte spectrin tetramerization domain complex. *Blood.* 2010; 115(23):4843-4852.
35. Ipsaro JJ, Mondragon A. Structural basis for spectrin recognition by ankyrin. *Blood.* 2010; 115(20):4093-4101.
36. Matsuoka Y, Li X, Bennett V. Adducin: structure, function and regulation. *Cell Mol Life Sci.* 2000; 57(6):884-895.
37. Kolch W, Pitt A. Functional proteomics to dissect tyrosine kinase signalling pathways in cancer. *Nat Rev Cancer.* 2010;10(9):618-629.

38. Gauthier EGX, Mohandas N, An X. Phosphorylation-dependent perturbations of the 4.1R associated multiprotein complex of the erythrocyte membrane. *Biochemistry*. 2011;50(21):4561-4567.
39. Lupas A, Van Dyke M, Stock J. Predicting coiled coils from protein sequences. *Science*. 1991; 252(5009):1162-1164.
40. Cooper RA, Durocher JR, Leslie MH. Decreased fluidity of red cell membrane lipids in abetalipoproteinemia. *J Clin Invest*. 1977;60(1):115-121.
41. Salomao M, Zhang X, Yang Y, et al. Protein 4.1R-dependent multiprotein complex: new insights into the structural organization of the red blood cell membrane. *Proc Natl Acad Sci U S A*. 2008; 105(23):8026-8031.
42. Stenberg PE, Pestina TI, Barrie RJ, Jackson CW. The Src family kinases, Fgr, Fyn, Lck, and Lyn, colocalize with coated membranes in platelets. *Blood*. 1997;89(7):2384-2393.
43. Evangelista V, Pamuklar Z, Piccoli A, et al. Src family kinases mediate neutrophil adhesion to adherent platelets. *Blood*. 2007;109(6):2461-2469.
44. de Gassart A, Geminard C, Fevrier B, Raposo G, Vidal M. Lipid raft-associated protein sorting in exosomes. *Blood*. 2003;102(13):4336-4344.
45. Savina A, Vidal M, Colombo MI. The exosome pathway in K562 cells is regulated by Rab11. *J Cell Sci*. 2002;115(12):2505-2515.
46. Harder T, Scheiffele P, Verkade P, Simons K. Lipid domain structure of the plasma membrane revealed by patching of membrane components. *J Cell Biol*. 1998;141(4):929-942.
47. Salzer U, Zhu R, Luten M, et al. Vesicles generated during storage of red cells are rich in the lipid raft marker stomatin. *Transfusion*. 2008;48(3): 451-462.

OPEN ACCESS Freely available online

PLoS one

Computational Identification of Phospho-Tyrosine Sub-Networks Related to Acanthocyte Generation in Neuroacanthocytosis

Lucia De Franceschi[1]*, Giovanni Scardoni[2,3☯], Carlo Tomelleri[1☯], Adrian Danek[4], Ruth H. Walker[5,6], Hans H. Jung[7], Benedikt Bader[4], Sara Mazzucco[8], Maria Teresa Dotti[9], Angela Siciliano[1], Antonella Pantaleo[10], Carlo Laudanna[2,3]

1 Department of Medicine, University of Verona, Verona, Italy, **2** Department of Pathology and Diagnosis, University of Verona, Verona, Italy, **3** The Center for Biomedical Computing, University of Verona, Verona, Italy, **4** Neurologische Klinik und Poliklinik, Klinicum der Universität München, Munich, Germany, **5** Department of Neurology, James J. Peters Veterans Affairs Medical Center, Bronx, New York, New York, United States of America, **6** Department of Neurology, Mount Sinai School of Medicine, New York, New York, United States of America, **7** Department of Neurology, University Hospital Zurich, Zurich, Switzerland, **8** Department of Neurosciences, University of Verona, Verona, Italy, **9** Department of Neurology, University of Siena, Siena, Italy, **10** Department of Biology, Molecular and Medical Chemistry, University of Torino, Torino, Italy

Abstract

Acanthocytes, abnormal thorny red blood cells (RBC), are one of the biological hallmarks of neuroacanthocytosis syndromes (NA), a group of rare hereditary neurodegenerative disorders. Since RBCs are easily accessible, the study of acanthocytes in NA may provide insights into potential mechanisms of neurodegeneration. Previous studies have shown that changes in RBC membrane protein phosphorylation state affect RBC membrane mechanical stability and morphology. Here, we coupled tyrosine-phosphoproteomic analysis to topological network analysis. We aimed to predict signaling sub-networks possibly involved in the generation of acanthocytes in patients affected by the two core NA disorders, namely McLeod syndrome (MLS, *XK*-related, Xk protein) and chorea-acanthocytosis (ChAc, *VPS13A*-related, chorein protein). The experimentally determined phosphoproteomic data-sets allowed us to relate the subsequent network analysis to the pathogenetic background. To reduce the network complexity, we combined several algorithms of topological network analysis including cluster determination by shortest path analysis, protein categorization based on centrality indexes, along with annotation-based node filtering. We first identified *XK*- and *VPS13A*-related protein-protein interaction networks by identifying all the interactomic shortest paths linking Xk and chorein to the corresponding set of proteins whose tyrosine phosphorylation was altered in patients. These networks include the most likely paths of functional influence of Xk and chorein on phosphorylated proteins. We further refined the analysis by extracting restricted sets of highly interacting signaling proteins representing a common molecular background bridging the generation of acanthocytes in MLS and ChAc. The final analysis pointed to a novel, very restricted, signaling module of 14 highly interconnected kinases, whose alteration is possibly involved in generation of acanthocytes in MLS and ChAc.

Citation: De Franceschi L, Scardoni G, Tomelleri C, Danek A, Walker RH, et al. (2012) Computational Identification of Phospho-Tyrosine Sub-Networks Related to Acanthocyte Generation in Neuroacanthocytosis. PLoS ONE 7(2): e31015. doi:10.1371/journal.pone.0031015

Editor: Hitoshi Okazawa, Tokyo Medical and Dental University, Japan

Received June 7, 2011; **Accepted** December 30, 2011; **Published** February 15, 2012

Funding: Grants from Telethon grant (GP07007, LDF) and Advocacy on Neuro-acanthocytosis (LDF, AD, BB, RW) and AIRC (Associazione Italiana per la Ricerca sul Cancro) e Fondazione Cariverona (CL). The funders had no role in study design, data collection and analysis, decision to publish, or preparation of the manuscript.

Competing Interests: The authors have declared that no competing interests exist.

* E-mail: lucia.defranceschi@univr.it

☯ These authors contributed equally to this work.

Introduction

Acanthocytes, abnormal thorny red cells in the peripheral circulation, are one of the biological hallmarks of a severe and underrecognised group of neurodegenerative group of disorders known as the neuroacanthocytosis syndromes (NA). Genetic studies in the two core NA disorders, McLeod syndrome (MLS) and chorea-acanthocytosis (ChAc), have resulted in the identification of mutations on (i) the *XK* gene (X-chromosome) encoding for Xk protein in MLS and (ii) the *VPS13A* gene (chromosome 9), encoding for chorein in ChAc [1,2,3,4,5]. These two disorders share a similar Huntington disease-like phenotype including chorea, psychiatric and cognitive abnormalities and additional neuromuscular involvement. The gap between genotype and phenotype in both disorders suggests an important role for post-translational protein modifications, such as phosphorylation, in abnormal cell functions. Since red cells are easily accessible and acanthocytes are part of the clinical presentation of NA, the study of acanthocytes in NA represents a convenient experimental model to be exploited.

Red cells are characterized by a typical biconcave shape, which is maintained through their 120 day life in the peripheral circulation. The red cell membrane is formed by a lipid bilayer bound to integral proteins, such as band 3, and connected with the spectrin-actin cytoskeleton network by multicomplex proteins bridging the membrane to the cytoskeleton. Quantitative or qualitative changes in protein membrane composition result in abnormal red cell morphology [6]. Although molecular and

functional studies in hereditary red cell membrane disorders such as hereditary spherocytosis (HS) or hereditary ovalocytosis (HOS) have highlighted the functional role of many of the membrane proteins, much still remains to be investigated in diseases characterized by abnormal red cell morphology and normal membrane protein composition. Recent studies have suggested a possible role of post-translational modifications, such as phosphorylation, in modulation of red cell membrane protein-protein function and/or structure. In addition, changes in the membrane protein phosphorylation state might result in loss of red cell membrane mechanical stability and abnormal morphology [7,8,9,10,11].

We applied methods of static network analysis derived from graph theory with the aim of identifying topological properties of signaling networks important in abnormal red cells from MLS and ChAc patients. We combined several algorithms of topological network analysis of the experimental data. In order to filter the network complexity, we combined cluster extraction and centrality analysis, coupled to multidimensional network node categorization. We extracted very restricted sub-networks with 14 highly interconnected kinases possibly involved in generation of acanthocytes in NA disorders.

Results

Sub network reconstruction and topological analysis

We performed comparative proteomic analysis combined with the identification of differently tyrosine phosphorylated proteins from red cell membranes of healthy and either ChAc or MLS subjects (Table 1). We observed no relation between the differently tyrosine phosphorylated proteins from red cells of either ChAc or MLS subjects and disease progression. Since the tyrosine phosphoproteomic analysis generated a significant amount of data, whose interpretation required a network level data analysis (Supplementary Table S1, S2, S3), we carried out a topological network analysis to identify potential new signaling pathways involved in generation of acanthocytes common to MLS and ChAc.

The first step of our analysis was intended to demonstrate signaling mechanisms possibly linking Xk and chorein protein to the specific pattern of protein tyrosine phosphorylation observed in red cells isolated from MLS and ChAc patients. We first reconstructed Xk and chorein-related networks by identifying all the interactomic shortest paths linking Xk and chorein to the corresponding set of proteins whose phosphorylations were altered in patients. In these sub-networks, we looked for a possible connection between defective Xk or chorein and the experimentally determined tyrosine phosphoproteomic patterns observed in red cells (see Methods). The Xk_to_P-tyr-network consisted of 129 proteins and 738 interactions (Appendix S1 and S2). The chorein_to_P-tyr-network consisted of 132 proteins and 1348 interactions (Appendix S3 and S4). These two networks could be considered clusters of signaling proteins controling membrane protein tyrosine phosphorylation by Xk and chorein. Since both Xk and chorein lack intrinsic kinase or phosphatase activity, their influence on the tyrosine phosphoproteome must be mediated by interacting kinases and/or phosphatases. In the Xk_to_P-tyr-network we identified 29 kinases (Appendix S13); two kinases, ABL2 and MARK1 belonged to the set of hyperphosphorylated proteins (both +2.84); three kinases, CSNK2A1, PRKACB and PRKCA, were first neighbors of Xk and directly interacted with all other 24 kinases. We also identified three phosphatases (Appendix S13), DUSP13, SET and PTPRC; DUSP13 belonged to the set of hyperphosphorylated proteins (+2.17). Since we experimentally identified proteins phosphorylated on tyrosine residues, the relevant kinases were the PTKs ABL2 and FYN, whereas the relevant phosphatases were DUSP13 and PTPRC. As PTPRC expression is restricted to leukocytes, we focused our analysis on ABL2, FYN and DUSP13.

To refine this first analysis we calculated the centrality scores for every node of the Xk_to_P-tyr-network (see Methods) (Appendix S14 and S15). This allowed us to rank nodes according to their topological weight in the network [12,13,14]. We found that all centrality indexes of FYN were well above the network average (Figure 1A). In particularly, the centroid was 2.1 times the average, betweenness was 1.7 times the average and stress was 1.92 times the average, thus ranking FYN in the top ten nodes. As the centroid indicates node tendency to organize functional modules, with betweenness and stress denoting the capability of a node to work as a critical linker between nodes, these elevated FYN centralities may suggest a critical regulatory role of FYN in this specific red cell context. In contrast, ABL2 had betweenness and stress well below the average, but centroid was over the average (Supplementary Figure S1). This may suggest a less critical role of ABL2 in maintaining node communication but still with a role in cluster formation. Finally, all centrality indexes of DUSP13 were well below the average (Supplementary Figure S2), suggesting a rather marginal role in network regulation. Calculation of shortest paths linking DUSP13 to the set of dephosphorylated proteins showed a rather indirect connection, with 3- to 4-degrees of separation (Figure 2, Appendix S5). Overall, the analysis suggests that FYN and ABL2 have a dominant topological role with respect to DUSP13. This suggests a dominant role in regulation of tyrosine phosphorylation in red cells from MLS patients in agreement with the observed hyperphosphorylating state of red cell membrane proteins in MLS. The previous conclusions are in accordance with previously reported data on other DUSP-related phosphatases, showing that phosphorylation of DUSPs may lead to their inhibition and/or degradation [15]. Four proteins were found to be dephosphorylated in red cells from MLS patients (ANXA4, PRPH, PRDX6 and INMT). Since the analysis suggests a marginal role of DUSP13, the only protein tyrosine phosphatase found by the analysis and possibly affecting protein tyrosine phosphorylation is PTPRC, which binds and modifies FYN activity [16]. Interestingly, at present no data are available on PTPRC expression in mature red cells.

ABL2 is another protein that can directly bind FYN and might be regulated by FYN-mediated phosphorylation of its SH2 and SH3 domains, suggesting a more complex scenario. In addition, FYN may interact with PRKCA [17], which may in turn directly interact with Xk. Finally, PTPRC binding CSNK2A1 and PRKCA may possibly participate in a multiprotein complex organized at the membrane by Xk. Altogether, these observations may indicate that a deficient Xk on red cells from MLS patients may alter the intracellular distribution and/or reciprocal interaction of FYN, ABL2, DUSP13 and, possibly, PTPRC. This promotes an imbalanced between kinases and phosphatases activity, leading in favour of FYN and ABL2.

In the chorein_to_P-tyr-network we identified 29 kinases (Appendix S16). Six kinases, AURKB (+2.6), CAMK1 (+2.5), PLK3 (+2.6), MPP1 (+2.6), PIP4K2A (+2.9) and PFTK1 (+2.4) belonged to the set of hyperphosphorylated proteins. Three kinases, FYN, ABL1 and PIK3R1, were first neighbors of chorein and directly interacted with all other 26 kinases. We also identified four phosphatases (Appendix S16), PPP3CB, PPP3CC, ACP1 and PTPRC; PPP3CC belonged to the set of hyperphosphorylated proteins (+2.2). Also in ChAc red cells we experimentally identified proteins phosphorylated on tyrosine residues. The relevant PTKs

Table 1. Demographic and molecular data of control subjects and McLeod Syndrome and chorea-acanthocytosis patients.

	Gender	Age of symptom onset (yrs)	Age at examination (yrs)	Abnormalities on Clinical Examination	Molecular Defect	Ref.
Healthy Controls	3M/9F	-	35.6±2.3	-	-	[34]
ChAc 1	F	16	35	Orofacial dyskinesias, tics, chorea, tongue protrusion dystonia, dysarthria, absent reflexes	Splice site mutation intron 3 (c.188-5T>G); mutation on the other allele unknown	[34], [38]
ChAc 2	M	47	49	Tongue and lip biting, dysarthria, orofacial dyskinesias, steppage gait, no cognitive impairment	Splice site mutations in exon 58 (c.8105+3_+6del) and exon 70 (c.9275G>A; Chorein absent	[34], [42], [43]
ChAc 3	F	28	30	Seizures, orofacial dyskinesias, chorea, tongue protrusion dystonia, dysarthria, obsessive compulsive disorder, absent reflexes, neuropathy	p.A1428P and splice site mutation intron 55 (c.7806G>A); Chorein absent	[34], [39]
ChAc 4	F	24	40	Seizures, orofacial dyskinesias, chorea, tongue protrusion dystonia, absent reflexes, myopathy, neuropathy	p.R1297X and p.V1406CfsX20	[5], [34]
ChAc 5	M	16	47	Orofacial dyskinesias, dysarthria, chorea, psychiatric disorder, no seizures and no parkinsonism at age 30, neuropathy	Splice site mutations intron 22 (c.2288+2T>C) and intron 61 (c.8472-1G>C); Chorein absent	[5], [34], [38]
ChAc 6	F	32	56	Seizures, orofacial dyskinesias, chorea, tongue protrusion dystonia, dysarthria, dysphagia, absent reflexes, myopathy	Homozygous p.K372SfsX2	[11], [34], [40], [41]
ChAc 7	M	24	32	Seizures, orofacial dyskinesias, chorea, tongue protrusion dystonia, dysarthria, parkinsonism, absent reflexes, neuropathy, myopathy	Chorein absent	[34]
ChAc 8	F	24	38	Seizures, orofacial dyskinesias, chorea, tongue protrusion dystonia, psychiatric disorder	Splice site mutation intron 6 (c.495+5G>A) and p.K1635VfsX6	[34]
ChAc 9	F	28	40	Seizures, Orofacial dyskinesias, chorea, dysarthria, dysphagia, absent reflexes, myopathy	Chorein absent	[34]
MLS 1	M	58	60	Yawning, belching, dystonia, no seizures, mild facial masking (no bradykinesia, tremor, or hypertonia)	p.R222G	[36]
MLS 2	M	56	60	Gait problems, tongue-biting, dystonia, atrial fibrillation, anxiety, depression, no seizures, mild truncal chorea, hyporeflexia, myopathy, neuropathy	Deletion of exons 1 and 2	[37]
MLS 3	M	26	54	Bipolar disorder, schizophrenia, moderate perioral dyskinesias, pronounced generalized chorea, mild generalized muscular atrophy, absent reflexes, cardiopathy,	p.Q299X	[35]
MLS 4	M	25	41	Personality disorder, mild generalized chorea, absent reflexes	p.Q299X	[35]
MLS 5	M	20	47	Swallowing difficulties, gait problems, pronounced generalized chorea, tongue protrusion dystonia, feeding dystonia, head dropping, mild cognitive impairment generalized muscular atrophy, absent reflexes	p.Q299X	[35]

M; male; F: female; yrs: years; ChAc: chorea-acanthocytosis; MLS: Mcleod Syndrome; Control age is presented as means ± SD. Molecular defect'' refers to the *VPS13A* and *XK* gene, respectively, that are responsible for ChAc and MLS.

doi:10.1371/journal.pone.0031015.t001

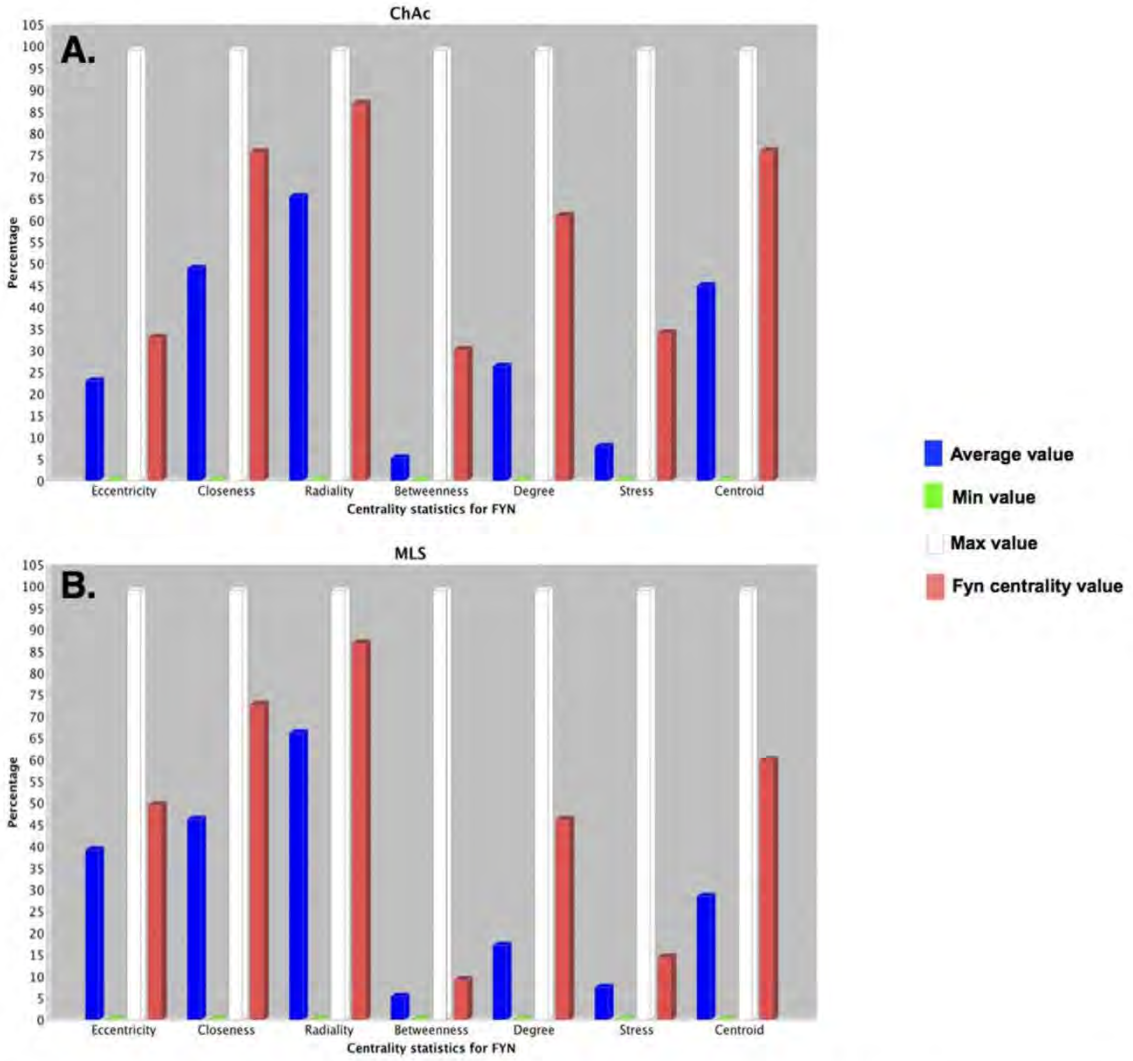

Figure 1. Scores of FYN centrality indexes in Xk_to_P-tyr- and chorein_to_P-tyr- networks. (**A**) Eccentricity, closeness, radiality, betweenness, degree, stress and centroid centrality indexes of the src-related, protein tyrosine kinase FYN in the chorea-acanthocytosis (ChAc; chorein_to_P-tyr)-related sub-network. (**B**) Eccentricity, closeness, radiality, betweenness, degree, stress and centroid centrality indexes of the src-related, protein tyrosine kinase FYN in McLeod syndrome (MLS; Xk_to_P-tyr)-related sub-network. The score of every index was normalized to the maximal value for every index, considered as 100%. Red columns are relative values for FYN. Blue columns are average values. White columns are maximal values. Green columns are minimal values.
doi:10.1371/journal.pone.0031015.g001

were FYN, ABL1, EGFR, FGFR1, IGF1R, TEC, TGFBR1 and BTK, whereas the relevant phosphatases were PTPRC and ACP1. As for the XK_to_P-tyr-network, we refined the analysis by calculating the centrality scores for every node of the chorein _to_P-tyr-network (Appendix S17 and S18), thus ranking nodes according to their topological relevance in the network. Among PTKs, FYN, ABL1 and EGFR had centralities values consistently above the average and ranked among the top ten nodes: (i) FYN had centroid 2.4 times the average, betweenness 5.6 times the average and stress 4.2 times the average; (ii) ABL1 had centroid 2.4 times the average, betweenness 6.6 times the average and stress 5.6 times the average (Supplementary Figure S3); (iii) EGFR had centroid 4 times the average, betweenness 5.5 times the average and stress 5 times the average (Supplementary Figure S4). In contrast, FGFR1, IGF1R, TEC, TGFBR1 and BTK had lower centrality scores and well below the network average (Supplementary Figure S5). Moreover, both identified phosphatases, PTPRC and ACP1 had very low centrality scores, suggesting a rather marginal role in network regulation with low influence on the tyrosine phosphoproteome (Supplementary Figure S5). Thus, centrality analysis not only suggests the absolute topological prevalence of FYN, ABL1 and EGFR over other PTKs but also on

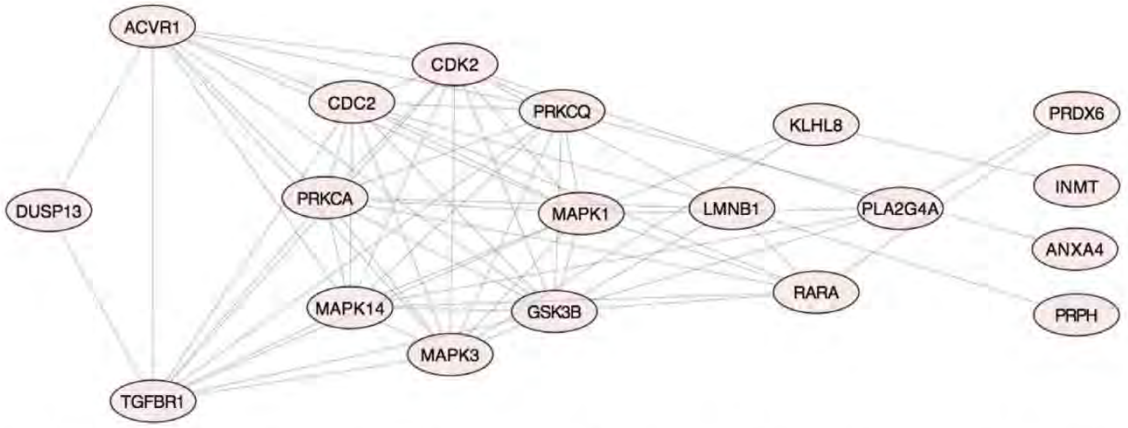

Figure 2. DUSP13 shortest paths to dephosphorylated proteins in Xk_to_P-tyr-network. Graph of all shortest paths linking DUSP13 to INMT, PRPH, PRDX6 and ANXA4. A distance of 3 (ANXA4) or 4 (INMT, PRPH, PRDX6) degree separates DUSP13 from the proteins found dephosphorylated in red cell from patients with McLeod syndrome (MLS).
doi:10.1371/journal.pone.0031015.g002

phosphatases in general. This is in agreement with the experimentally determined definitive tendency to protein hyperphosphorylation in ChAc red cells, with limited dephosphorylated proteins. During the analysis GRB2 attracted our attention. Indeed, GRB2 had the highest scores for all calculated centrality indexes in the chorein _to_P-tyr-network (Supplementary Figure S6). GRB2 is a direct interactor of chorein and directly interacts with FYN, ABL1, EGFR and PTPRC, and, through FYN and SPTAN1, with ACP1. Since FYN and ABL1 also directly interact with chorein, in ChAc red cells the absence of VPS13A may potentially affect the organization and localization of a signaling complex including GRB2, FYN, ABL1, EGFR, PTPRC, and ACP1. Due to the docking role of GRB2 (more than 700 signaling proteins, including several PTKs, directly dock on GRB2), it is possible that delocalization of GRB2 from chorein in red cells isolated from ChAc patients may modify the docking role of GRB2. This would lead to the generation of PTKs signaling complexes whose activity is not balanced by phosphatases. This conclusion seems supported by the absolutely prevalent topological relevance of FYN, ABL1 and EGFR versus PTPRC and ACP1 and by the interaction-phosphorylation relationships. Indeed, FYN directly interacts with ACTB (+2.3) and AURKB (+2.6); ABL1 directly interacts with ACTB (+2.3), AURKB (+2.6) and CAT (+2.5); ACP1 directly interact with EPB41 (+4.3).

Overall, this first analysis suggests that an altered plasma membrane localization of FYN, ABL1, ABL2 and EGFR, not balanced by a concurrent co-localization of ACP1 and PTPRC, may explain the pattern of protein tyrosine phosphorylation observed in red cells from MLS and ChAc patients.

Combined network analysis and generation of shared regulatory cluster of kinases

The second step of our analysis was intended to unveil common signaling mechanisms shared by MLS and ChAc in acanthocytes. To this end, we first reconstructed two Xk- and chorein – "enriched" networks consisting of the previous Xk_to_P-tyr-network and chorein _to_P-tyr-network respectively combined with two networks generated by computing the first neighbors of the proteins belonging to the MLS and ChAc tyrosine phosphoproteomic data sets.

The Xk-PY_probe-FN network consisted of 316 nodes and 16702 interactions (Appendix S6); the chorein-PY_probe-FN network consisted of 930 nodes and 30351 interactions (Appendix S7). Upon network union, the Xk-enriched network consisted of 373 nodes and 17080 interactions (Appendix S8), whereas the chorein-enriched network consisted of 941 nodes and 30549 interactions (Appendix S9). These two networks represent interactomic spaces related to Xk and chorein signaling activities. To identify a common interactomic background shared by MLS and ChAc, we applied an intersection algorithm generating a unique, fully connected, interactomic network component. This Xk_ chorein-intersected network consisted of 249 nodes and 16131 interactions (Appendix S10). Every protein and interaction belonging to the Xk_ chorein-intersected network is present in both in Xk- and in chorein-union networks. This intersected network is likely the common interactomic space where shared signaling mechanisms may emerge.

To further focus the analysis we calculated the centrality score for every node of the Xk_ chorein-intersected network (Appendix S19 and S20, Appendix Figure 1). We, then, computed the most represented Gene Onthologies (GO) categories (www.geneontology.org) in the Xk_chorein-intersected network (Appendix S21). Finally, we filtered the Xk_ chorein-intersected network toward the node centralities scores, the GO categories and the biochemical activity. By applying this network filtering procedure we better focused the analysis and generated a number of interesting output. First, network filtering by kinase and phosphatases activity revealed 144 protein kinases but only 3 protein phosphatases, suggesting an absolutely imbalanced activity toward protein phosphorylation present in the Xk_chorein-intersected network. Notably, we found 4 proteins (ACTB, CAT, AURKB and RAB3C) hyperphosphorylated in ChAc red cells and 3 proteins (MARK1, ABL2, RPH3AL) hyperphosphorylated in MLS red cells.

Secondly, analysis of centroid demonstrated an organization of the Xk_chorein-intersected network in at least 4 main protein clusters (Figure 3A). This suggested the possibility of a further focusing of the analysis. We plotted centroid versus betweenness (Figure 3B) to evidence a concurrent discretization of the betweenness. We then filtered out the Xk_chorein-intersected

network by extracting a sub-network of nodes having both centroid and betweenness above the average (far and top right of the Figure 3B; Appendix S11). All proteins belonging to this sub-network (41 nodes - 818 interactions) were kinases (Figure 4, Appendix S22). We finally extracted all proteins from this sub-network, which show the highest statistical scores in the GO categories "erythrocyte development" and "neurogenesis". The resulting highly restricted sub-network consisted of 14 proteins and 89 interactions (Figure 5, Appendix S12, Appendix S23 and S24). This network was extremely connected with an average shortest path of 1, a neighborhood connectivity of 12 and a clustering coefficient of 1, indicating that this network works as a unique, fully integrated, functional signaling module. The network included ABL2, FYN and ABL1 along with other 11 kinases. FYN, LYN, ABL2, TTN and PDPK1 are involved in rho small GTPases activity and cytoskeleton regulation (see http://www.signaling-gateway.org/molecule and http://www.geneontology.org/); RPS6KA3, EPHB2, EPHB4 and CDK5 regulate neurogenesis (see http://www.signaling-gateway.org/molecule and http://www.geneontology.org/); TGFBR1 regulates development; MAP4K2 and MAPK14 are involved in response to stress (see http://www.signaling-gateway.org/molecule and http://www.geneontology.org/); LYN regulate erythrocyte differentiation and band 3 tyrosine phosphorylation state [18,19]; ABL1 and ABL2 are related to oxidoreductase activity and oxidative stress. Of particular interest is the presence in this highly connected sub-network of TTN (Titin), which is a muscle giant (4.3 MD) scaffolding protein characterized by intrinsic viscous-elastic stiffness and kinase activity, involved in cytoskeleton regulation and contractility in the sarcomere [20].

Interrogation of the 8 manually curated data-bases from which we derived the interactomic data-set used in this study (HPRD, BioGRID, MINT, IntAct, Reactome, CELL-MAP, NCI_Nature and Pathway Commons), show interactions between the 14 proteins described in various publications. Interactions have been shown both *in vitro* (cell-free system) and/or *in vivo* depending of data-bases, some representative references are shown in Appendix S25.

Overall, the two combined analyses point to a very restricted group of highly interconnected kinases including ABL1, ABL2, AURKA, CDK5, EPHB2, EPHB4, FYN, LYN, MAP4K2, MAPK14, PDPK1, RPS6KA3, TGFBR1 and TTN (Figure 5, see Appendix S24), regulating rho small GTPase-mediated signaling, cytoskeleton network, erythropoiesis and neurogenesis. This network may represent a shared regulatory cluster of kinases whose alteration is most likely involved in generation of the abnormal red cells that characterize MLS and ChAc.

Discussion

The maintenance of the red cell membrane mechanical stability is crucial for red cell functions and survival in peripheral circulation. The mechanisms involved in this process are complex and only partially understood. Recent proteomic studies have identified more than 300 erythrocyte membrane proteins indicating that most of the available information is limited to less than 15% of total membrane proteins [8,21,22,23,24]. In addition, changes in phosphorylation state of some of the most abundant red cell membrane proteins have been reported to affect the red cell membrane organization with loss of mechanical membrane stability and abnormal red cell morphology [7,8,9]. This indicates that the red cell membrane contains a consistent number of regulatory structures characterized by unexpected complexity. The events involved in generation of acanthocytes associated with NA syndromes are only partially known. In this context, a proteomic approach enable the rapid identification of new functional pathways. In previous reports we have shown abnormalities in protein tyrosine-phosphorylation state of few red cell membrane proteins, suggesting abnormalities of intracellular signaling pathways involved in acanthocytosis in NA [11,25].

To infer potential mechanisms of disease shared by MLS and ChAc we performed a bioinformatic analysis of the experimentally-determined Tyr-phosphoproteomic data sets by implementing an articulated procedure of topological network analysis [26,27,28,29]. In the first level of analysis when the phosphoproteomic data from MLS and ChAc were separately reconstructed and analyzed, we observed an imbalance between kinase/phosphatase membrane translocation compared to controls. The centrality index analysis suggests that the absolute topological prevalence of few tyrosine kinases, such as FYN and ABL1, over other PTKs may contribute to the imbalanced activity between kinases and phosphatases in acanthocytes. This is in agreement with the experimentally determined definitive tendency to protein hyperphosphorylation in ChAc red cells, with limited dephosphorylated proteins. Notably, the analysis suggested a negligible topological role for ACP1, a low molecular weight protein tyrosine phosphatase, in the ChAc signaling network. In other cell models ACP1 may modulate the activation state of rho small GTPases [30], which in turn are involved in cytoskeleton remodeling [31,32]. The recent data on erythrocytes from mice genetically lacking the small G protein Rac1 indicate that these proteins are involved in the dynamic regulation of the red cell membrane network [33]. This suggests that a perturbation in the events involved in cytoskeleton rearrangement might participate to the generation of acanthocytes in ChAc and MLS. Based on this analysis we obtained preliminary data showing increased membrane association of small G proteins in ChAc red cells compared to normal controls, supporting the network modeling [34].

The topological network analysis of red cells from MLS patients indicated that a defective Xk protein on red cells may possibly alter the intracellular distribution and/or reciprocal interaction of FYN, ABL2, DUSP13 and, possibly, PTPRC. This would generate an imbalanced activity of tyrosine kinases versus phosphatases in MLS also. To address whether shared signaling mechanisms operate in acanthocytes from MLS and ChAc, NA disorders caused by different genes, we finally combined the two network analyses. We found a very restricted group of highly interconnected kinases including ABL1, ABL2, AURKA, CDK5, EPHB2, EPHB4, FYN, LYN, MAP4K2, MAPK14, PDPK1, RPS6KA3, TGFBR1 and TTN (Figure 5, see Appendix Table 12), regulating rho small GTPases-mediated signaling, cytoskeleton network, erythropoiesis and neurogenesis. This network could likely represent a shared regulatory cluster of kinases whose alteration is responsible for abnormal red cells in MLS and ChAc.

Previous studies have shown that FYN and LYN, two tyrosine kinase of the Src family, are present in red cells [7,19]. Alteration of Fyn activity and generation of red cells with abnormal morphology has been previously described in a mouse model genetically lacking the protein tyrosine phosphatase epsilon (PTPε).This supports the crucial role of FYN in modulating the tyrosine phosphorylation state of red cell membrane protein and emphasizes the balance between phosphatase and kinase activities in the maintenance of red cell membrane mechanical stability [7]. The identification of LYN as another candidate of this shared signaling network is very interesting because of the increased tyrosine phosphorylation state of band 3 reported in red cells from ChAc [7,25]. In normal red cells, the translocation of functionally active LYN to red cell membrane is a sequential process of

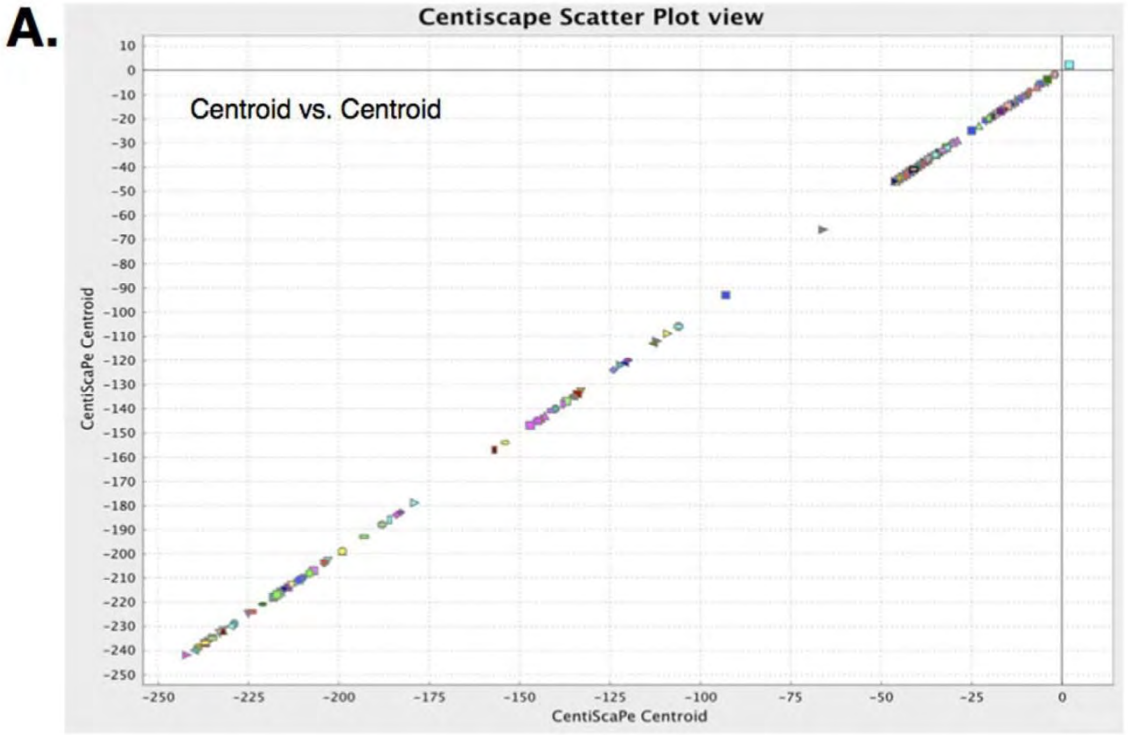
A.
Centiscape Scatter Plot view
Centroid vs. Centroid
CentiScaPe Centroid
CentiScaPe Centroid

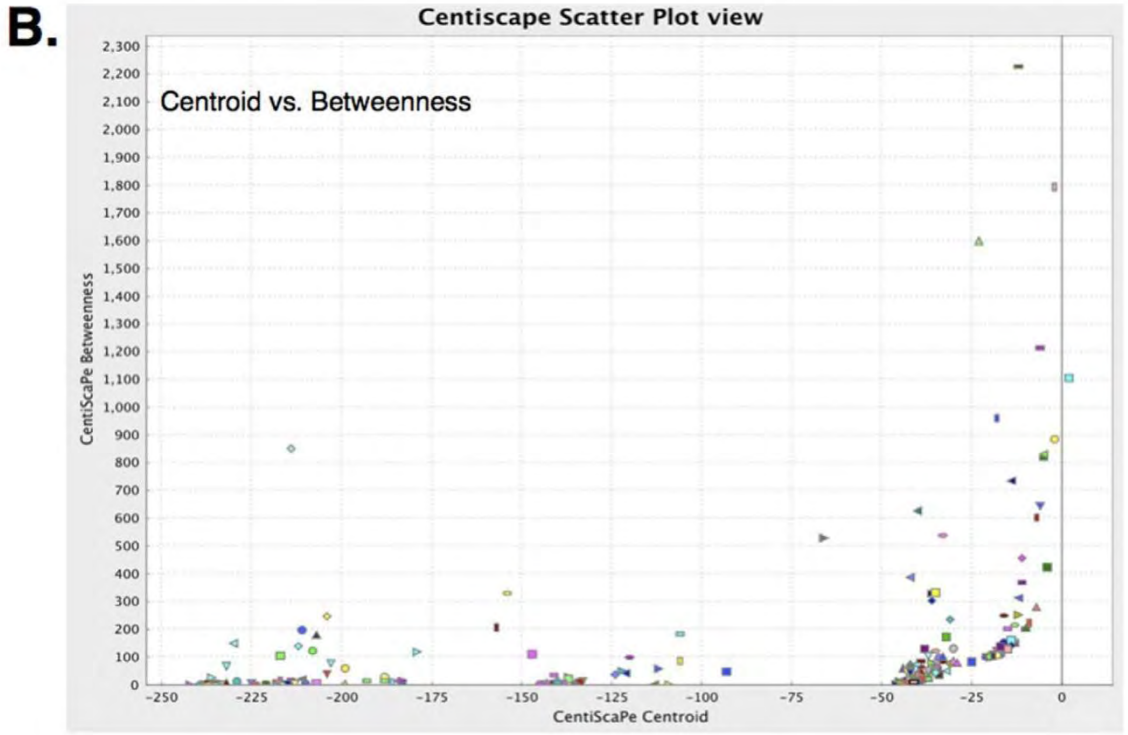
B.
Centiscape Scatter Plot view
Centroid vs. Betweenness
CentiScaPe Betweenness
CentiScaPe Centroid

Figure 3. Centrality discretization in Xk_VPS13A-intersected network. (**A**) Plot of centroid vs. centroid centrality index values of all nodes in the Xk_ chorein-intersected network. (**B**) Plot of centroid vs. betweenness centrality index values of all nodes in the Xk_chorein-intersected network; the plot shows a concurrent discretization of centroid and betweenness, highlighting a cluster of 41 proteins having centroid and betweenness above the network average.
doi:10.1371/journal.pone.0031015.g003

phosphorylation synergistically mediated by SYK, a ZAP-70 related tyrosine kinase. SYK generates a binding site for the Src SH2 domain followed by LYN membrane association [19]. It is of interest that SYK is not present in the MLS and ChAc-related shared kinase network, suggesting either abnormal LYN activation, possibly SYK-independent as we recently reported in ChAc red cells [34], or changes in the accessibility of the membrane docking site for LYN in abnormal red cells from ChAc and MLS patients.

Overall, we believe that the results of the present work may impact the study of signaling networks in red cells. Indeed, dynamics of protein-protein kinase interactions could provide the

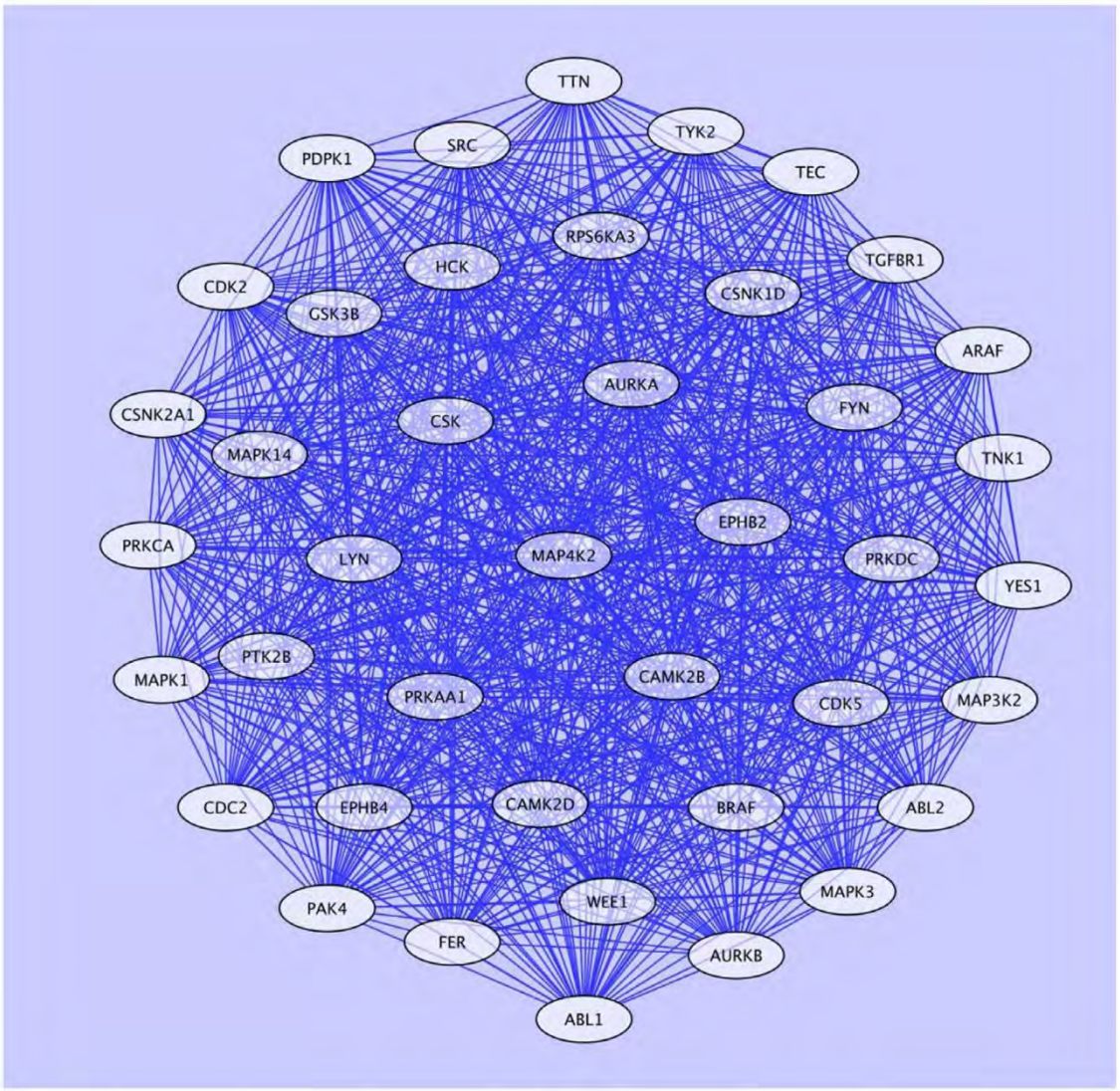

Figure 4. Sub-network of proteins in the Xk_ chorein-intersected network. Sub-network of proteins in the Xk_chorein-intersected network having centroid and betweenness over the network average. The sub-network contains 41 proteins connected by 818 interactions. All proteins are kinases.
doi:10.1371/journal.pone.0031015.g004

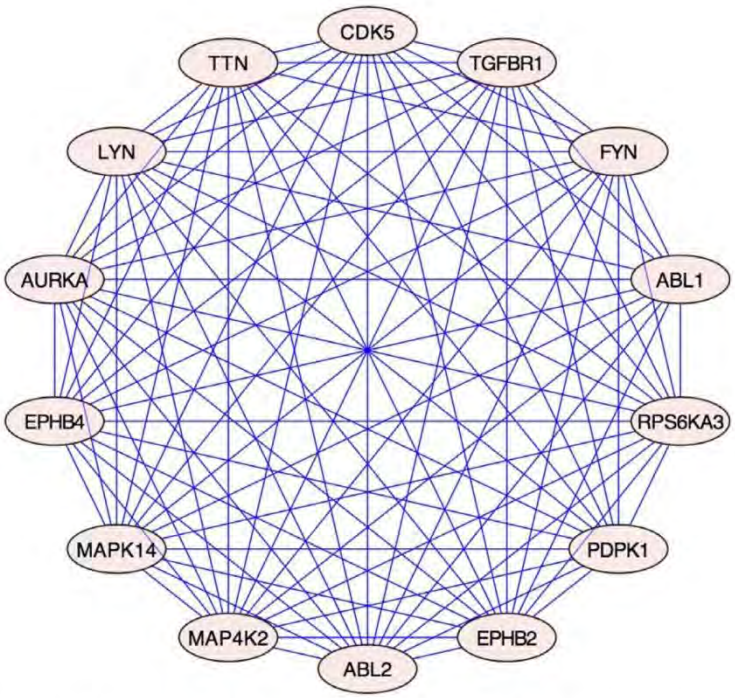

Figure 5. Highly restricted sub-network of, GO categorized, clustered proteins isolated from the Xk_chorein-intersected network. Sub-network of proteins in the Xk_chorein-intersected network having centroid and betweenness above the network average and enriched in the GO categories "erythrocyte development" and "neurogenesis". The sub-network consists of 14 proteins connected by 89 interactions. All proteins are kinases.
doi:10.1371/journal.pone.0031015.g005

molecular context necessary for cell plasticity, in turn required to maintain erythrocyte shape, steadiness and for long-term survival of red cells. This aspect needs to be investigated especially in diseased red cells. Our results provide a proof-of-principle for a potentially useful bioinformatic approach by combining several algorithms of topological network analysis coupled to multidimensional network node categorization to allow consistent filtering of network complexity. We believe that this approach may accelerate the progress in kinome characterization in MLS and ChAc diseases and will possibly become informative for the analysis of signaling networks in normal and diseased red cells.

Materials and Methods

Proteomic data generation

We studied nine patients with chorea-acanthocytosis (ChAc) and five patients with McLeod syndrome (MLS), in whom the diagnosis was based on the clinical neurological manifestation, the presence of acanthocytes and the molecular analysis of either *VSPA13* (chorein) or *XK* (Xk) mutations as previously described [1,2,3,4,5,35]. Table 1 reports the demographic, clinical and molecular data of the patients studied [5,11,35,36,37,38,39,40,41,42,43]. The study was approved by either Ethic Committees or the Istitutional review boards for human subject study of the James J. Peters VAMC (Bronx, NY, USA), of Mount Sinai School of Medicine (NYC, NY, USA), of Zurich University (Zurich, Switzerland) and of Siena University (Siena, Italy). Blood was collected after informed written consent had been obtained from each subject. Plasma and buffy coat were removed after centrifugation at 1,200 *g* for 10 minutes and the cells were washed four times with a choline washing solution containing: 152 mmol/L choline chloride, 1 mmol/L MgCl2, 10 mmol/L TRIS-MOPS, pH 7.40 at 4°C as previously described [44]. Packed red cells were lysed in ice cold Phosphate Lysis Buffer (LB: 5 mM Na2HPO4, pH 8 containing: protease inhibitor cocktail tablets (Roche), 3 mM benzamidine, final concentration) and centrifuged 10 min at 4°C at 12,000 *g*. The red cell membrane were washed several times in LB and protein content was quantified using DC Protein Assay (Biorad) [7]. The red cell membrane proteins were separated by bidimensional electrophoresis as previously reported [7,8] and the 2D colloidal Coommassie stained gels were scanned and digitized with Progenesis Same Spots software (Nonlinear Dynamics, Newcastle-Upon-Tyne, UK) to generate a general pattern in the 3–10 pH rage. Using the twofold abundance change criteria combined with one-way ANOVA analysis we found 91 spots differently expressed in ChAc *vs* control as previously reported [34] and 28 spots differently expressed in MLS *vs* control (Supplementary Table S1). The spots differently expressed were identified by MALDI-TOF MS analysis as previously described [7,8]. The tyrosine phosphorylation profile of ChAc and MLS red cell membrane was analyzed as previously reported [7,8]. The bands or spots differently tyrosine phosphorylated were identified by Progenesis Same Spots software (Nonlinear Dynamics, Newcastle-Upon-Tyne, UK) following the densitometric analysis of the scanned images of unsaturated films (ImageJ v 1.28 software). The selected bands or spots were identified by MALDI-TOF MS/MS [7,8] are shown in Supplementary Table S2, S3.

Building of a Global Mammalian Protein Interactomic network

A Global Mammalian Protein Interactomic network was built by combining the interactomic data sets from HPRD, MINT, BioGrid, IntAct, DIP, BIND and Pathway Commons online databases, complemented by in-house manually curated data derived from the literature. The combined data set included only manually curated protein-protein binary interactions, inferred by two to six independent methods. Functional, protein-DNA, protein-RNA, protein-metabolite and protein-drug interactions, eventually present in the data sets, were removed. To avoid miscalculations of topological parameters, duplicates and self-interactions, leading to self-loops, were also removed. All molecule identifiers were normalized to HGNC official symbols (www.genenames.org) by using Babelomics 4 (http://babelomics.bioinfo.cipf.es/index.html) and Clone/Gene ID converter (http://idconverter.bioinfo.cnio.es/). The entire set of gene IDs derived from HGNC was also incorporated in the interactomic set to facilitate full interrogation of the data set, thus considering proteins for which direct, physical, interactions were still not described. The resulting data set consisted of 29012 unique gene IDs (nodes) and 149967 binary interactions (edges). The data set contained a PPI network consisting of a unique connected giant component including 11976 nodes (all proteins) and 149879 edges, 68 isolated sub-components, including a total of 159 nodes and 88 edges connected by a maximum of 5 to a minimum of 2 edges, and 16877 isolated nodes. 20451 edges were functionally tagged, with 18286 directed edges accounting for the biochemical activity "state change", and 2165 undirected edges accounting for the biochemical activity "complex formation". Where unambiguously defined, the category "state change" was further specified as "activation" or "inhibition". 94% of total interactions were human and 6% were mouse and rat interactions. The combined data set was compiled in .sif (network) and .txt (attribute) formats to be analyzed in the network analysis environment Cytoscape (www.cytoscape.org) [45,46]. This interactomic data set can be considered a sort of virtual cell including all known protein-protein binary interactions and represents the protein interactomic context where cell regulation originates.

Node annotation and mapping

Protein annotations were extracted from protein annotation data files obtained from HPRD, BioGRID, HGNC and GO databases. Annotations were mapped to all proteins present in the Global Mammalian Protein Interactomic network upon normalization to HGNC protein IDs and were compiled in a single TAB-delimited file to be loaded, as a multidimensional layer of protein properties, in the network analysis software Cytoscape. Node annotations were used to filter sub-networks versus specific protein biochemical or functional properties thus allowing further functional focusing of the analysis.

Sub-network reconstruction and analysis

To perform network topological analysis in the context of MLS and ChAc, the two experimentally determined sets of phosphorylated proteins, derived form the analysis of Red cells isolated from MLS and ChAc patients, were considered as "bioinformatic probes". These were used to interrogate the Global Mammalian Protein Interactomic network and extract enriched sub-networks of proteins related to the activity of Xk or chorein proteins and of the two tyr-phosphoproteomic sets. To perform the reconstruction of MLS and ChAc. PPI sub-networks, we used standard tools of network interrogation, reconstruction, filtering and manipulation provided by the core code of the Cytoscape network analysis environment. Additionally, we applied computational features provided by dedicated plug-ins.

To calculate all shortest paths linking Xk and chorein to the corresponding set of phosphorylated proteins, we developed the Cytoscape plug-in Pesca 3.0 (under submission). The plug-in computes all the shortest paths from a root node to all the other nodes in the network. Formally, given a network described as an undirected graph $G=(N,E)$, where N is the set of nodes and E is the set of edges, a path from node n_1 to node n_k is an alternative sequence $n_0,e_1,n_1,e_2,n_2,\ldots,e_k,n_k$ such that $e_i=\{n_i,n_{i+1}\}$, where $e_i \neq e_j$, if $i \neq j$. The length of a path is the number of edges it has. A path P from a source node s to a target node t is the shortest path if its length is the smallest possible among all paths from s to t. The algorithm used by the Pesca 3.0 plugin to find the shortest paths is based on the Dijkstra algorithm [47]. To compute all the shortest paths the Dijkstra algorithm has been adjusted as follows. Exploring the graph when calculating the shortest path between two nodes s and t, the Dijkstra algorithm keeps for each node n a predecessor node p. To have all the shortest paths, we replace the predecessor p with a set of predecessors for each node n. The set of predecessors of the node n is the set of all the predecessors of the node n in the shortest paths set between s and t, i.e. one node is in the set of predecessors of n if and only if it is a predecessor of n in one of the shortest paths between s and t containing n. Once the predecessors set of each node n has been computed, the tree of all the shortest paths between s and t can also be easily computed.

In biological term, the shortest path is the minimal path of functional influence of an agent A on a target B. Thus, the shorter the path the more likely is the functional influence of A on B. This principle was applied to generate the two MLS- and ChAC-related clusters of signaling proteins most likely mediating protein phosphorylation by Xk and chorein. To gain maximal significance, the network reconstruction based on direct interactor identification was limited to the first neighbor determination. Thus, only first neighbors of the proteins belonging to the two phosphoproteomic data sets were extracted from the Global Mammalian Protein Interactomic data set. This procedure generated the most likely cluster of signaling proteins functionally related to the activity of the proteins belonging to the phosphoproteomic data sets.

Table 2. Stress, Betweenness and Centroid centrality indexes.

Centralities definitions	
σ_{st} is the number of shortest paths from node s to node t $\sigma_{st}(v)$ is the number of shortest paths from node s to node t passing through node v	
Stress(v)	$\sum_{s \neq v \in V} \sum_{t \neq v \in V} \sigma_{st}(v)$
Betweenness(v)	$\sum_{s \neq v \in V} \sum_{t \neq v \in V} \delta_{st}$ *where* $\delta_{st}(v) = \frac{\sigma_{st}(v)}{\sigma(v)}$
Centroid(v)	$C_{cen}(v) = min\{f(v,w) : w \in V/\{v\}\}$ *where* $f(v,w) = \gamma_v(w) - \gamma_w(v)$ *and* $\gamma_v(w)$ *is the number of vertex closer to* v *than* w

doi:10.1371/journal.pone.0031015.t002

Protein categorization based on topological relevance in the network was performed by means of centrality index calculation. The analysis of network centrality indexes was performed by computing node-by-node centrality scores with the Cytoscape plug-in CentiScaPe [12]. Node centrality indexes are complex topological parameters allowing quantitative local measurement of the position of a node relative to the other nodes, and can be used to infer node relative importance in global network organization. Thus, centrality index calculation allows categorization of nodes in a network according to their specific regulatory relevance with respect to other nodes in a network. Particularly we focused on betweenness, stress and centroid indexes (Table 2). Scatter plots of centrality scores were generated within CentiScaPe. Determination of Gene Ontology (GO) categories and calculation of statistical prevalence within the extracted sub-networks were automatically generated by applying the two Cytoscape plug-ins BiNGO [48] and ClueGO [49].

Supporting Information

Figure S1 Scores of ABL2 centrality indexes in the XK_to_P-tyr-network. Eccentricity, closeness, radiality, betweenness, degree, stress and centroid centrality indexes of the protein tyrosine kinase ABL2 in the McLeod syndrome (XK_to_P-tyr)-related sub-network. The score of every index was normalized to the maximal value for every index, considered as 100%. Red columns are relative values for ABL2. Blue columns are average values. White columns are maximal values. Green columns are minimal values.
(TIFF)

Figure S2 Scores of DUSP13 centrality indexes in the XK_to_P-tyr-network. Eccentricity, closeness, radiality, betweenness, degree, stress and centroid centrality indexes of the protein tyrosine phosphatase DUSP13 in the Mcleod syndrome (XK_to_P-tyr)-related sub-network. The score of every index was normalized to the maximal value for every index, considered as 100%. Red columns are relative values for DUSP13. Blue columns are average values. White columns are maximal values. Green columns are minimal values.
(TIFF)

Figure S3 Scores of ABL1 centrality indexes in the VPS13A_to_P-tyr-network. Eccentricity, closeness, radiality, betweenness, degree, stress and centroid centrality indexes of the protein tyrosine kinase ABL1 in the ChAc (VPS13A_to_P-tyr)-related sub-network. The score of every index was normalized to the maximal value for every index, considered as 100%. Red columns are relative values for ABL1. Blue columns are average values. White columns are maximal values. Green columns are minimal values.
(TIFF)

Figure S4 Scores of EGFR centrality indexes in the VPS13A_to_P-tyr-network. Eccentricity, closeness, radiality, betweenness, degree, stress and centroid centrality indexes of the protein tyrosine kinase EGFR in the ChAc (VPS13A_to_P-tyr)-related sub-network. The score of every index was normalized to the maximal value for every index, considered as 100%. Red columns are relative values for EGFR. Blue columns are average values. White columns are maximal values. Green columns are minimal values.
(TIFF)

Figure S5 Scores of FGFR1, IGF1R, TEC, TGFBR1, BTK, PTPRC and ACP1 centrality indexes in the VPS13A_to_P-tyr-network. Eccentricity, closeness, radiality, betweenness, degree, stress and centroid centrality indexes of the protein tyrosine kinases FGFR1, IGF1R, TEC, TGFBR1, BTK, and protein tyrosine phosphatases PTPRC, ACP1 in the ChAc (VPS13A_to_P-tyr)-related sub-network. The score of every index was normalized to the maximal value for every index, considered as 100%. Red columns are relative values for FGFR1, IGF1R, TEC, TGFBR1, BTK, PTPRC and ACP1. Blue columns are average values. White columns are maximal values. Green columns are minimal values.
(TIFF)

Figure S6 Scores of GRB2 centrality indexes in the VPS13A_to_P-tyr-network. Eccentricity, closeness, radiality, betweenness, degree, stress and centroid centrality indexes of the docking protein GRB2 in the ChAc (VPS13A_to_P-tyr)-related sub-network. The score of every index was normalized to the maximal value for every index, considered as 100%. Red columns are relative values for GRB2. Blue columns are average values. White columns are maximal values. Green columns are minimal values.
(TIFF)

Table S1 List of identified proteins in comparative analysis between control and McLeod red cell membrane.
(DOC)

Table S2 List of identified proteins displaying different degrees of tyrosine phosphorylation in control and chorea-acanthocytosis red cell membrane.
(DOC)

Table S3 List of identified proteins displaying different degrees of tyrosine phosphorylation in control and McLeod red cell membrane.
(DOC)

Appendix S1 Network of proteins connecting, by means of shortest paths, Xk to proteins whose phosphorylation in tyrosine was found altered in RBCs from McLeod patients.
(TXT)

Appendix S2 List of all shortest paths connecting Xk to proteins whose phosphorylation in tyrosine was found altered in RBCs from McLeod patients.
(TXT)

Appendix S3 Network of proteins connecting, by means of shortest paths, chorein to proteins whose phosphorylation in tyrosine was found altered in RBCs from ChAc patients.
(TXT)

Appendix S4 List of all shortest paths connecting chorein to proteins whose phosphorylation in tyrosine was found altered in RBCs from ChAc patients.
(TXT)

Appendix S5 Network cluster of proteins linking DUSP13 to proteins found de-phosphorylated in tyrosine in RBCs from McLeod patients.
(TXT)

Appendix S6 Network of proteins including Xk and all proteins whose phosphorylation was found altered in RBCs from McLeod patients, expanded to the first neighbor (FN).
(TXT)

Appendix S7 Network of proteins including chorein and all proteins whose phosphorylation was found altered in RBCs from ChAc patients, expanded to the first neighbor (FN).
(TXT)

Appendix S8 Network derived form fusion of Appendix S1 and Appendix S6 McLeod networks.
(TXT)

Appendix S9 Network derived form fusion of Appendix S3 and Appendix S7 ChAc networks.
(TXT)

Appendix S10 Connected network derived from the intersection between Appendix S8 and Appendix S9 networks. This network only includes proteins relevant to both McLeod and ChAc RBCs phenotypes.
(TXT)

Appendix S11 Network as in Appendix S10, but reduced to include only proteins having both centroid and betweenness centrality indexes over the total network average.
(TXT)

Appendix S12 Network as in Appendix S11, but reduced to include only proteins having gene ontology (GO) attributes in the domains: erythrocyte development; neurogenesis (shown in Figure 5).
(TXT)

Appendix S13 Table of protein attributes for Appendix S1 network in the categories: Approved Name, Name Aliases, Chromosome, Entrez Gene ID, Kinases, MLS_PY, Phosphatases.
(TXT)

Appendix S14 Table of protein attributes for Appendix S1 network in the category: Node centrality indexes.
(TXT)

Appendix S15 Table of attributes for Appendix S1 network in the category: Network centrality indexes.
(TXT)

Appendix S16 Table of protein attributes for Appendix S3 network in the categories: Approved Name, Name Aliases, Chromosome, Entrez Gene ID, Kinases, MLS_PY, Phosphatases.
(TXT)

Appendix S17 Table of protein attributes for Appendix S3 network in the category: Node centrality indexes.
(TXT)

Appendix S18 Table of attributes for Appendix S3 network in the category: Network centrality indexes.
(TXT)

Appendix S19 Table of protein attributes for Appendix S10 network in the category: Node centrality indexes.
(TXT)

Appendix S20 Table of attributes for Appendix S10 network in the category: Network centrality indexes.
(TXT)

Appendix S21 Table of protein attributes for Appendix S10 network in the categories: GO BIOLOGICAL_PROCESS.
(TXT)

Appendix S22 Table of protein attributes for Appendix S10 network in the categories: Approved Name, Kinases, Phosphatases, ChAC_PY, MLS_PY, Bottom_acanthocytes, Betweenness, Centroid, Closeness, Eccentricity, Node degree, Radiality, Stress.
(TXT)

Appendix S23 Table of protein attributes for Appendix S11 network in the categories: Approved Name, GO BIOLOGICAL_PROCESS.
(TXT)

Appendix S24 Table of protein attributes for Appendix S12 network (shown in Figure 5) in the categories: Approved Name, Kinases, Phosphatases, ChAC_PY, MLS_PY, Bottom_acanthocytes, Betweenness, Centroid, Closeness, Eccentricity, Node degree, Radiality, Stress.
(TXT)

Appendix S25 Table of protein attributes for Appendix S12 network (shown in Figure 5) in the categories: in vitro evidence of interaction, in vivo evidence of interaction, PubMed reference.
(TXT)

Author Contributions

Performed the experiments: CT AS AP GS. Analyzed the data: CT AS AP GS LDF CL. Wrote the paper: LDF CL. Conceived and designed the study: LDF CL. Identified the patients and provided the blood samples: AD BB RHW HHJ MD SM.

References

1. Walker RH, Danek A, Dobson-Stone C, Guerrini R, Jung HH, et al. (2006) Developments in neuroacanthocytosis: expanding the spectrum of choreatic syndromes. Mov Disord 21: 1794–1805.
2. Danek A, Walker RH (2005) Neuroacanthocytosis. Curr Opin Neurol 18: 386–392.
3. Danek A, Jung HH, Melone MA, Rampoldi L, Broccoli V, et al. (2005) Neuroacanthocytosis: new developments in a neglected group of dementing disorders. J Neurol Sci 229–230: 171–186.
4. Rampoldi L, Danek A, Monaco AP (2002) Clinical features and molecular bases of neuroacanthocytosis. J Mol Med 80: 475–491.
5. Dobson-Stone C, Danek A, Rampoldi L, Hardie RJ, Chalmers RM, et al. (2002) Mutational spectrum of the CHAC gene in patients with chorea-acanthocytosis. Eur J Hum Genet 10: 773–781.
6. Mohandas N, Gallagher PG (2008) Red cell membrane: past, present, and future. Blood 112: 3939–3948.
7. De Franceschi L, Biondani A, Carta F, Turrini F, Laudanna C, et al. (2008) PTPepsilon has a critical role in signaling transduction pathways and phosphoprotein network topology in red cells. Proteomics 8: 4695–4708.
8. Siciliano A, Turrini F, Bertoldi M, Matte A, Pantaleo A, et al. Deoxygenation affects tyrosine phosphoproteome of red cell membrane from patients with sickle cell disease. Blood Cells Mol Dis 44: 233–242.
9. Pantaleo A, De Franceschi L, Ferru E, Vono R, Turrini F (2010) Current knowledge about the functional roles of phosphorylative changes of membrane proteins in normal and diseased red cells. J Proteomics 73: 445–455.
10. De Franceschi L, Turrini F, del Giudice EM, Perrotta S, Olivieri O, et al. (1998) Decreased band 3 anion transport activity and band 3 clusterization in congenital dyserythropoietic anemia type II. Exp Hematol 26: 869–873.
11. Olivieri O, De Franceschi L, Bordin L, Manfredi M, Miraglia del Giudice E, et al. (1997) Increased membrane protein phosphorylation and anion transport activity in chorea-acanthocytosis. Haematologica 82: 648–653.
12. Scardoni G, Petterlini M, Laudanna C (2009) Analyzing biological network parameters with CentiScaPe. Bioinformatics 25: 2857–2859.
13. Pieroni E, de la Fuente van Bentem S, Mancosu G, Capobianco E, Hirt H, et al. (2008) Protein networking: insights into global functional organization of proteomes. Proteomics 8: 799–816.
14. Ma'ayan A (2009) Insights into the organization of biochemical regulatory networks using graph theory analyses. J Biol Chem 284: 5451–5455.
15. Patterson KI, Brummer T, O'Brien PM, Daly RJ (2009) Dual-specificity phosphatases: critical regulators with diverse cellular targets. Biochem J 418: 475–489.
16. zur Hausen JD, Burn P, Amrein KE (1997) Co-localization of Fyn with CD3 complex, CD45 or CD28 depends on different mechanisms. Eur J Immunol 27: 2643–2649.
17. Hsu KL, Fan HJ, Chen YC, Huang YS, Chen CH, et al. (2009) Protein kinase C-Fyn kinase cascade mediates the oleic acid-induced disassembly of neonatal rat cardiomyocyte adherens junctions. Int J Biochem Cell Biol 41: 1536–1546.
18. Karur VG, Lowell CA, Besmer P, Agosti V, Wojchowski DM (2006) Lyn kinase promotes erythroblast expansion and late-stage development. Blood 108: 1524–1532.
19. Brunati AM, Bordin L, Clari G, James P, Quadroni M, et al. (2000) Sequential phosphorylation of protein band 3 by Syk and Lyn tyrosine kinases in intact

human erythrocytes: identification of primary and secondary phosphorylation sites. Blood 96: 1550–1557.
20. Kruger M, Linke WA (2011) The Giant Protein Titin: A Regulatory Node that Integrates Myocyte Signaling Pathways. J Biol Chem.
21. Candiano G, Musante L, Bruschi M, Ghiggeri GM, Herbert B, et al. (2002) Two-dimensional maps in soft immobilized pH gradient gels: a new approach to the proteome of the Third Millennium. Electrophoresis 23: 292–297.
22. Pasini EM, Kirkegaard M, Mortensen P, Lutz HU, Thomas AW, et al. (2006) In-depth analysis of the membrane and cytosolic proteome of red blood cells. Blood 108: 791–801.
23. Pasini EM, Lutz HU, Mann M, Thomas AW (2010) Red blood cell (RBC) membrane proteomics–Part II: Comparative proteomics and RBC pathophysiology. J Proteomics 73: 421–435.
24. Pasini EM, Lutz HU, Mann M, Thomas AW (2010) Red blood cell (RBC) membrane proteomics–Part I: Proteomics and RBC physiology. J Proteomics 73: 403–420.
25. Bosman GJCGM, de Franceschi L (2008) Neuroacanthocytosis-related changes in erythrocyte membrane organization and function. In: Walker RHSS, Danek A, eds. Neuroacanthocytosis syndromes II. Berlin, Germany: Springer.
26. Aittokallio T, Schwikowski B (2006) Graph-based methods for analysing networks in cell biology. Brief Bioinform 7: 243–255.
27. Chautard E, Thierry-Mieg N, Ricard-Blum S (2009) Interaction networks: from protein functions to drug discovery. A review. Pathol Biol (Paris) 57: 324–333.
28. Li X, Wu M, Kwoh CK, Ng SK (2010) Computational approaches for detecting protein complexes from protein interaction networks: a survey. BMC Genomics 11 Suppl 1: S3.
29. Kwoh CK, Ng PY (2007) Network analysis approach for biology. Cell Mol Life Sci 64: 1739–1751.
30. Faggioni G, Grassi S, Fillo S, Stefanini L, Bottini E, et al. (2006) Rapid single tube genotyping of ACP1 by FRET based amplification and dual color melting curve analysis. Mol Cell Probes 20: 27–30.
31. Nimnual AS, Taylor LJ, Bar-Sagi D (2003) Redox-dependent downregulation of Rho by Rac. Nat Cell Biol 5: 236–241.
32. Chiarugi P, Cirri P, Taddei L, Giannoni E, Camici G, et al. (2000) The low M(r) protein-tyrosine phosphatase is involved in Rho-mediated cytoskeleton rearrangement after integrin and platelet-derived growth factor stimulation. J Biol Chem 275: 4640–4646.
33. Kalfa TA, Pushkaran S, Mohandas N, Hartwig JH, Fowler VM, et al. (2006) Rac GTPases regulate the morphology and deformability of the erythrocyte cytoskeleton. Blood 108: 3637–3645.
34. De Franceschi L TC, Matte A, Bovee-Guerts PH, Brunati A, Bertoldi M, et al. (2011) Chorea-acanthocytosis related changes in erythrocyte membrane are associated with abnormal activation of Lyn kinase independent from Syk sequential phosphorylation. Blood 118: 5652–5663.
35. Jung HH, Hergersberg M, Kneifel S, Alkadhi H, Schiess R, et al. (2001) McLeod syndrome: a novel mutation, predominant psychiatric manifestations, and distinct striatal imaging findings. Ann Neurol 49: 384–392.
36. Walker RH, Danek A, Uttner I, Offner R, Reid M, et al. (2007) McLeod phenotype without the McLeod syndrome. Transfusion 47: 299–305.
37. Walker RH, Jung HH, Tison F, Lee S, Danek A (2007) Phenotypic variation among brothers with the McLeod neuroacanthocytosis syndrome. Mov Disord 22: 244–248.
38. Dobson-Stone C, Velayos-Baeza A, Filippone LA, Westbury S, Storch A, et al. (2004) Chorein detection for the diagnosis of chorea-acanthocytosis. Ann Neurol 56: 299–302.
39. Bader B, Walker RH, Vogel M, Prosiegel M, McIntosh J, et al. (2011) Tongue protrusion and feeding dystonia: a hallmark of chorea-acanthocytosis. Mov Disord 25: 127–129.
40. Rubio JP, Danek A, Stone C, Chalmers R, Wood N, et al. (1997) Chorea-acanthocytosis: genetic linkage to chromosome 9q21. Am J Hum Genet 61: 899–908.
41. Rampoldi L, Dobson-Stone C, Rubio JP, Danek A, Chalmers RM, et al. (2001) A conserved sorting-associated protein is mutant in chorea-acanthocytosis. Nat Genet 28: 119–120.
42. Gan JJ GF, Alterman RL, Cheung T, Gora-stahlberg G, Tagliati M (2011) Long-term benefit of pallidal stimulation in chorea-acanthocytosis. Neurology 76: A590.
43. Walker RH SV, Tikhonova IR, Mahajan MC, Mane S, Arroyo Muniz M, et al. (2011) Genetic diagnosis of neuroacanthocytosis disorders using exosome sequencing. Movement Disorders;(in press).
44. Olivieri O, De Franceschi L, Capellini MD, Girelli D, Corrocher R, et al. (1994) Oxidative damage and erythrocyte membrane transport abnormalities in thalassemias. Blood 84: 315–320.
45. Cline MS, Smoot M, Cerami E, Kuchinsky A, Landys N, et al. (2007) Integration of biological networks and gene expression data using Cytoscape. Nat Protoc 2: 2366–2382.
46. Shannon P, Markiel A, Ozier O, Baliga NS, Wang JT, et al. (2003) Cytoscape: a software environment for integrated models of biomolecular interaction networks. Genome Res 13: 2498–2504.
47. Dijkstra E (1959) A note on two problems in connexion with graphs. Numerische Mathematik 1: 269–227.
48. Maere S, Heymans K, Kuiper M (2005) BiNGO: a Cytoscape plugin to assess overrepresentation of gene ontology categories in biological networks. Bioinformatics 21: 3448–3449.
49. Bindea G, Mlecnik B, Hackl H, Charoentong P, Tosolini M, et al. (2009) ClueGO: a Cytoscape plug-in to decipher functionally grouped gene ontology and pathway annotation networks. Bioinformatics 25: 1091–1093.

PRELIMINARY STUDY ON ERYTHROCYTES FROM PATIENTS WITH NEURODEGENERATION WITH BRAIN IRON ACCUMULATION (NBIA)

In the context of an international collaboration on NA syndromes we have analysed red cells from Turkish patients and their first grade relatives. Based on neurological clinical manifestations and image analysis these patients have been diagnosed of Neurodegeneration with Brain Iron Accumulation without identification of molecular defects. To our knowledge this is the first time that an analysis of red cells from patients affected by this rare disease together with their relatives has been carried out. The family tree for patient A3 and O3 is shown below.

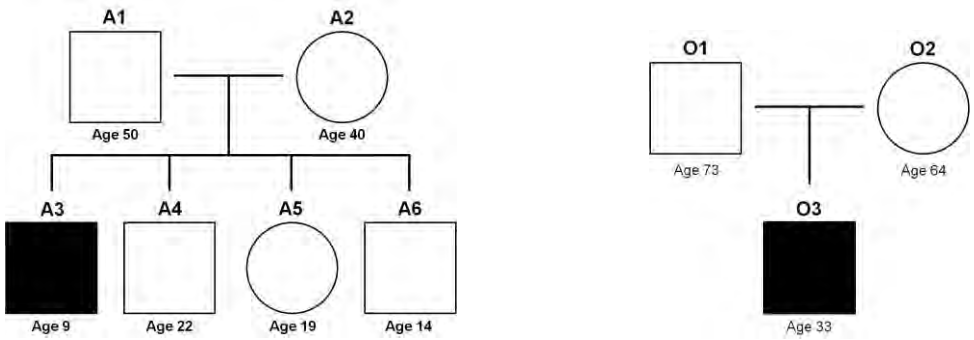

Fig. 1 *Family trees for patients A3 and O3. Age at time of analysis is indicated.*

We first evaluated whether acanthocytes might be present in patients' relatives in absence of neurological manifestations.

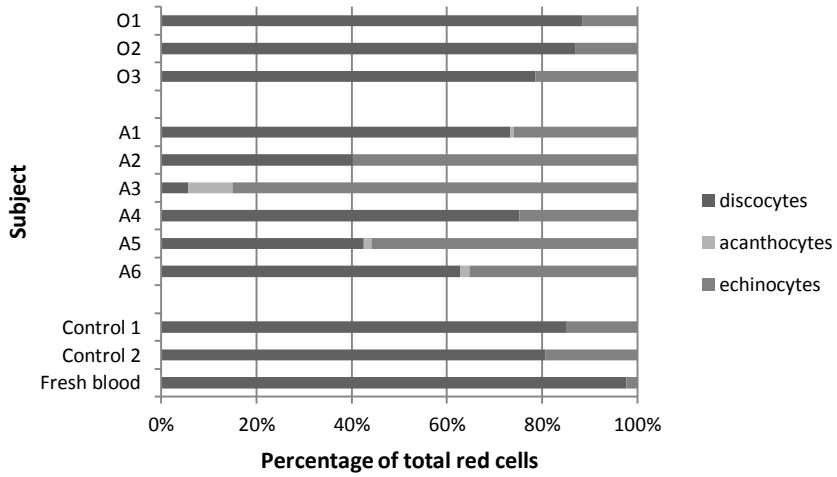

Fig. 2 *Red cell morphology in samples from family O, A and controls, data are presented as percentage of total red cells. Controls 1 and 2 have been shipped with patients' samples. A3 and O3 are the two patients; O1/A1 and O2/A2 are respectively fathers and mothers of the patients; A4, A5, A6 are unaffected siblings.*

We analysed red cell morphology by phase contrast microscopy. We divided red cells into the following populations: discocytes, echinocytes and acanthocytes. Echinocyte population includes cells with very different shapes going from slightly crenated cells to sphero-echinocyes, for the sake of simplicity we did not further classify such cells.

As shown in Fig. 2, patient O3 and his family did not present acanthocytes and the amount of echinocytes was comparable to that observed control samples. However, the percentage of echinocyte was slightly higher in patient sample compared to his parents.

Samples from family A differed from those of family O. Patient (A3) showed more than 80% abnormally shaped red cells, with ~5% acanthocytes. The mother (A2) and two siblings (A5 and A6) showed some acanthocytes as well as high numbers of echinocytes. Of note that the samples with higher values of echinocytes, that are nowadays considered artifactual cells due to manipulation of the samples, were also the ones showing acanthocytes. .

We then studied red cells from these patients by immunofluorescence assay with confocal microscopy to quantitate total internal fluorescence after staining with specific antibodies against the integral membrane protein band 3, the cytoskeleton component β-spectrin and the membrane associated protein stomatin.

We fixed and permeabilized cells as previously reported by Matte et al. [50]. We stained control cells with a rabbit polyclonal antibody against band 3 membrane domain (K2N6B). These cells were mixed with red cells from all samples which were probed with either mouse antibodies against band 3 cytoplasmic domain (B3-136, Sigma-Aldrich, St. Louis, USA), β-spectrin (4C3, Acris, Herford, Germany) or stomatin (GARP-50, kindly provided by Prof. R. Prohaska). After reaction with Alexa 633 anti-rabbit and Alexa 488 anti-mouse, we mounted red cells on poly-L-lysine coated coverslips and took Z-stacks of the appropriate thickness with a Leica TCS SP5 II confocal microscope (63x, 1.2 NA objective, Leica Microsystems, Wetzlar, Germany).

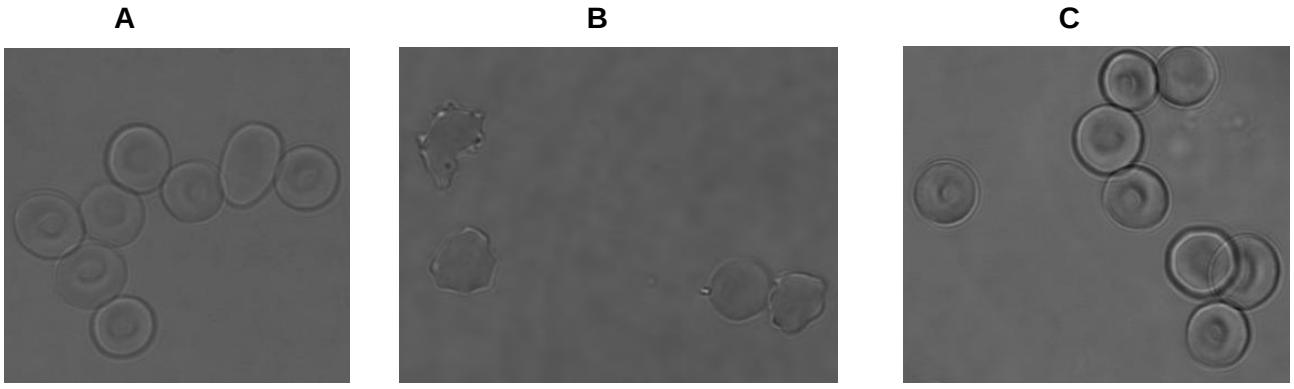

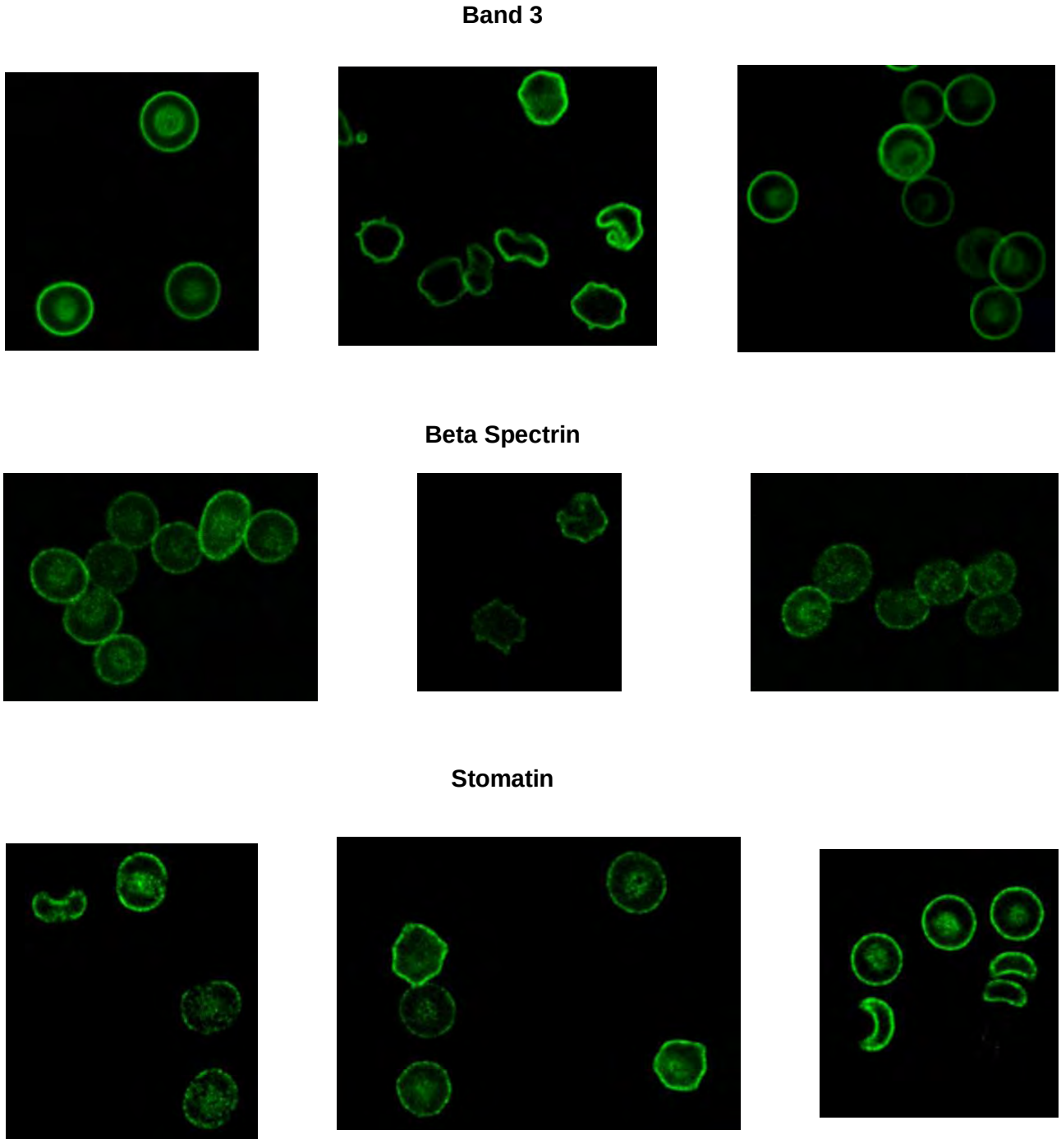

Fig. 3 *Confocal images of red cells from patient O3 (A), A3 (B) and healthy Control (C). Staining has been carried out as described in the text. All images have been taken with the same settings and magnification.*

Z-stacks were post-processed with ImageJ (version 1.45, NIH, Bethesda, USA) to quantify total internal fluorescence for each cell. Total internal fluorescence for band 3 membrane domain was used as an internal control to correct data values grouped by cell shape.

We designed the experiments to avoid artifacts due to slide-to-slide variations and detection fluctuations, allowing us to discriminate red cells by shape. The major limitations of this

approach are the low throughput of confocal microscopy and the time-consuming post-processing of the images. Although we analysed several microscopic fields using this strategy, we could not obtain enough data to carry out statistical analysis for all the different groups. Since all the cells in a single sample share the same genetic background, we compared total red cell population for each sample with the two controls.

A

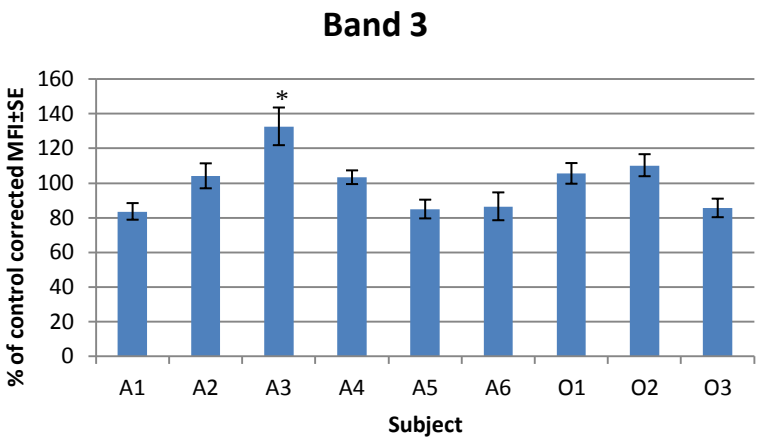

B

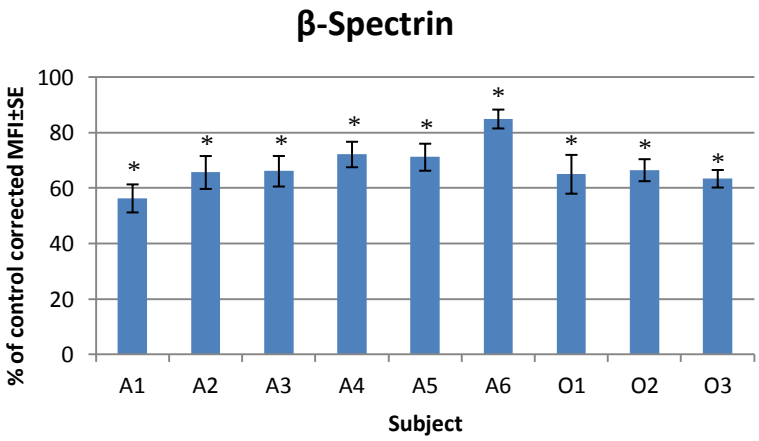

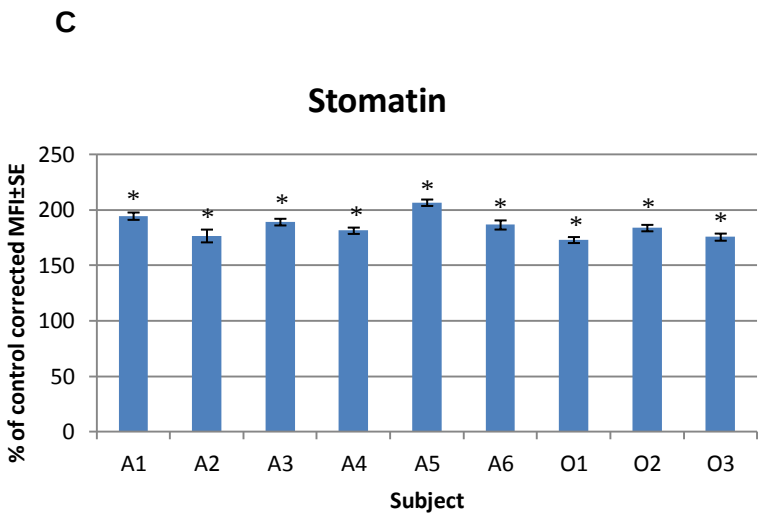

Fig. 4 *Confocal microscopy quantitation of (A) Band 3, (B) β-Spectrin and (C) Stomatin. Mean fluorescence intensity per cell, percentage of control ± SE; ANOVA and Tukey's test. * p<0.05.*

Interestingly band 3 fluorescence for patient A3 resulted significantly higher than control, whereas band 3 fluorescence was significantly lower in patient O3 and samples A1 and A5 compared to controls. We did not find any correlation between abnormal red cell shape and band 3 fluorescence levels. Otherwise, we found that β-spectrin fluorescence was significantly lower in all samples from the two families compared to normal controls. Stomatin fluorescence was significantly higher in all the analyzed samples compared to controls.

In order to discriminate whether the differences in protein fluorescence might be related to either differences in the amount of protein or in the accessibility of protein epitope to specific antibodies in fixed red cells, we carried out immuno-blot analysis of patients' and relatives' red cells compared to controls. No major differences in either band 3 or beta spectrin amount were present. Thus, the differences in protein fluorescence detected by confocal microscopy might be related to conformational changes/epitope availability of these proteins more than differences in protein abundance. It is of interest to note that we found differences in the degradation pattern of band 3 in patients red cells, which were not possible to correlate with the disease or the family lineage.

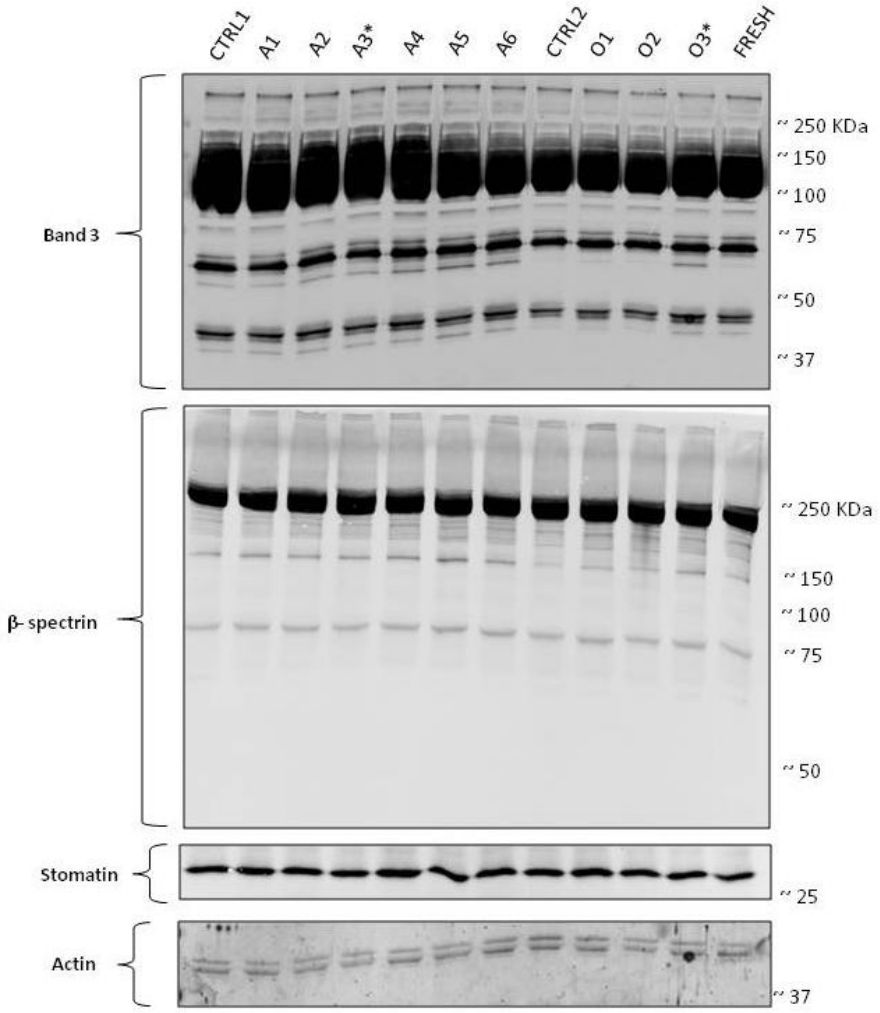

Fig. 5 *Immunoblot analysis with specific antibodies against respectively band 3 (B3-136), β-spectrin (4C3), stomatin (GARP-50). Actin was used as loading control (A-2066, Sigma-Aldrich, St. Louis, USA). Proteins were quantified by Biorad Protein Assay (Biorad, Hercules, USA), solubilized with Laemmli Buffer and 5 or 10 µg for each lane were loaded.*

These preliminary data on NBIA patients and their families suggest that perturbation of membrane organization is not only limited to the homozygous state, but it is also present in a different grade in the carriers. The immunofluoresence data combined with the evidences that there are not significant differences in the abundance of band 3 and β-spectrin in patients red cells compared to controls, suggest that possible changes in protein epitope accessibility to specific antibodies might sustain this discrepancy.

Future studies will be designed to further characterize red cells from NBIA patients also in the view of our recently reported data on different tyrosine-phosphorylation state of red cell membrane proteins from patients with Chorea-Acanthocytosis and McLeod Syndrome. Proper genetic analysis of the patients studied will be also carried out in order to better understand the genotype-phenotype connection in red cells from NBIA patients.

PERFORMANCE OF A NOVEL SIEVING MATRIX OF POLY(VINYL ALCOHOL)/ACRYLAMIDE COPOLYMER IN ELECTROPHORETIC SEPARATIONS OF HIGH MOLECULAR WEIGHT PROTEINS FROM RED CELL MEMBRANE

Carlo Tomelleri [1°] , Marcella Chiari [2] , Alessandro Matte' [1°] , Laura Sola [2] , Franco Turrini [3] , Lucia De Franceschi [1]

[1] Department of Medicine, University of Verona, Verona, Italy

[2] Istituto di Chimica del Riconoscimento Molecolare, CNR, Milan, Italy

[3] Department of Biology, Genetic and Chemical Medicine, University of Torino, Torino, Italy

[°] These Authors have equally contributed to the paper

Corresponding Author:
Dr. Marcella Chiari
Istituto di Chimica del Riconoscimento Molecolare, CNR
Via Mario Bianco, 9
20131 Milano, Italy
E-mail: marcella.chiari@icrm.cnr.it
Tel +39 02 28500035
Fax +39 02 28901239

ABBREVIATIONS

PAA/PA polyacrylamide; HMW High Molecular Weight; APS, ammonium persulfate; Cymal 6, 6-cyclohexyl β-D-maltoside; LM, low melting; CWS, choline washing solution; LB, lysis buffer; DS, destaining solution;

Key words: Macroporous sieving matrix, agarose, polyacrylamide, High molecular weight proteins, separation, two dimensional electrophoresis, proteomics

ABSTRACT

The analysis of high molecular weight (HMW) proteins from complex mixtures is still a challenge in proteomic investigations. Here, we developed a novel hydrogel for electrophoretic separation of HMW proteins. The new sieving matrix is formed by copolymerization of polyvinyl alcohol bearing olefinic moieties (allyl PVA) with acrylamide and bisacrylamide. By inducing gelation of polyacrylamide in the presence of variable amounts of allyl PVA polymer, it is possible to control and vary the average gel porosity. This gel is easy to produce and handle and offers the advantage of being highly mechanically resistant and macroporous. The new matrix was tested in mono- and bi-dimensional gels for separating complex mixture of proteins from red cell membranes extracted with different detergents. New proteins, separated within this matrix, were identified both by mass spectrometry and immunoblot analysis using specific antibodies.

Resolution of oxidized red cell membranes, which was limited in standard polyacrylamide gels, was greatly improved by the new allyl PVA based gels allowing a better separation of proteins ranging in size between 97 and 279 kDa. These data indicate the allyl-PVA new matrix as novel feasible tool in routine application for analysis of HMW proteins in cell biology.

1. INTRODUCTION

The analysis of high molecular size proteins is still only partially covered by the methodological strategies presently available in proteomics as demonstrated by the small number of studies on high molecular weight (HMW) proteins in various cell models [1-3].

In the past 20 years there have been many attempts to optimize the composition of protein sieving matrices to improve the electrophoretic resolution of high molecular weight proteins using classical polyacrylamide or agarose and agarose related polymers [1-4].

Although polyacrylamide pore size can be increased by varying bisacrylamide concentration, this is not the best approach for separating HMW proteins [5, 6]. Agarose and related polymers have shown some advantages over polyacrylamide in the resolution of HMW proteins such as myosin heavy chains (200 kDa), dystrophin (400 kDa), tyroglobulin (330 kDa), spectrins (250 kDa) or von Willebrand factor [3, 7-10]. However, agarose and related polymers have some major limitations in routine application such as the equilibrium condition, the mechanical stability, the long working time of the procedure. In a previous work we have synthesized and characterized covalently cross-linked, mixed-bed agarose-polyacrylamide gels for electrophoresis formed by copolymerization of allyl modified agarose with acrylamide [3]. The cross linking mechanism enabled the formation of gels with higher porosity and elasticity. However, being weekly cross-linked, these gels tend to considerably overswell in buffer and, as a consequence, their application as SDS-sieving matrices is limited.

This work reports on the development of a hydrogel for electrophoretic separation of high molecular weight proteins characterized by high mechanical stability, optimal swelling properties and soft rubberlike behavior. This hydrogel is formed by a combination of polyvinyl alcohol, bearing olefinic moieties, physically entangled and covalently cross-linked with polyacrylamide and bisacrylamide (BIS) which reinforces the cross-linking of the two polymers thus strengthening its mechanical strength.

This new gel was applied to the study of HMW proteins from red cells. The resolution of high molecular weight proteins, separated by mono and bi-dimensional gel electrophoresis using different strategy to extract proteins from red cells, was the parameter considered in this study. The new hydrogel is an excellent and easy to handle matrix to study HMW proteins, suitable for application in classical proteomic techniques such as tryptic digestion, peptide extraction and identification or immunoblot analysis with specific antibodies.

2 MATERIALS AND METHODS

2.1 Chemicals

NaCl, KCl, Na 2 HPO 4 , Na 3 VO 4 , KH 2 PO 4 , MgCl 2 , NH 4 HCO 3, MOPS, TRIS, choline chloride, benzamidine, β -mercaptoethanol, glycine, bromphenol blue, trypsin, sodium dodecyl sulfate (SDS), 6-cyclohexylhexyl β-D-maltoside (Cymal-6), Nonylphenol ethoxylate (Tergitol type NP40) and glycerol were purchased from Sigma/Aldrich (St Louis, MO, USA); urea, thiourea, dithiotreithol (DTT), iodoacetamide, tri-n-butylphosphate, trifluoroacetic acid and α -cyano-4-hydroxy cynnamic acid were from Fluka (Buchs, Switzerland); CHAPS and low melting (LM) agarose were from USB (Cleveland, OH, USA); acetone, methanol, and acetonitrile were from Baker (Deventer, The Netherlands); protease inhibitor cocktail tablets were from Roche (Basel, Switzerland); Immobiline DryStrip 7 cm pH 4-7 gels, IPG buffer pH 3-10, Triton X-100, ECL-Plus, Percoll were purchased from GE Healthcare (Little Chalfont, UK); 40% Acrylamide/Bis Solution, 37.5:1 was from BIO-RAD (Hercules, CA, USA); Immobilon Western Chemiluminescent HRP Substrate was from Millipore (Billerica, MA, USA).

2.2 Synthesis of Allyl Polyvinyl Alcohol (Allyl PVA)

Three grams of PVA, 99% hydrolized, with a Mw ranging from 89000-98000 Da, were dissolved in 70 mL of water at boiling temperature. To the solution, cooled at room temperature, 30 mL of 1M NaOH solution are added, followed by the addition of 66 mg of sodium borohydride and of 3.2 mL of allylglycidyl ether (Figure 1A). The reaction was stirred overnight at room temperature. The solution was then diluted 1:1 with milliQ water and neutralized with 1 N hydrochloric acid; finally it was dialyzed against water and freeze-dried to recover the polymer.

2.3 Gel preparation

An allyl PVA stock solution (5% w/v) was prepared by dissolving the polymer powder in water at boiling temperature; the stock solution was diluted to a final concentration of 1% with a solution of PAAA/BIS, (7% T, 0.5% C in 375 mM Tris, pH 8.9, 0.1% SDS). TEMED (0.05% w/v) and APS (0.015% w/v) were added to initiate the polymerization. Polyacrylamide control gel (PA) (7% T, 2.6% C) was cast using a classical procedure [3, 11-14]. In both gels monomer solutions were polymerized for 2h at room temperature before overlaying the stacking gel (3% T, 1.3% C in 0.125 M Tris-HCl buffer, pH 6.8).

2.4 Red cell membranes preparation

Whole blood was centrifuged at 2,500 g at 4°C in order to remove plasma, filtered through cotton to remove white cells, and rinsed three times with choline washing solution (CWS: 150 mM choline, 1 mM MgCl 2 , 10 mM Tris-MOPS pH 7.4 at 4°C). Packed red cells were lysed in ice cold phosphate lysis buffer (LB: 5 mM Na 2 HPO 4 pH 8.0, containing: protease inhibitor cocktail tablets, 3 mM benzamidine, 1 mM Na 3 VO 4) [13, 14]. Red cell ghosts were washed several times in LB to obtain white membranes and used for mono and bi-dimensional electrophoresis. The use of human samples was approved by the Ethical Committee of Verona University and the informed consent of all healthy participating subjects was obtained.

2.5 Mono- and bi-dimensional analysis

Monodimensional electrophoresis (1DE). Red cell ghosts were solubilized in the standard sample buffer (SB: 50 mM Tris, pH 6.8, 2% SDS, 10% glycerol, 100 mM β-mercaptoethanol, few grains of bromophenol blue) either alone or with different detergents and chaotropes (see Results section 3.2 and Figure 1B). The solubilized proteins were then separated by mono-dimensional electrophoresis using a Mini-Protean II dual slab gel cell (BIO-RAD), 7 cm long, 5.5-6.5 cm wide 1.5 mm thick.

Gels were either stained with Colloidal Coomassie or transferred to nitrocellulose membranes for immuno-blot analysis with specific antibody against β-spectrin (Acris, Herford Germany) as previously described [14].

Bi-dimensional electrophoresis (2DE). Red cell ghosts were solubilized using different protocols as reported in Table 1, starting from the standard solubilization method (protocol A1) for 2DE of RBC membrane ghosts [11, 14]. Samples underwent to a delipidization step as previously described [11, 14]. The delipidized samples were then dried under nitrogen flow and solubilized by vigorous shacking in 40 mM TRIS/HCl pH 8.8 buffer containing 7M urea, 2M thiourea, 2.7% IPG buffer, 3% Cymal-6, 1% DTT for 8 h at 25°C.

IPG strips were passively rehydrated overnight at 20°C with the solubilized samples; focusing was carried out on Ettan IPGphor II (GE Healthcare, Little Chalfont, UK). The isoelectrofocusing (IEF) in pH 4-7 strips (7 cm) was 50V for 3h, 100V for 3h, 200V for 3h, 500V for 2h, 1000V for 2h, 3000V for 2h and 4500V to reach a total of 32000V/h; while in non-linear pH 3-10 strips (13 cm) the IEF was 50V 3h, 100V 3 h, 300V 3 h, 1000V 2 h, 2000V 2 h, 4500V to reach a total of 60000V/h. After focusing, both types of IPG strips were reduced using 50 mM TRIS/HCl pH 8.8, 6 M urea, 30% v/v glycerol, 2% SDS, 1% DTT for 15 min at 30°C and then alkylated with 2.5% iodoacetamide dissolved in 50 mM TRIS/HCl pH 8.8, 6 M urea, 30% v/v glycerol, 2% SDS, for 15 min. This two reactions were carried out both, at room temperature and at 30°C.

Strips were included in 0.5% agarose stacking gel on second dimension gels for electrophoresis whic was carried out as stated in Materials and methods section 2.4 for the pH 4-7 (7 cm) strips, while we used the HoeferSE 600 Ruby (Amersham) gel cell apparatus for the 13 cm gels (18 cm wide and 0.75 mm thick). Proteins were visualized by double staining procedure: first colloidal Comassie then silver staining [11, 14].

2.6 Image analysis and protein identification

1DE gels underwent image analysis using Quantity One (BIO-RAD, Hercules, CA, USA) while 2DE gels were analyzed using both ImageJ (NIH, USA) and 2D-Platinum software (version 5.0 Amersham-Bioscience). Bands (see numbered bands in Figure 1B, lane 4) were excised from the colloidal Coomassie stained gels for mass spectrometry and were destained in DS (50% Acetonitrile, 5 mM NH 4 HCO 3), dehydrated in 100% Acetonitrile and digested overnight at 37°C with 20 µ l of trypsin solution (0.01 mg/ml trypsin, 5 mM NH 4 HCO 3) [11, 14]. Mass spectrometry was performed using a Tofspec SE (Micromass, Manchester, UK) equipped with a delayed extraction unit. for mass spectrometry analysis and were destained in DS (50% Acetonitrile, 5 mM NH 4 HCO 3), dehydrated in 100% Acetonitrile and digested overnight at 37°C using 20 µ l of trypsin solution (0.01 mg/ml trypsin, 5 mM NH 4 HCO 3) [11, 14]. Peptide desorption was achieved using a laser wavelength of 337 nm, and mass spectra were obtained in the reflectron mode in the mass range 800-4000 Da. Peptide solutions were mixed 1:1 v/v with a saturated alpha-cyano-4 hydroxycinnamic acid solution containing 40% acetonitrile and 0.1% trifluoroacetic acid (v/v). External calibration was performed using fragment ions from standard peptides: adrenocorticotropic hormone 18-39 and angiotensin I. Each mass spectrum was generated by accumulating data from 100-120 laser pulses. Database searches of peptide masses were performed using the search program “Mascot, Peptide Mass Fingerprint” (available at http://www.matrixscience.com) using the following search criteria: taxa Homo sapiens protein molecular mass range from 10 to 300 kDa, trypsin digest, monoisotopic peptide masses, one missed cleavage by trypsin and a mass deviation of 100 ppm allowed in the NCBI database searches [11, 12, 14].

3 RESULTS AND DISCUSSION

3.1 Polyvinyl alcohol Polyacrylamide gel

The pore size of a polyacrylamide gel is determined by the total amount of acrylamide and cross-linker: the lower the total monomer and cross-linker concentration, the higher the pore size is. However, gels with low cross linking density are soft and prone to change their swelling degree. By inducing gelation of polyacrylamide in the presence of variable amounts of a pre-formed polymer, it is possible to control the average gel porosity and to vary its pore size in a wide range. Righetti et al. have exploited this concept to produce “macroporous” gels back in 1995 [15]. According to their view, if constraints to chain motion are imposed during gel polymerization, large pores are formed. It was suggested that the presence of preformed polymers in the gelling solution forces the growing chains to “laterally aggregate” via inter-chain hydrogen bond formation. Upon consumption of pendant double bonds, such bundles chains are frozen in the three-dimensional space by permanent cross-links.

In a previous work, we suggested that polymerization of linear acrylamide in the presence of acryl modified agarose induces formation of a macroporous gel due to combination of hydrogen bonds between agarose chains and cross-linking of acrylamide through a macromolecular cross-linker. The gel obtained was successfully used in two dimensional electrophoresis to separate large proteins. However, several drawbacks have hampered its widespread use: first of all, the agarose/polyacrylamide mixed bed must be cast above agarose gelling temperature to prevent gelation. In addition the absence of bisacrylamide leads to significant changes in gel swelling during staining and post processing. In an effort to overcome such drawbacks, a new system is here proposed, based on the copolymerization of acrylamide with an allyl derivatized polyvinyl alcohol macromonomer in the presence of bisacrylamide. Each macromonomer bears a number of allyl groups pending from the backbone. It is sufficient that, at least, one of them reacts with acrylamide to promote the covalent binding of the two polymers. This new gel, comprising void regions separated by highly cross-linked chains, is easy to produce and handle and offers the advantage of being highly mechanically resistant and macroporous. Its unique structure results from physical entanglement of the two polymer networks stabilized by the covalent cross-linking. In fact, the insertion of allyl moieties pending from PVA to the growing chains of polyacrylamide together with inter-chain hydrogen bonds established immediately before and during acrylamide gelation is responsible for the formation of thicker gel fibers. This mechanism of chain aggregation makes the gel pore size insensitive to temperature and urea, allowing the use of the system in a broader range of conditions.

3.2 Monodimensional electrophoresis: high molecular weight protein resolution and identification from red cell membrane

In order to evaluate the performance of the new matrix, red cells were used as a model since their membrane organization is well known and has been previously used as a reference system in the development of protein separation strategies [16, 17]. Figure 1B shows a typical separation of red cell membranes in the PA gel (10%T- 2.6% C, left panel) compared to that obtained in allyl PVA copolymer gel (1% PVA-7% T-0.5% C, right panel).

PA and allyl PVA gels were run side by side and analyzed to detect the resolved bands. In allyl PVA gels, proteins located between 97 and 240 kDa displayed higher mobility and better resolution. In particular, allyl PVA provided an higher number of bands for proteins with Mw from 160 to 240 kDa, or higher than 240 kDa. The increased pore size in allyl PVA gels allowed to improve the separation of the HMW proteins while maintaining acceptable handling properties.

Since previous studies have shown that a treatment with the nonionic detergent Triton-X100 favored the separation between membrane proteins and cytoskeleton network (formed by the α-β spectrins and actins) [18], additional detergents were added to the sample buffer to solubilize red cell membrane ghosts before separation by mono-dimensional electrophoresis. Several nonionic detergents were tested such as Triton X-100, NP40 as well as glycol-based detergents (Brji-56 and -96 detergents) [17, 19-23].

The best results in terms of resolution, in particular for proteins with molecular weight between 240 and 160 kDa (Figure 1B, C), were obtained with a combination of Triton-X100 (1%) with Cymal-6 (1%), a glycosidic detergent. It's possible that this detergent formulation leads to optimal denaturation of HMW proteins, avoiding possible sticking that could occur while exposing hydrophobic surfaces during unfolding of proteins.

The possible synergic effect of detergents and chaotropes to facilitate HMW protein unfolding was also evaluated. However, addition of 2M or 8 M urea to the Triton-X100 (1%) Cymal-6 (1%) solubilization buffer, did not significantly modify mobility and resolution (Figure 1B, C), thus indicating that a complete denaturation was already obtained in the presence of detergents.

After electrophoresis, proteins were identified both by mass spectrometry and immunoblot analysis using specific antibodies. Ten bands, excised from allyl PVA gel (Figure 1B, lane 4), were destained (in DS: 50% Acetonitrile, 5 mM NH 4 HCO 3), dehydrated in 100% acetonitrile and digested overnight at 37°C with 20 µ l of trypsin solution (0.01 mg/ml trypsin, 5 mM NH 4 HCO 3). As shown in Table 2 various HMW proteins were identified, such as the inositol triphosphate receptor type 3 (ITPR3, Mw 304 KDa) or the alpha spectrin chain (SPTA1, Mw 280 KDa). Cystic fibrosis transmembrane conductors regulator CFTR, previously detected in red cells by functional test (immunoblot analysis with specific antibody and by combination of atomic force microscopy with quantum-dot labeled CFTR antibodies) was also found [24-26]).

Palladin, an interesting and still partially unknown protein in red cells, involved in organization of actin based cytoskeleton structure [27-29], was highlighted by running electrophoresis with this new separation matrix. Furthermore one protein containing the armadillo repeat domain (ARMC4) was identified. The interaction between ARMC4 and prolin-rich domain proteins promotes proteasomal-dependent degradation of cytoskeletal components in other cell types [30, 31]. For example, α -spectrin, a component of cytoskeleton contained in red cells, has a proline-rich domain that might interact with proteins containing the ARCM4, possibly participating in ubiquitination processes. Since red cells survive long time in circulation without the possibility of new protein synthesis in response to different stress (such as oxidative or shear stress in microcirculation), the "ubiquitin/proteasome dependent" or the "ubiquitin/ proteasome independent" proteolysis might represent a very interesting and still unknown element in red cell homeostasis. Finally membrane associated protein such as Rab GTPase, recently described as partecipating in red cell membrane-cytoskeleton organization [32], were identified.

In a second time, the transfer of proteins, separated in allyl PVA gels to a nitrocellulose membrane for immunoblot analysis was investigated. Considering that spectrins represent 25-30% of total red cell membrane proteins and are organized in tetramers and high order oligomers, β-spectrin was chosen as a model to carry out this study. Samples were run in the two gels using both, reducing and not reducing conditions, so to detect β-spectrin as monomers and high order oligomers; gels were both stained with Colloidal Coomassie (Figure 2A) and transferred to nitrocellulose membrane utilizing a buffer containing 5% methanol. As shown in Figure 2B , proteins were efficiently transferred to nitrocellulose membrane and detected by specific anti β-spectrin antibody. The results of Fig 1 and 2 indicate that the porosity of the allyl PVA gel allows the identification of resolved HMW proteins by two different methodological approaches: mass spectrometry and immunoblot analysis.

3.3 Separation of membrane proteins from red cells exposed to oxidative stress

Since the oxidative damage plays an important role in shortening red cell survival in the peripheral circulation, normal red cells were exposed to diamide (20 mM in a buffer containing: 10 mM NaCl, 140 mM KCl, 1 mM MgCl2, 10 mM glucose, 2.5 mM K-phosphate), a cysteine specific thiol oxidizer [12]. As shown in Figure 3, the resolution of diamide oxidized red cell membranes was limited in standard PA gels, while allyl PVA gels allowed a better separation of proteins located between 121 and 279 kDa (Figure 3 A and B). When the diamide oxidized red cell ghosts were solubilized in presence of the thiol-direct reagent N-ethylmaleimide (NEM), an alkylating reagent that blocks cysteine residues in their oxidized or

reduced state, the quality of protein separation in allyl PVA gels compared to that obtained in standard PA was further improved.

3.4 Bi-dimensional electrophoresis

Bi-dimensional analysis of red cell membrane proteins using commercial IPG strips (non-linear pH range 3-10 or pH range 4-7, 4% T, 3% C) was carried out using either allyl PVA or PA gels in the second dimension (Figure 4). Starting from a protocol previously developed for 2D electrophoresis of red cell membrane in PA gel (protocol A of Table 1) different other protocols were evaluated to improve HMW protein separation from red cell membrane [3, 14]. As shown in Table 1, the combination of different detergents was tested based on the number of detectable spots in the 2D maps [17, 19-23] and protocol D4 was found to be the most efficient one (Table 1). Since the red cell membrane underwent through a delipidization step before 2DE analysis, we did not expect to observed the integral membrane protein band 3 in the 2D maps of red cell membrane in agreement with a previous report by Candiano et al. [33]. The 2D maps obtained with allyl PVA allowed the resolution of reference protein as actin and showed well defined spots in the range from 97 to 240 kDa, while the PA 2D map showed only smears and unresolved spots (pH 3-10 strips, Figure 4A), The differences in the 2D maps were not related to the separation in the first dimension but to improvement of second dimension by PVA matrix. We then re-examined PVA matrix in bidimensional analysis of red cell membrane proteins using commercial IPG strips with shorter pH range (pH 4-7) (Figure 4B). An image analysis of both gel PVA and PAA gels allowed us to detect (i) 6 spots with molecular weight higher than 240 kDa in allyl PVA while no detectable spots were present in the conventional PA; (ii) 70 spots in in the new matrix compared to 26 in the control gels with proteins ranging from 160 to 240 kDa and (iii) 12 spots compared to 9 spots in the molecular weight range between 97 and 160 kDa (Figure 4). The proteins ranged between 160 and 240 kDa were better focused in PVA than in PAA gels. The 3D view of the selected area in the 2D maps(Figure 4 A and B) shows that allyl PVA improved the quality of second dimension allowing detection of a larger number of spots compared to conventional gels.In addition, PVA 2DE required the same working time of PA 2DE and PVA was more easy to handle than other matrix for HMW analysis such as agarose and agarose related polymers in 2DE.

4. CONCLUSIVE REMARKS

A new mixed bed gel matrix obtained by copolymerizing acrylamide and bisacrylamide with polyvinyl alcohol chemically modified by reaction with allyl glycidyl ether was used as sieving matrix in SDS gel electrophoresis. It has been demonstrated that the allyl PVA containing gel is easy to handle for both mono and bi-dimensional gel electrophoresis and is fully compatible with protein identification by mass spectrometry and immunoblot- analysis with specific antibodies. It' is also more efficient in HMW protein separation of red cells exposed to oxidative stress than standard PA matrix, suggesting its possible use in studying pathological red cells or other cell types characterized by oxidative damage.

Detergent selection for the analysis of HMW proteins from red cell membrane was carried out on empirical trial based strategy and indicates 6-Cyclohexylhexyl β-D-maltoside as the most efficient detergent in extraction of HMW proteins from red cell membrane. In conclusion, allyl PVA gels represent an excellent for the characterization and identification of HMW proteins from complex mixture of proteins such those from cell system(s).

ACKNOWLEDGEMENTS

This study was funded by grants from Istituto Italiano di Tecnologia IIT, PRIN (LDF) and Telethon grant GP07007 (LDF).

The authors have declared no conflict of interest.

REFERENCES

[1] Rabilloud, T., Two-dimensional gel electrophoresis in proteomics: old, old fashioned, but it still climbs up the mountains. *Proteomics 2002, 2, 3-10.*

[2] Miller, I., Eberini, I., Gianazza, E., Other than IPG-DALT: 2-DE variants. *Proteomics 2010, 10, 586-610.*

[3] Roncada, P., Cretich, M., Fortin, R., Agosti, S., et al., Acrylamide-agarose copolymers: improved resolution of high molecular mass proteins in two-dimensional gel electrophoresis. *Proteomics 2005, 5, 2331-2339.*

[4] Fritz JD, Swartz DR, Greaser ML. Factors affecting polyacrylamide gel electrophoresis and electroblotting of high-molecular-weight myofibrillar proteins. *Anal Biochem 1989, 180, 205-210*

[5] Wenisch, E., de Besi, P., Righetti, P. G., Conventional isoelectric focusing and immobilized pH gradients in 'macroporous' polyacrylamide gels. *Electrophoresis 1993, 14, 583-590.*

[6] Righetti, P. G., Bossi, A., Wenisch, E., Orsini, G., Protein purification in multicompartment electrolyzers with isoelectric membranes. *J Chromatogr B Biomed Sci Appl 1997, 699, 105-115.*

[7] Oh-Ishi, M., Satoh, M., Maeda, T., Preparative two-dimensional gel electrophoresis with agarose gels in the first dimension for high molecular mass proteins. *Electrophoresis 2000, 21, 1653-1669.*

[8] Oh-Ishi, M., Maeda, T., Separation techniques for high-molecular-mass proteins. *J Chromatogr B Analyt Technol Biomed Life Sci 2002, 771, 49-66.*

[9] Hirabayashi, T., Agarose isoelectric focusing for the detection of many isoforms and high molecules in muscle protein analysis. *Electrophoresis 2000, 21, 446-451.*

[10] Lombardi R, Gelfi C, Righetti PG, Lattuada A, Mannucci PM, Electroblot and immunoperoxidase staining for rapid screening of the abnormalities of the multimeric structure of von Willebrand factor in von Willebrand's disease. *Thromb Haemost. 1986, 30;55(2):246-9.*

[11] Siciliano, A., Turrini, F., Bertoldi, M., Matte, A., et al., Deoxygenation affects tyrosine phosphoproteome of red cell membrane from patients with sickle cell disease. *Blood Cells Mol Dis, 44, 233-242.*

[12] Matte, A., Low, P. S., Turrini, F., Bertoldi, M., et al., Peroxiredoxin-2 expression is increased in beta-thalassemic mouse red cells but is displaced from the membrane as a marker of oxidative stress. *Free Radic Biol Med, 49, 457-466.*

[13] Biondani, A., Turrini, F., Carta, F., Matte, A., et al., Heat-shock protein-27, -70 and peroxiredoxin-II show molecular chaperone function in sickle red cells: Evidence from transgenic sickle cell mouse model. *Proteomics Clin Appl 2008, 2, 706-719.*

[14] De Franceschi, L., Biondani, A., Carta, F., Turrini, F., et al., PTPepsilon has a critical role in signaling transduction pathways and phosphoprotein network topology in red cells. *Proteomics 2008, 8, 4695-4708.*

[15] Righetti, P.G., Macroporous gel: facts and misfatcs. *J Chromatogr A 1995, 698, 3-17.*

[16] Candiano, G., Musante, L., Zennaro, C., Bruschi, M., et al., Inhibition of renal permeability towards albumin: a new function of apolipoproteins with possible pathogenetic relevance in focal glomerulosclerosis. *Electrophoresis 2001, 22, 1819-1825.*

[17] Luche, S., Santoni, V., Rabilloud, T., Evaluation of nonionic and zwitterionic detergents as membrane protein solubilizers in two-dimensional electrophoresis. *Proteomics 2003, 3, 249-253.*

[18] Mohandas, N., Gallagher, P. G., Red cell membrane: past, present, and future. *Blood 2008, 112, 3939-3948.*

[19] Tastet, C., Charmont, S., Chevallet, M., Luche, S., Rabilloud, T., Structure-efficiency relationships of zwitterionic detergents as protein solubilizers in two-dimensional electrophoresis. *Proteomics 2003, 3, 111-121.*

[20] O'Farrell, P. H., High resolution two-dimensional electrophoresis of proteins. *J Biol Chem 1975, 250, 4007-4021.*

[21] Witzmann, F., Jarnot, B., Parker, D., Dodecyl maltoside detergent improves resolution of hepatic membrane proteins in two-dimensional gels. *Electrophoresis 1991, 12, 687-688.*

[22] Rabilloud, T., Detergents and chaotropes for protein solubilization before two-dimensional electrophoresis. *Methods Mol Biol 2009, 528, 259-267.*

[23] Rabilloud, T., Solubilization of proteins in 2DE: an outline. *Methods Mol Biol 2009, 519, 19-30.*

[24] Stumpf, A., Wenners-Epping, K., Walte, M., Lange, T., et al., Physiological concept for a blood based CFTR test. *Cell Physiol Biochem 2006, 17, 29-36.*

[25] Sprague, R. S., Ellsworth, M. L., Stephenson, A. H., Kleinhenz, M. E., Lonigro, A. J., Deformation-induced ATP release from red blood cells requires CFTR activity. *Am J Physiol 1998, 275, H1726-1732.*

[26] Sterling, K. M., Jr., Shah, S., Kim, R. J., Johnston, N. I., et al., Cystic fibrosis transmembrane conductance regulator in human and mouse red blood cell membranes and its interaction with ecto-apyrase. *J Cell Biochem 2004, 91, 1174-1182.*

[27] Liu, X. S., Li, X. H., Wang, Y., Shu, R. Z., et al., Disruption of palladin leads to defects in definitive erythropoiesis by interfering with erythroblastic island formation in mouse fetal liver. *Blood 2007, 110, 870-876.*

[28] Jin, L., Yoshida, T., Ho, R., Owens, G. K., Somlyo, A. V., The actin-associated protein Palladin is required for development of normal contractile properties of smooth muscle cells derived from embryoid bodies. *J Biol Chem 2009, 284, 2121-2130.*

[29] Alekperova, G. A., Orudzhev, A. G., Javadov, S. A., Analysis of erythrocyte and platelet membrane proteins in various forms of beta-thalassemia. *Biochemistry (Mosc) 2004, 69, 748-753.*

[30] Tomaru, K., Ueda, A., Suzuki, T., Kobayashi, N., et al., Armadillo Repeat Containing 8alpha Binds to HRS and Promotes HRS Interaction with Ubiquitinated Proteins. *Open Biochem J, 4, 1-8.*

[31] Suzuki, T., Ueda, A., Kobayashi, N., Yang, J., et al., Proteasome-dependent degradation of alpha-catenin is regulated by interaction with ARMc8alpha. *Biochem J 2008, 411, 581-591.*

[32] Kalfa, T. A., Pushkaran, S., Mohandas, N., Hartwig, J. H., et al., Rac GTPases regulate the morphology and deformability of the erythrocyte cytoskeleton. *Blood 2006, 108, 3637-3645.*

[33] Candiano, G., Musante, L., Bruschi, M., Ghiggeri, G.M., Herbert, B., Antonucci, F., Righetti, P.G. Soft immobilized pH gradients in proteome analysis: a follow up. *Electrophoresis 23, 2002, 292-297*

FIGURE LEGENDS

Figure 1. A. allyl PVA synthesis Schematic representation of Allyl-PVA synthesis. **B. Analysis of red cell membrane proteins by 1DE in PA and allyl PVA gels.** Left panel: 75 µg of red cell membrane proteins were solubilized in standard sample buffer (see section 2.4 for buffer composition) and separated in PAA gel (7%T-2.6% C), M: high molecular weight commercial marker (HiMark™ unstained protein standard, Invitrogen). Right panel: 75 µg of red cell membrane proteins were solubilized with Triton X-100 and Cymal-6 in addition to standard sample buffer and separated in allyl PVA gel (1% PVA-7% T-0.5% C). The gels were stained with Colloidal Coomassie to evaluate protein separation and analysed by image analysis software (Quantity One, BIO-RAD, Hercules, CA, USA). The selected bands for spectrometric analysis are indicated by numbers from 1 to 10. **C. Histogram of the resolved bands from PAA and PVA gels run as shown in Figure 1B.** Data are shown as means ± SD (n=3). We considered gel areas corresponding to three molecular weight ranges: > 240 kDa, 160-240 KDa, 97-160 KDa.

Figure 2. Immunoblot analysis with specific anti-beta spectrin antibody of red cell membrane proteins separated in PVA gel. Twin allyl PVA gels (1% PVA, 7% T, 0.5% C) gels were run 5h at 20 mA): one was stained with Colloidal Coomassie (left panel) and the other transferred to a nitrocellulose membrane for immunoblot analysis (right panel). The red cell membrane ghosts (75 µg) were solubilized with 1% Triton X-100 and 1% Cymal-6 added to the standard sample buffer (see also section 2.4 and Figure 1B right panel) in presence (lane 1) or absence of β-mercaptoethanol (lane 2), M: high molecular weight commercial marker (HiMark™ pre-stained protein standard, Invitrogen).

Figure 3. Analysis of diamide oxidized red cell membrane proteins by 1DE. Red cells were incubated with diamide (20 mM) in a buffer containing: 10 mM NaCl, 140 mM KCl, 1 mM MgCl 2 , 10 mM glucose, 2.5 mM K 2 HPO 4, 20 min at 37° in a shaking waterbath [10]. The oxidized red cells were then washed several times with choline washing solution and red cell membrane ghost were prepared as detailed in Materials and Methods (Paragraph 2.4) with and without N-ethylmaleimide (NEM, 100 mM). Red cell membrane (35 µg) were solubilized with standard sample buffer containing 1% v/v Triton X-100 and 1% Cymal-6.

Figure 4. 2DE gel images of red cell membrane protein solubilized following protocol D4 (see Table 1). Red cell membrane proteins were separated in PA gels or PVA gels using either 1000 µg in non-linear pH 3-10 strips (13 cm gels) (A) or 600 µg in pH 4-7 strips (7 cm gels) (B); the first and second dimension were run in parallel in PVA and PA gels. Silver (A) and colloidal Coomassie (B) stained gels underwent to image analysis as described in point

2.6. The insets show the 3D reconstruction of representative gel areas from both PAA and PVA gels (2D-Platinum software, Amersham-Bioscience).

Figure 1 A

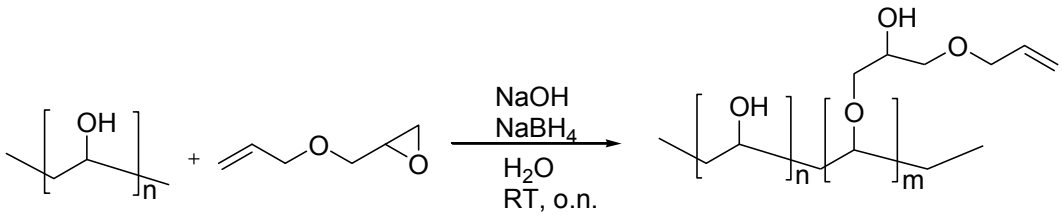

Figure 1 B

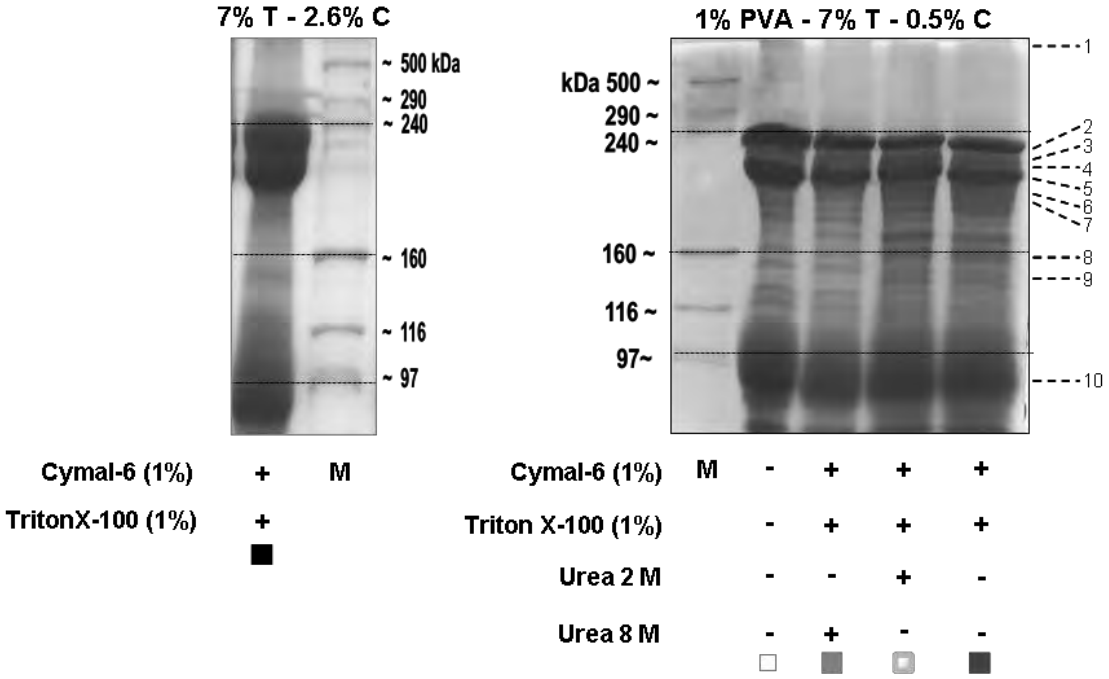

Figure 1 C

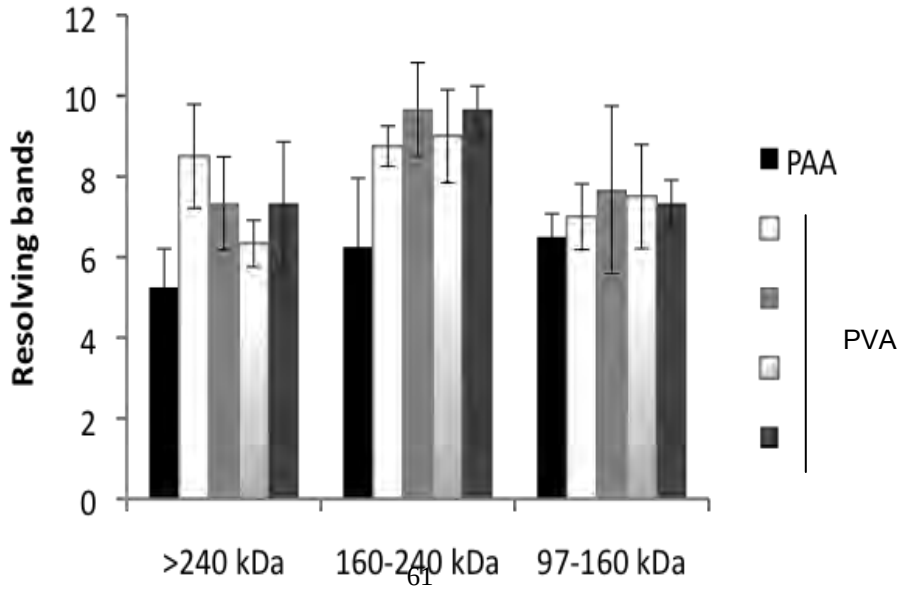

Figure 2

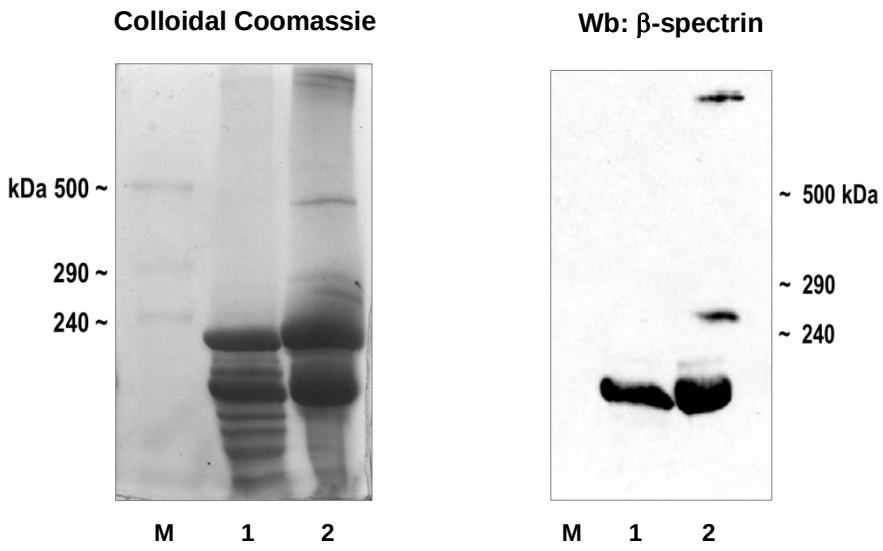

Figure 3

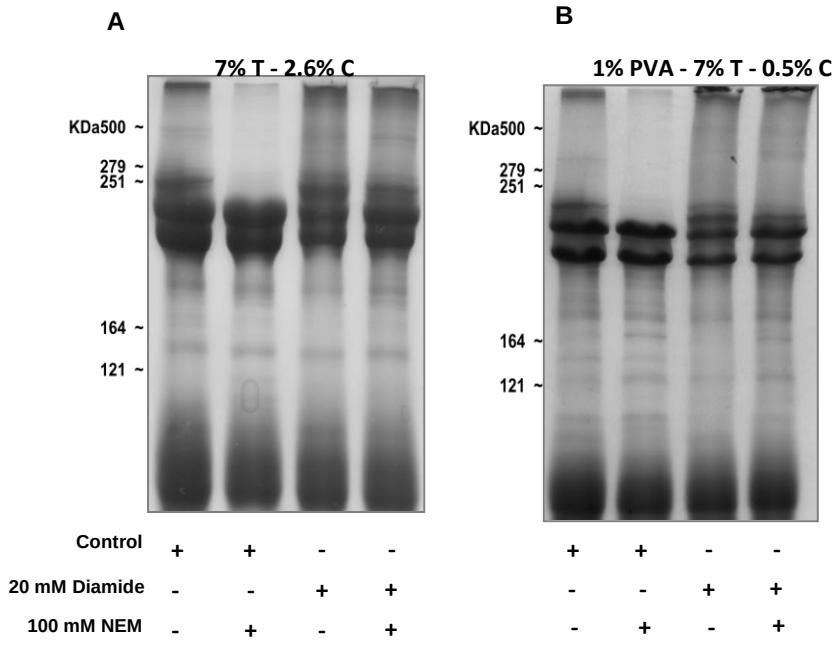

Figure 4

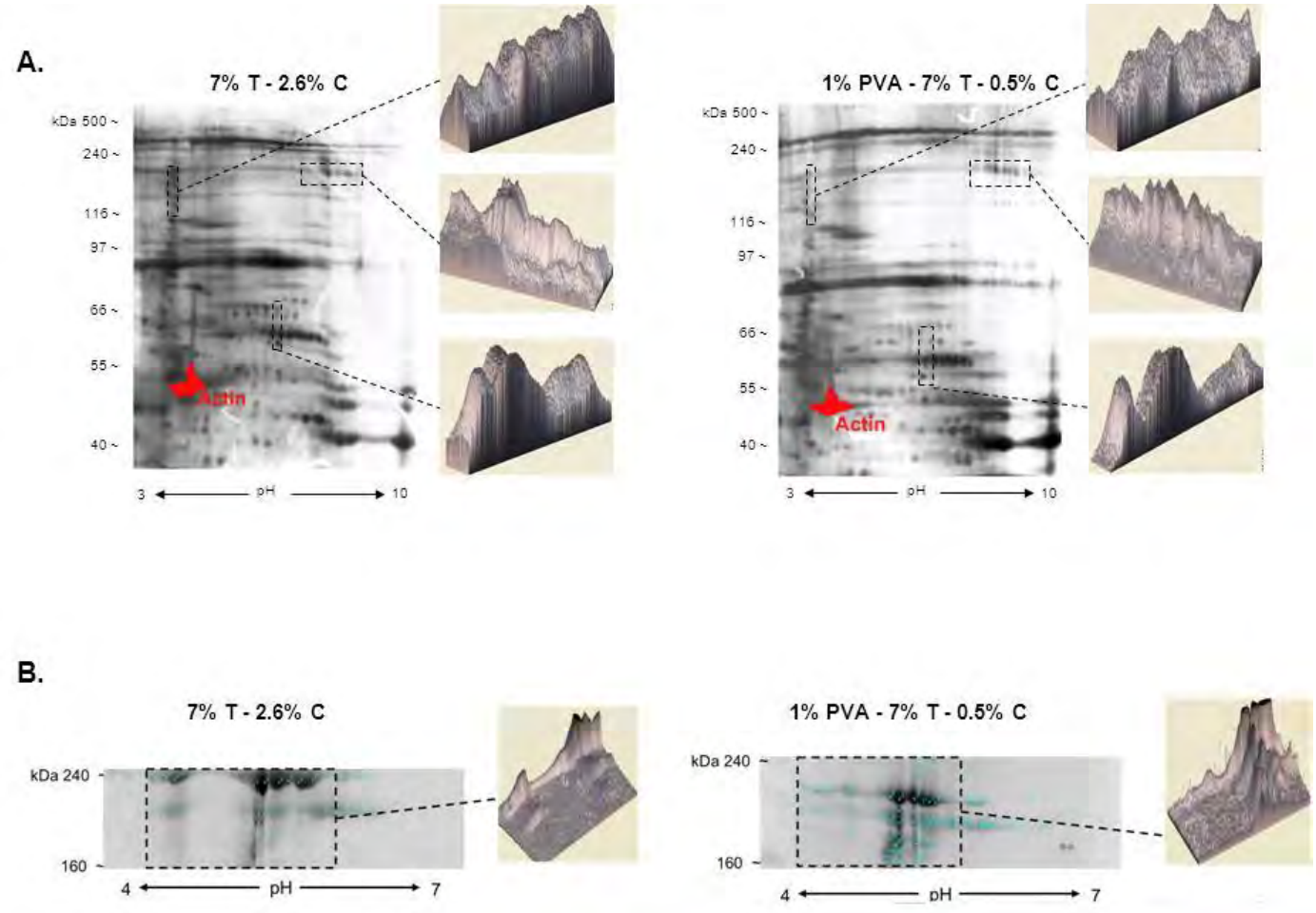
A.
7% T - 2.6% C
1% PVA - 7% T - 0.5% C
kDa 500
240
116
97
66
55
40
Actin
3
pH
10
B.
7% T - 2.6% C
1% PVA - 7% T - 0.5% C
kDa 240
160
4
pH
7